THE UNIVERSITY of ADELAIDE

Thermoresponsive Hydrogels for Mimicking Three-dimensional Microenvironment of Mesenchymal Stem Cells in Cartilage Tissue Engineering

Amir Mellati

This thesis is submitted for the degree of Doctor of Philosophy

in

School of Chemical Engineering

Faculty of Engineering, Computer and Mathematical Sciences

at

The University of Adelaide

January 2015

To my Lovely wife

Hosna

and my sweet daughter

Rasta

PANEL OF SUPERVISORS

Principal Supervisor

Dr. Hu Zhang (PhD)
School of Chemical Engineering
The University of Adelaide
Email: hu.zhang@adelaide.edu.au
Phone: + 61 8 831 33810

Co-supervisor

A/Prof. Bo Jin (PhD)
School of Chemical Engineering
The University of Adelaide
Email: bo.jin@adelaide.edu.au
Phone: +61 8 831 37056

Declaration for a thesis that contains publications

I certify that this work contains no material which has been accepted for the award of any other degree or diploma in my name, in any university or other tertiary institution and, to the best of my knowledge and belief, contains no material previously published or written by another person, except where due reference has been made in the text. In addition, I certify that no part of this work will, in the future, be used in a submission in my name, for any other degree or diploma in any university or other tertiary institution without the prior approval of the University of Adelaide and where applicable, any partner institution responsible for the joint-award of this degree.

I give consent to this copy of my thesis when deposited in the University Library, being made available for loan and photocopying, subject to the provisions of the Copyright Act 1968.

The author acknowledges that copyright of published works contained within this thesis resides with the copyright holder(s) of those works.

I also give permission for the digital version of my thesis to be made available on the web, via the University's digital research repository, the Library Search and also through web search engines, unless permission has been granted by the University to restrict access for a period of time.

Name: Amir Mellati

Signature:…… Date:……

Preface

This doctoral thesis is prepared in "Publication" format according to the "Specifications for Thesis (2015)" of the University of Adelaide. It includes publications that have been published, submitted for publication, or prepared in publication format:

1- A. Mellati and H. Zhang. Expansion of stem cells by nanotissue engineering, in Stem-cell nanoengineering (eds H. Baharvand and N. Aghdami), 2015, John Wiley & Sons Inc., Hoboken, NJ. DOI: 10.1002/9781118540640.ch14

2- A. Mellati, S. Dai, J. Bi, B. Jin, and H. Zhang. A biodegradable thermoresponsive hydrogel with tunable properties for mimicking three-dimensional microenvironments of stem cells. RSC Advances, 2014, 4(109): 63951-63961. DOI: 10.1039/C4RA12215A

3- A. Mellati, M. Valizadeh, S. Dai, J. Bi, B. Jin, and H. Zhang. Influence of polymer molecular weight on the cytotoxicity of poly (N-isopropylacrylamide). Colloid and Interface Science Communications. (Submitted and under review, Reference number: COLCOM-D-14-00131)

4- A. Mellati, C.M. Fan, A. Tamayol, S. Dai, J. Bi, B. Jin, C. Xian, A. Khademhosseini and H. Zhang. Microengineered 3D cell-laden thermoresponsive hydrogels as a platform for bi-zonal cartilage tissue engineering using mesenchymal stem cells. (Prepared in publication style)

5- A. Mellati, M. Valizadeh, S. H. Madani, S. Dai, J. Bi, B. Jin and H. Zhang. Poly (N-isopropylacrylamide)/chitosan hybrid as a three-dimensional microenvironment for stem cells in cartilage tissue engineering. (Prepared in publication style)

Some relevant components of the work have been presented in conferences:

1- H. Zhang, A. Mellati, S. Dai. A thermoresponsive hydrogel-based stem cell culture platform, Tissue Engineering & Regenerative Medicine International Society Asia-Pacific Annual Conference 2014 (TERMIS-AP 2014), 24-27 Sep 2014, Daegu, South Korea (Oral presentation)

2- A. Mellati, S. Dai, B. Jin, H. Zhang. Chitosan-g-PNIPAAm: A thermoresponsive hydrogel as a 3D microenvironment for MSCs. 2013 Royal Australian Chemical Institute SA Student Polymer & Bionanotechnology Symposium (SASPBS'13), 4 Oct 2013, Adelaide (Poster presentation)

During the PhD candidature, some relevant researches were conducted in collaboration with other researchers which led to a publication or conference presentation. The finalized works are:

1- S. Zheyu, A. Mellati, J. Bi, H. Zhang and S. Dai. A thermally responsive cationic nanogel-based platform for three-dimensional cell culture and recovery. 2014, *RSC Advances* 4(55): 29146-29156. DOI: 10.1039/C4RA02852J

2- A.W. Thomson, A. Mellati and H. Zhang. Chitosan-nanoparticle hydrogel complexes for bone tissue engineering. BioProcessing Network 2011 (BPN 2011), October 18-20, 2011, Adelaide (Poster presentation)

In addition, some awards were achieved during the PhD work:

1- Research Abroad Scholarship, The University of Adelaide, 2014 (The scholarship was awarded upon receiving an offer of pre-doctoral research fellow from Prof. Khademhosseini Lab, Harvard-MIT Division of Health Science and Technology, Cambridge, USA, May-June 2014)

2- Young Investigator Award 2011, BioProcessing Network, 2011

3- Adelaide Scholarship International, the University of Adelaide, 2011

Acknowledgement

I would like to acknowledge all the people who had a significant role in my achievements as without their help I would not have been able to get to this point.

I gratefully acknowledge my supervisor Dr. Hu Zhang for his tremendous effort and support during my candidature. His valuable scientific support, encouragement and constructive criticisms led me to the goal. In stressful moments of research his availability, patience and guidance were vital for my success. I also would like to thank my co-supervisor A/Prof. Bo Jin for not only giving research supports but also polishing my publications. I am particularly grateful to A/Prof. Sheng Dai for his guidance, suggestions and support. What I learnt from him is beyond the science. I would like to thank A/Prof. Jingxiu Bi for her great advices and support. The knowledge that I have gained from my supervisors and academic members of research group is not only valuable for my PhD, but also benefit my whole career and life. I also thank A/Prof. Zheyu Shen for his support during his stay in the lab.

I would like to acknowledge heads of school during these years, Prof. Mark Biggs and Prof. Peter Ashman for their willingness to support.

Many thanks go to Prof. Cory Xian for letting me work in his lab and learning from his great team in Sansom Institute for Health Research. I also thank Dr. Chi-ming Fan and Dr. Rosa Chung to help me in performing experiments there.

I would like to acknowledge Prof. Ali Khademhosseini for giving me the chance to work in his lab at Harvard-MIT Division of Health Sciences and Technology (USA). It helped me to develop my technical skills and broaden my perspective. I also thank Dr. Ali Tamayol who provides me with his support to conduct my experiments there.

Many thanks go to all my lab members, staff of the School of Chemical Engineering, Adelaide Microscopy and the University of Adelaide for their scientific, technical and administrative help and support.

I would like to specially thank the University of Adelaide for providing me a full scholarship to study and live in Australia.

Special thanks go to all my wonderful friends in the School of Chemical Engineering, in particular Meisam Valizadeh and Hadi Madani for their support and scientific collaboration.

The place I stand today would not be possible without my wife's patience and devotement. Thank you Hosna, for accompanying and supporting me on my PhD journey, and my little daughter, Rasta, thank you for giving unsparing love to your busy dad.

Finally, I would also like to thank my parents for their endless love and encouragement throughout my life and studies.

Abstract

Articular cartilage covers the bone heads of articulating joints to decrease the friction between bones. Unfortunately, articular cartilage has limited self-repair potential. Cartilage tissue engineering is a promising therapeutic approach, and its success strongly depends on our understanding and ability to mimic the complex three-dimensional microenvironment for cells and their surrounding native extracellular matrix (ECM) in articular cartilage. In particular, recreating the zonal organisation of articular cartilages makes the process more challenging.

My PhD thesis aims to design and develop chitosan-based thermoresponsive matrices with tailored physical, mechanical and chemical properties to fulfill microenvironmental requirements of mesenchymal stem cells (MSCs) in order to promote functional articular cartilage regeneration. The matrices are then micro-manipulated for resembling the spatially varying architecture of articular cartilage zones.

To achieve these aims, chitosan-g-poly (N-isopropylacrylamide) (CS-g-PNIPAAm) hydrogel with a random chain length of grafts was synthesized through free radical polymerization. The influence of various polymerization conditions on physical and mechanical properties was systematically investigated. Its suitability for mimicking microenvironment for MSC culture was studied using cell viability assays. The best CS-g-PNIPAAm in terms of its cell compatibility and cell culture performance was used in fabrication of microengineered constructs for regenerating the superficial zone and the middle zone of articular cartilage. Chondrogenic differentiation of embedded MSCs was evaluated through ECM components (glycosaminoglycan (GAG), total collagen and collagen type II) analysis. Cellular organisation and morphology within microchannels were determined using cell alignment and elongation quantification methods. To further control the chain length of PNIPAAm, well-defined and narrow-dispersed molecular weights of PNIPAAm were synthesized through atom transfer radical polymerization (ATRP). Influence of the polymer molecular weight on cytotoxicity and the cell death mechanisms were investigated through standard assays. Finally, chitosan/well-defined PNIPAAm (CSNI) hybrids were prepared using low/no toxic PNIPAAms. MSCs mixed with PNIPAAm solution and were seeded in the voids of the chitosan scaffolds. The phase separation of PNIPAAm at 37 ^{o}C led to a hybrid matrix for MSCs. The structural characteristics of the hybrids were studied and chondrogenic

differentiation of incorporated MSCs was evaluated through measuring GAG and total collagen deposition.

Various copolymerization conditions of CS-g-PNIPAAm have been optimised to obtain the best hydrogel for MSC culture with desired physical and mechanical properties. After MSC proliferation, MSCs can be recovered by separating cells from the polymer solution at room temperature using the sol-gel thermo-reversible property of the CS-g-PNIPAAm copolymer. It has been demonstrated that the CS-g-PNIPAAm copolymer hydrogel can provide an appropriate microenvironment for 3D cultivation of MSCs.

Biochemical analysis demonstrates that the CS-g-PNIPAAm hydrogel can support the embedded MSCs differentiation into chondrocytes in 3D. Histological and immunohistochemical stainings also confirm the increasing accumulation of GAG and collagen type II. The CS-g-PNIPAAm hydrogel with manipulated properties can be micropatterned for regenerating the superficial zone and the middle zone of articular cartilage. The cell-laden hydrogel micropatterned in 50-100 μm constructs can organize cells along the microchannel horizontal axis. The cell shape and alignment in the constructs is very similar to the superficial zone of chondrocytes of the native cartilage. Meanwhile, cells in the microchannel with the gap above 150 μm are randomly distributed which can be used to mimic the middle zone of the cartilage tissue.

The cytotoxicity of PNIPAAm is molecular weight dependent, and varies with the PNIPAAm chain length. Low molecular weight PNIPAAm (degree of polymerization (DP) = 35) is inherently toxic to cells, and necrosis is the dominant cell death mechanism. Moderate-sized PNIPAAms with their DP between 100 and 200 are non-cytotoxic. For the PNIPAAm with a higher molecular weight (DP = 400, P-400), cell viability is dependent on the assay method. The P-400 hydrogel is detrimental to stem cells when the cells are covered with a thick layer of gel, and this layer may become a barrier for nutrient or oxygen delivery to cells.

The CSNI hybrid matrices composed of chitosan scaffolds and well-defined PNIPAAm with a degree of polymerization of 400 (CSNI400) can provide a supporting platform for 3D stem cell culture and cartilage tissue engineering. Matrix characterization shows improved structural properties of CSNI400 in comparison with CSNI100 and the chitosan-alone scaffold.

In conclusion, we are able to create and refine 3D microenvironment for stem cells through manipulation of matrices in order to enhance cell proliferation and chondrogenic differentiation. Our results reveal that graft copolymer of chitosan and PNIPAAm with tailored properties and microengineered architecture is appealing for zonal cartilage tissue engineering. The hybrid matrices from chitosan scaffolds with well-defined PNIPAAm hydrogels promote chondrogenesis, better than the graft copolymer.

Graft copolymerization of chitosan and well-defined PNIPAAms (CS-g-W-PNIPAAm), microengineering of CSNI hybrids, and CS-g-W-PNIPAAm, stacking the microengineered constructs to form a macroscale 3D cartilage tissue, and *in vivo* implantation of engineered tissues should be addressed in future projects.

Table of Contents

CHAPTER ONE

1. Introduction

1.1 Background: cartilage failures and tissue engineering

Cartilage-related diseases are one of the most reasons for disabilities around the world. Osteoarthritis is already one of the ten most disabling diseases in developed countries. 55.3 million people are affected by arthritis diseases worldwide (1). 9.6% of men and 18.0% of women aged over 60 years have symptomatic osteoarthritis (2). In Australia, osteoarthritis is a major cause of disability, psychological distress and poor quality of life (3). In 2007-08, 15% of people reported that they currently had arthritis (4). 62.5% of people with profound/severe disability and 32% of people without disability reported to have arthritis in the 75 and over age group (5). It was 4% of the disease burden in Australia in 2007-08 and cost 7.5% ($4.0 billion) of total allocated health expenditure in 2004-05 (6). 4.6% of deaths registered in 2009 were due to arthritis and musculoskeletal diseases (underlying or associated) (7). Other countries also suffer from the same problem. These diseases cost $128 billion for US economy per annum (5). In Canada, a 2006 study found that for adults aged 15 years and over with disabilities, the most common issue was arthritis (1). On the other hand, cartilage can be damaged from accidents such as car crashes or work and sport injuries. Articular cartilage injuries of the knee are reported as the most common reason of permanent disabilities in athletes (8). According to the "Australian Safety and Compensation Council" report, over 76,000 compensation claims for acute and chronic musculoskeletal disorders in 2003 were made, representing 43% of all injuries and disease-related claims (9). Unfortunately, articular cartilage has limited repair potential (10). Poor self-repair capacity of cartilages becomes the major challenge for the therapeutic strategy especially in young and active individuals, because they need to return to sport and working activities quickly.

There are different approaches to repair a damaged articular cartilage. These therapeutic strategies can be divided into two major categories (11). The first category is "without biologic therapies", such as lavage and arthroscopy, chondral shaving, laser abrasion/ laser chondroplasty, abrasion chondroplasty, pridie drilling and microfracture, spongialization, debridement and extensive surgical interventions e.g. osteotomy and distraction of joints. The second category consists of "with active biologic therapies", such as autologous tissue

transplantation, osteochondral transplantation (mosaicplasty), allogenic osteochondral, chondral grafting, and tissue engineering.

Tissue engineering is one of the most promising therapies for patients with organ failure and damaged or diseased tissues. The appropriate cells are incorporated within a three-dimensional (3D) matrix and grown under a suitable condition to form the new functional tissue. There are two major elements to be considered in tissue engineering: cells and cell microenvironment. Matrices are the main component of the cellular microenvironment. They serve as artificial temporary scaffolds for cells. These scaffolds are often made by mimicking the native extracellular matrix (ECM). The cell-ECM interactions are essential requirements for cell and tissue functionality. Other signaling factors such as bioactive molecules and mechanical or electrical stimulations may also be considered in designing a microenvironment. Controlling the variables of microenvironment in order to provide mimicking physiological conditions in a 3D manner forms the key component of tissue engineering.

1.2 Aims and objectives

Many research groups and scientists have been working on regenerating functional cartilage tissues and implanting them into the patient body. Despite of many promising trials, there are still no off-the-shelf products in the market which can fully address all the clinical needs for treatment and many challenges remain to be resolved. Successful cartilage tissue engineering requires more efforts to control microenvironmental cues. Novel biomaterials with precisely engineered properties should be prepared to provide a suitable 3D microenvironment to regulate cell fate and cellular activities, including adequate proliferation to obtain sufficient homogenous cells, and differentiation toward the desired cell line and deposition of extracellular matrix with chondrogenic phenotype. Hence, in this PhD project, I aim to design and develop a serial of chitosan-based thermoresponsive matrices with controlled properties to fulfill microenvironmental requirements of mesenchymal stem cells (MSCs) in order to promote functional articular cartilage regeneration.

Specific objectives of my PhD project are:

- To synthesize and characterize a range of chitosan-based thermoresponsive matrices with different mechanical properties for cartilage tissue engineering;
- To correlate the synthesized polymer chemical structure and its physical, mechanical and biological properties with cellular responses, and to exploit matrices with tailored properties for recreating the most appropriate 3D microenvironment for cells;
- To replicate the zonal structure of native cartilages using micro-engineered cell-laden thermoresponsive hydrogels;
- To evaluate the biological characteristics of engineered cartilages through standard assays.

1.3 Thesis structure

The thesis is written in a paper-based format. I start my thesis with the Introduction chapter to highlight the importance of my PhD work, and critically review the recent contributions to cartilage tissue engineering to identify research gaps in the second chapter. Major experimental results are written in Chapter 3 to 6. The thesis finishes with the conclusion and future directions derived from my experiments.

In the first chapter of this thesis, the background, research gaps, aims and objectives, and the thesis outline are introduced.

In the second chapter, the biological background of native articular cartilage structure and functions is described. Cells and their microenvironments are further discussed in cartilage tissue engineering. Biomaterials, particularly nanostructured biomaterials, developed for 3D stem cell culture and expansion are reviewed. The effect of nanoscale features of microenvironment on stem cell infiltration, adhesion, migration and proliferation is discussed.

In chapter three, based on the literature review, chitosan was selected as the base material for cartilage tissue engineering. Poly (N-isopropylacrylamide) was grafted onto chitosan to

make it thermo-responsive. These thermo-responsive hydrogels can be injected into cartilage defect sites in a minimally invasive manner. Therefore, chitosan-g-poly(N-isopropylacrylamide) (CS-g-PNIPAAm) copolymers were synthesized. The influence of various polymerization conditions, such as acid concentration, reaction temperature and monomer feed, on the grafting parameters of this thermo-responsive hydrogel, was systematically investigated. In a physiological pH, optimized balance between the solubility (as the pre-requirement for cell dispersion and injectability) of copolymers at ambient temperature and enhanced gel mechanical strength (as the essential parameter of stem cell microenvironments) at body temperature was achieved through controlled reaction conditions. The viability and proliferation of mesenchymal stem cells (MSCs) in this hydrogel was investigated.

In the fourth chapter, MSCs were incorporated within CS-g-PNIPAAm hydrogel and their chondrogenic differentiation was studied quantitatively by biochemical assays and qualitatively by histological and immunohistochemical assessments. Micropatterning was employed to mimic cellular shape and orientation within the superficial and middle zones of the natural cartilage. Thermo-responsiveness of CS-g-PNIPAAm was exploited to cast the cell-laden gels within micromolds. Cell alignment and elongation within three-dimensional micropatterned cell-laden hydrogels were evaluated.

In the fifth chapter, a serial of PNIPAAms with well-defined molecular weights were synthesized through atom transfer radical polymerisation (ATRP) and polymer molecular weight-dependent cytotoxicity was examined in order to obtain the less toxic PNIPAAm chain length for thermoresponsive scaffold design in the next chapter.

In the sixth chapter, another form of chitosan and PNIPAAm was investigated. Non-toxic or low-toxic PNIPAAms were chosen based on the results of Chapter 5 for fabrication of a hybrid chitosan and PNIPAAm scaffold. The scaffold was characterized using thermal analysis, dynamic light scattering and swelling ratio measurement. The morphological structure of the scaffold was investigated in micro- and nano-scale. Influence of PNIPAAm molecular weight on cell viability and self-renewal in a 3D microenvironment was studied and the suitability of the hybrid scaffold for cartilage tissue engineering was evaluated using biochemical assays.

Chapter Seven comprises the conclusions and future directions derived from current findings in this PhD project.

1.4 References

1. Selected long-tem health conditions, aspects of disability and health in Australia (2007-2008): Australian Bureau of Statistics2011.
2. Chronic rheumatic conditions: World Health Organization, Department of Chronic Diseases and Health Promotion, Respiratory Diseases and Arthristis2011.
3. A picture of osteoarthritis in Australia: Department of Health and Ageing, Australian Institute of Health and Welfare2007.
4. Year book Australia, 2009–10, chronic disease: Australian Bureau of Statistics2010.
5. Spiller KL, Maher SA, Lowman AM. Hydrogels for the Repair of Articular Cartilage Defects. Tissue Engineering Part B: Reviews. 2011;17(4):281-99.
6. Arthritis and osteoporosis in Australia - a snapshot (2007-08) Australian Bureau of Statistics2011.
7. Causes of death 2009: Australian Bureau of Statistics2011.
8. McAdams TR, Mithoefer K, Scopp JM, Mandelbaum BR. Articular cartilage injury in athletes. Cartilage. 2010;1(3):165-79.
9. Worked related musculoskeletal disease in Australia: Australian Saftey and Compensation Council2006.
10. Haleem AM, Chu CR. Advances in tissue engineering techniques for articular cartilage repair. Operative Techniques in Orthopaedics. 2010;20(2):76-89.
11. Hunziker EB. Articular cartilage repair: basic science and clinical progress. A review of the current status and prospects. Osteoarthritis and Cartilage. 2002;10(6):432-63.

CHAPTER TWO

2. Literature Review

2.1 Biology, structure and functions of native cartilage

Cartilage is a connective tissue in human or animal bodies. Three different types of cartilages are distinguishable: hyaline cartilages (e.g. articular cartilages), elastic cartilages in epiglottis and eustachian tube, and fibrocartilages in intervertebral discs, temporomandibular joint and meniscus (1). Articular cartilage is a thin layer of hyaline cartilage covering the bone heads of articulating joints to decrease the friction between bones of a joint. These soft tissues have outstanding properties such as shock absorption, wear resistance and high lubrication (2). There are no blood vessels and nerves within articular cartilages. Articular cartilage is a multiphasic tissue consisting of chondrocyte cells (less than 10% of the total volume), interstitial fluid (approximately 80% by wet weight), which is mostly water, and solid phase or extracellular matrix (ECM) (approximately 20% by wet weight). ECM contains collagen fibers (approx. 60% of dry weight), proteoglycans (PGs) (10-15% of wet weight) and other protein and glycoprotein macromolecules (Fig.2-1). 90-95% of the collagen content is collagen type II and a minor amount of types V, VI, IX, X and XI are also present in articular cartilages (2). Collagens provide tensile stiffness of cartilage and proteoglycans are responsible for its compressive strength.

Four zones or layers are identified in articular cartilages (2, 3) as shown in Fig.2-2. The superficial or tangential zone is the closest layer to the cartilage surface. This layer represents 10-20% of the total thickness. This zone is rich in water and PGs are at the minimum level. Chondrocytes are ellipsoidal and parallel to the surface. Collagen fibrils lie also parallel to the surface. The middle or transitional zone is laid under the superficial zone. Its thickness is 40-60% of the total thickness. Chondrocytes are rounder and collagen fibrils are larger in diameter in comparison to the superficial zone. Both chondrocytes and collagen fibrils are randomly aligned. The PG content is at its highest level. The deep zone is below the middle layer and contains the minimum water amount. Chondrocytes are spherical in shape and are aligned columnar and perpendicular to the tidemark which is a boundary line between the deep zone and the lowest layer (i.e. calcified zone) of the cartilage. Collagens are perpendicular to the tidemark too. The calcified zone anchors the

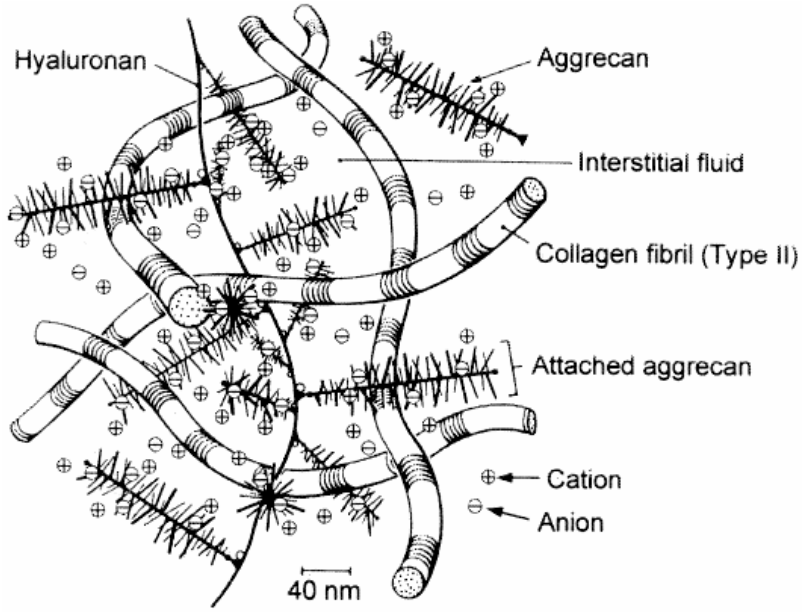

Figure 2-1. Structure of articular cartilage extracellular matrix. (Reprinted with permission from (3))

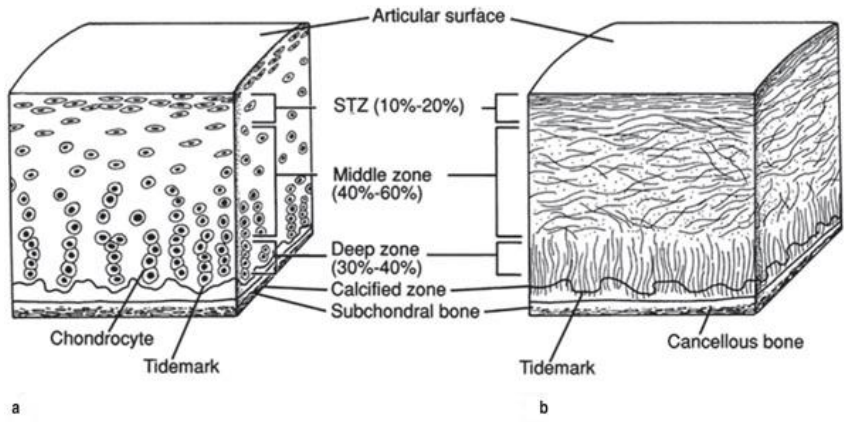

Figure 2-2. Zonal organisation of articular cartilage. (a) Chondrocyte shape and alignment, (b) collagen alignment. (Reproduced with permission from (3))

hyaline cartilage to the subchondral bone. Chondrocytes are small and randomly distributed in a matrix of apatitic salts.

Due to its avascular nature, articular cartilage has limited capacity for self-repair. Articular cartilage also contains a sophisticated zonal structure. To restore the normal functions of the cartilage, a myriad of issues have to be addressed for regenerating functional cartilage, especially on optimizing the microenvironment for stem cell culture and differentiation. The objective of this study was to regenerate articular cartilage by synthesizing biomaterials with tailored properties for 3D stem cell expansion and differentiation as well as cartilage formation. Therefore, we will discuss important features of biomaterials as cell matrices. Then we will review the literature on biomaterials and their nano-level aspects for 3D cell culture and expansion, followed by a specific focus on biomaterials for mimicking matrices for tissue engineering, especially cartilage tissue engineering.

2.2 General features of biomaterials as cell matrices

The matrices should be biocompatible. Matrices and their degradation by-products should be safe to the host tissue with no inflammatory responses and they should be nontoxic to seeded cells. The matrices should be able to provide supports for cells to adhere and function. They need to provide the primary mechanical strength of the defect site during the tissue regeneration *in vivo* (4). Sufficient mechanical strength in highly stressed joints to match those of native tissue is another necessity (5, 6). They may also mediate mechanical signals to cells for stimulating cell proliferation and differentiation (7). Porous matrices are often required for regenerating cartilage tissues. Cartilage tissues are avascular. Hence, the matrix should have a suitable architecture to deliver nutrients and exhaust cell wastes. Porous structure provides essential pathways to deliver nutrients to the cells which are attached within scaffold pores. Moreover, pores allow cells to attach, spread, proliferate, migrate and produce extracellular matrix. Furthermore, biodegradability of the matrices is an important parameter. They need to be eliminated as a result of biological reactions in a timely manner that matches cell modeling/remodeling,

ECM production and neo-tissue formation (4). The matrices may also provide physical, mechanical, or biological cues for cells. The matrix-cell dynamic interactions can regulate cell behaviours and fate (157). Bioactive molecules may be encapsulated in the matrices and then released from them in a temporal and spatial way to induce cells to grow and differentiate into specific tissue with desired functionality (8).

2.3 Structural features of matrices

Tissue engineers have recognized that structural aspects can have profound influences on cell behaviours (9). Recent studies show that cell adhesion, migration, proliferation, differentiation, morphogenesis and apoptosis, not only depend on macrostructure of the microenvironment, but also rely on nano- and micro-scale features of the ECM in the microenvironment (10). Therefore, the success in tissue engineering strongly depends on our understanding and ability to mimic the complex 3D architecture of the native ECM in a multiple length scale (11).

Macro-scale structure is important to make the desired shape and size of the defect site, and to offer enough mechanical strength for tissue formation. Micro-scale level of scaffold design is usually related to tissue architectures. For example, oriented parallel fibres are beneficial for reconstructing peripheral nerve (12), while random non-woven fibres may be more important for dermal replacement (13,14). Micro-structural features are also essential for ensuring cell adhesion and migration and determining the overall mechanical properties (15). Particular attention has been drawn to pore size, connectivity, and geometry of 3D matrices (16). Pore size should be relatively large because most of the adherent stem cells have a size ranging from 10 to 150 μm. A large-pore structure allows delivering a sufficient number of cells and cell migration, while the inter-connected porosity offers efficient diffusion of nutrients and metabolic waste removal (17,18).

The multi-scale requirements have motivated the development of new fabrication processes that can produce biomaterials with specific three-dimensional (3D) micro- and nanostructures in which pore structure, surface area to volume ratio, texture and surface topography can be manipulated to control cell-matrix and cell-cell interactions (9).

Microfabrication technologies such as emulsification (to produce microgels), photolithography, micromolding, microfluidics, 3D bioprinting are emerging approaches to replicate cellular microenvironment *in vitro* or to fabricate tissue engineering matrices with microscale resolutions (19-21). Microtechnologies can be employed in various orders to control individual cell-cell interactions, to control the structure of clusters of cells, or to control interactions between multiple cell clusters (21). For example, they can be utilized to generate microvasculature within scaffolds (22). Micromolded poly(glycerol sebacate) (PGS) (23) capillaries and cell-laden agarose microfluidic channels (24) were fabricated as vascularized scaffolds. Furthermore, in a bottom up approach, microengineered constructs can be assembled as building blocks to fabricate larger tissues with controlled biomimetic microarchitecture (25, 26).

Microfabrication techniques can also be used to control the porosity and microarchitecture of pores (pore size, pore shape, interconnectivity and etc.) (27). These structural features play an important role in regulating engineered tissue properties. Various methods have been utilized to fabricate porous scaffolds, such as solvent casting/particle leaching, freeze-drying, gas foaming, and electrospinning. Porosity and microarchitectural features of pores can be tailored by changing the preparation conditions in various methods (27). Scaffold nanopores are also important jn controlling over tissue architecture and they expand our ability to direct cell fate and improve tissue growth and function (28). Nanoporous structure of membranes has been shown to significantly affect cellular response (29). Nanoporous membranes can also provide an antigen barrier around encapsulated cells to prevent host immune rejection, while preserve their capabilities for nutrient and oxygen delivery and metabolic waste removal (30). Nanopores are useful for the crystallization of hydroxycarbonate apatite (HCA) and cell adhesion in bone tissue engineering (31). Change in nanoscale textural porosity of macropore walls can alter their mechanical strength which has a significant effect on cellular activity (32). Besides the nanoporous structures, some platforms with nano-scaled features such as nano-fibres, nano-composites and surface-modified nano-structures are being used to control cell behaviors. We will describe these platforms as matrices for 3D stem cell culture in the following section.

2.4 Nanostructured platforms as matrices for 3D stem cell culture[1]

Nano-scale elements of native cells and tissues have become more important for understanding stem cell behaviours. Especially, nano features of ECM have a big impact on stem cell adhesion, migration, proliferation and controlled differentiation. Fig. 2-3 summarized the nano-level aspects of ECM and benefits of resembling these features using nano-structured matrices.

ECM consists of structural protein fibres (collagen and elastin), adhesive proteins (fibronectin and laminin), glycosaminoglycans (GAGs) and proteoglycans (PGs). These proteins have dimensions between 10 to several hundred nanometers (34).

ECM nano-topology also regulates stem cell behaviours, ranging from changes in cell adhesion, cell orientation, cell motility, surface antigen display, cytoskeletal condensation, activation of tyrosine kinases, and modulation of intracellular signaling pathways that regulate transcriptional activity and gene expression (35). The nano-topology may include dimensional scale from nanometer to micrometer and types of topological forms such as ridges, steps, grooves, pillars and pits (35). Structural ECM features, such as fibrils and pores, are often of a size compatible with cellular processes involved in migration, which may influence the strategy by which cells migrate through ECM. This size ratio between cell (1 to 100 µm) and surrounding fibres (1-100 nm) enables the cell to be in direct contact with the fibres of the ECM thus creating a 3D orientation (34).

---

[1] **The section was published as a book chapter in: Stem-Cell Nanoengineering (eds H. Baharvand and N. Aghdami), John Wiley & Sons, Inc., Hoboken, NJ. DOI: 10.1002/9781118540640.ch14 (33). It is partially reorganized to be adapted to this literature review.**

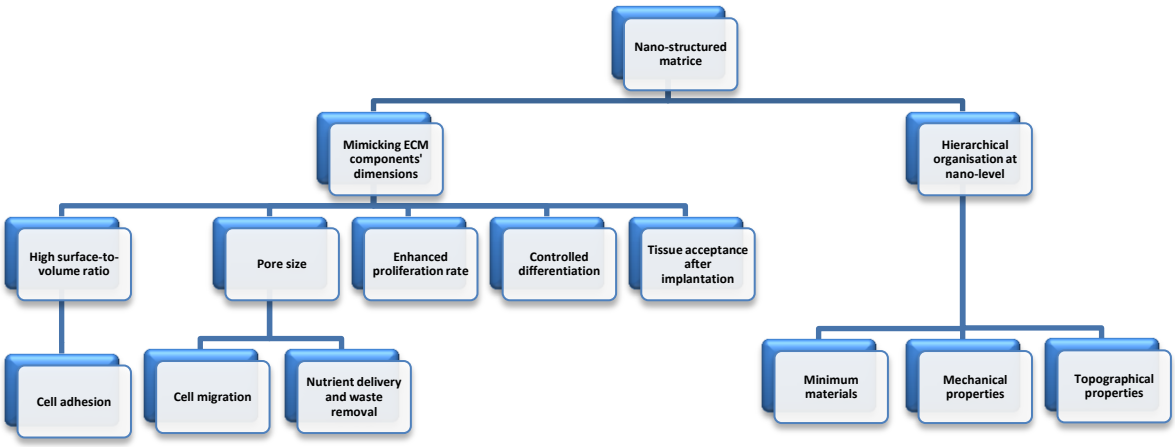

Figure 2-3 Advantages of nano-structured matrices for regulating stem cell behaviours

Nano-scale ECM also plays a significant role in signal transduction. Stem cells respond to the ECM through nano-sized membrane receptors that connect the matrix to the cytoskeleton. Integrin is one of the main receptors which can recognise Arg-Gly-Asp (RGD) sequences of ECM proteins. After integrins bind to ECM proteins (such as fibronectin or vitronectin); the integrin ligation would activate focal adhesion kinase (FAK) signalling. The activated FAK undergoes auto-phosphorylation and triggers a downstream signalling of extracellular signal regulated kinase (ERK)/ mitogen activated protein kinase (MAPK) pathway to transfer mechanical information to the cell nucleus where the cell DNA reacts to extracellular stimulus by producing changes such as proliferation and differentiation to cells. Ras homolog gene family, member A (RhoA)/ Rho associated coiled-coil protein kinase (ROCK) pathway can also be triggered by activated FAK and subsequently activate ERK/MAPK pathway to influence stem cells. The schematic description of this process is shown in Fig. 2-4. The signaling pathways

may be regulated from different ECM protein composition, and density and distribution of ECM ligands. Through these pathways, cells detect and respond to the mechanical, chemical and biological characteristics of their surrounding microenvironment (36). A variety of strategies have been formulated to engineering ECM ligands, such as RGD, in artificial 3D matrices through self-assembly of peptides and surface modifications.

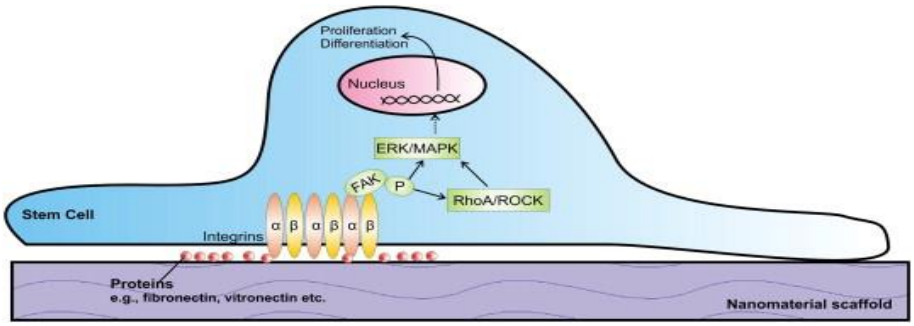

Figure 2-4 Schematic pathways involved in the interaction of stem cells and nano-structured matrices: After integrins on the cell membranes bind to nano-structured ECM components, cascades of signal transduction occur for translating physical contact with nano-structures into biological responses, such as cell morphological change, proliferation and differentiation. (Reprinted from (36) with permission)

Nature manages to make structures with the minimum amount of essential chemicals. The natural ECM includes less than 1% solid materials, yet they are mechanically strong and have various functionality. Nature regulates the mechanical characteristics of a biological tissue by fine adjustment of its composition with alteration of its nano-scale structure from molecular level up to macroscopic scale (37).

Investigators have tried to engineer artificial matrices that resemble the nano-scale features of the natural ECM. The matrices with nano-scale features can be categorized into nano-fibres, nano-composites, and nano-structured surfaces.

2.4.1.1 Nano-fibres

Nano-fibres, diameters ranging from 1 to 1000 nm, are the most popular nano-structured biomaterials which have been widely used in tissue engineering due to the similarity between nano-fibre structures and ECM fibres diameter size scales, and large surface area which is favorable for cell adhesion and bioactive factor encapsulation.

There are three commonly used methods to produce nano-fibres: electrospinning, self-assembly and phase separation (38), and the fibre composition, alignment, diameter, degradation, and mechanical characteristics can be controlled for different types of tissue regeneration. Fibres have been fabricated for stem cell expansion using self-assembly peptides and a range of polymers such as Poly (ε-caprolactone) (PCL), Poly (lactic acid) (PLA), Poly (D, L-lactide-co-glycolide) (PLGA), and other synthetic or natural polymers and also their blends or copolymers (Table 2-1).

2.4.1.1.1 PCL

PCL is widely chosen as a FDA-approved model polymer due to its low toxicity, low cost and ease of fabrication. Disadvantages of unmodified PCL are slow degradation rate (weeks to months), weak mechanical properties, non-reactivity and hydrophobicity. Intensive attempts have been made at fabricating PCL fibres for tissue engineering based on mesenchymal stem cells (MSCs) (39,40-42), ESCs (43), somatic stem cells (SSCs) (44) and neural stem cells (NSCs) (110) .

In 2003, Yushimoto et al. explored PCL nano-fibre matrices for expanding MSCs. Penetration of cells and abundant ECM were observed in the cell-fibre constructs after 1 week. SEM images showed that the surfaces of the constructs were covered with several layers of cells at fourth weeks (40). Ruckh et al. further quantified cell growth along with live cell imaging. After a short-term (7 days) culture of MSCs in PCL nano-fibres, live cell fluorescence staining and MTT assay showed significantly higher proliferation of MSCs on nano-fibres than 2D control surfaces. SEM analysis also supported the fluorescence microscopy results that the

Table 2-1- Nano-fibres for stem cells expansion

Category	Nanomaterial	Stem Cell	Significance/Result (s)	References
Synthetic Polymers	PCL[b]	MSC[a]	SEM images showed good cell attachment	(40)
		MSC	successful 7 days cell proliferation before adding differentiation medium	(39)
		MSC	surface modification led to improved cell adhesion and proliferation	(42)
		CSC[c]-MSC	the higher the scaffold thickness, the more the cell proliferation	(41)
		ESC[d]	ESCs successfully cultured	(43)
		SSC[e]	SSCs successfully cultured	(44)
		NSC[f]	NSCs successfully cultured	(110)
	PCL nano/microfibre	MSC	multilayer of nano(for higher ECM mimicary) and micro(for better cell migration) fibres	(45)
	PCL nano-fibre/ PCL strands	MSC	combining good architecture control of strands with good cell attachment of nano-fibres	(47)
	Poly (lactic acid)	NSC	Cell adhesion is near TCPS[g]	(50), (49)
		MSC	Microfibre constructs:cells were aggregate within the larger inter-fibre space- Nano-fibre constructs: cells spread across multiple nano-fibres	(54)
		TSC[h]	Effect of fibre orientation on cell morphlogy and orientation- Increased cell proliferation	(55)
	PLGA[i]	MSC	Nano-fibres increased proliferation rather than microfibres	(62)
		MSC	Good proliferation and morphology- Retaining the differentiation abilities after 14 days culture (prior to differentiation)	(61)
		ESC	ESCs successfully cultured	(57), (58)
		NSC	High cell attachment on nano-fibre surfaces	(63)

Synthetic Polymers (Continued)	PLGA/Collagen	HSC[j]	rapid and rich cell attachment	(65)
	Polyurethane	MSC	enhanced attachment and proliferation	(66)
	polyamide	ESC	enhanced attachment and proliferation	(67)
	PES[k]	HSC	Surface-aminated nano-fibres enhance adhesion and expansion	(68)
	PES	HSC	aminated chain length is important factor	(69)
	Self-assembeled RAD16 peptide and its motifs	ESC	ESCs successfully cultured	(80)
		NSC	NSCs successfully cultured	(82)
		hASC[l]	hASCs successfully cultured	(81)
	Self-assembeled Multi Domain Peptide	MSC	promoted cell adhesion,migration and expansion	(83)
	Self-assembeled Peptide-amphiphiles	NSC	NSCs successfully cultured	(84)
		MSC	MSCs successfully cultured	(85), (86), (87)
Natural Polymers	Collagen	MSC	MSCs successfully cultured	(70)
	Silk/PEO[m]	MSC	PEO was added to improve processability- Improved adhesion and proliferation	(71), (72)
Other Modifications	PCLnano-fibre/ PLLA nano-fibre	ESC-MSC	Cells infiltrated into the scaffold rather than migration along the surface - enhanced proliferation	(78)
	P(LLA-CL) [n]	SMC[m]	enhanced proliferation	(73)
	starch/PCL	MSC	Example of blending with natural materials - combination of micro and nano-fibres- better morphology and cell growth	(79)
	P(EOT-BT)[o]	MSC	microfibres with nanopores are great for cell adhesion and proliferation	(77)

a: Mesenchymal Stem Cell , b: Poly (ε -caprolactone) , c: Carcinoma Stem Cell , d: Embryonic Stem Cell , e: Somatic Stem Cell , f: Neural Stem Cell , g: Tissue Culture Polystyrene , h: Tendon Stem Cell , i: Poly (D, L-lactide-co-glycolide) , j: Hematopoietic Stem Cell, k: polyethersulfone , l: human Adipose Stem Cell , m: poly(ethylene oxide) , n: poly (l-lactic-co- ε -caprolactone) , m: Smooth Muscle Cell , o: Poly (ethylene oxide terephthalate)–poly(butyleneterephthalate)

MSCs preferentially adhere, spread and colonize on nano-fibre matrices compared to 2D surfaces (39). The physical parameters of PCL nano-fibres, such as diameter of the fibres and morphology of the fibre surface, can influence cell attachment and growth. This has been confirmed by a study using mouse ESCs (P19) and mouse MSCs. Matrices with a thickness of 0.6 mm were found to provide a better substrate for cell proliferation rather than scaffolds with the thickness of 0.1 mm, possibly due to more dimensional stability (41). To demonstrate that nano-fibre surface modification affects stem cell behaviour, the surface of the PCL nano-fibres was modified by He^+-irradiation which led to slight smooth surface and different nano-scale surface chemical structures. The results showed that early attachment, further proliferation as well as osteoblastic markers, were higher for MSC on He^+-irradiated PCL (42).

One of the drawbacks of nano-fibre matrices is their small pore size which results in poor cell infiltration and migration. To capitalize on the properties of micro-fibres (i.e., pores large enough for cell migration) and nano-fibres (i.e., physical mimicking of native ECM), multilayered matrices can be fabricated to increase the pore size for cell migration. MSCs were attached well on both single and bi-layered matrices but were more spread when nano-fibres were present. However, increasing the thickness of the nano-fibre layer reduced the infiltration of cells into the matrices (45).

The pore size of fibrous structure can be controlled with melt-plotted strands from CAD/CAM technologies. In this method, the melted polymer was plotted with a 250 mm dispensing needle tip, laid down layer by layer. The resulting fabricated matrices have smooth strand surfaces and large pore size between the strands. These characteristics limit the initial cell adhesion. To overcome these disadvantages, micro/nano-fibre electrospun with PCL were layered between micro-sized PCL strands (46). The cell attachment was further improved by two natural biomaterials (small intestinal submucosa (SIS) and silk fibroin. Bone marrow-derived rat MSCs revealed an incredible increase in initial cell attachment and cell expansion on the 3D hierarchical PCL fibrous matrices modified with two natural biomaterials (47).

2.4.1.1.2 PLLA

PLLA is a biodegradable, biocompatible polymer and it has better thermal processability than other biopolymers such as poly (ethylene glycol) (PEG) and PCL. However, unmodified PLLA has limited applications in tissue engineering due to its poor toughness, very slow degradation (more than 3 years), relatively hydrophobicity that results in low cell affinity, and Lack of reactive side-chain groups (48).

One modification for PLLA is to fabricate PLLA nano-fibres using a liquid–liquid phase separation method (49). This method can create nano-fibrous matrices with controlled and carefully designed macro-porous architecture. However, the nano-fibre diameter is not adjustable in this method. Electrospinning method has been exploited to produce PLLA nano-fibres with variable diameters. Liquid surface separation method may produce nano-fibrous matrices with soft surface, while electrospinning methods may result in nano-fibrous with increased surface roughness. Results showed that the NSC attachment was better at surface fabricated from electrospinning method (50,51) since the more the roughness, the higher the cell adhesion (52,53). However, increasing the roughness will lead to an increase in the hydrophobicity as well, which impels the nutrients from pores.

Micro- and nano-sized PLLA fibrous matrices were also fabricated to study effect of architectural characteristics on cell spreading, migration and proliferation. The micro-fibrous meshes with a large pore size enhanced cell aggregation while small-pore nano-fibre structures presented a spread, spindle-shape morphology. Cell attachment may be higher on the nano-fibre scaffolds because the fibres were highly packed in matrices. By increasing the fibre diameter size, cells were aggregate within the larger inter-fibre distance/pore space rather than spread across multiple fibres (54).

PLLA nano-fibres were also fabricated to have aligned or random-oriented structures. Human tendon stem/progenitor cells (hTSPCs) were seeded onto both nano-fibres. They were adhered very well and the cell number was increased about 3 folds in 14 days for both nano-fibres. However, histological staining and confocal images (Fig 2-5) showed that hTSPCs were spindle-shaped and well orientated on the aligned nano-fibres (55). This

demonstrates that nano-fibrous aligned structure can influence stem cell morphology and orientation.

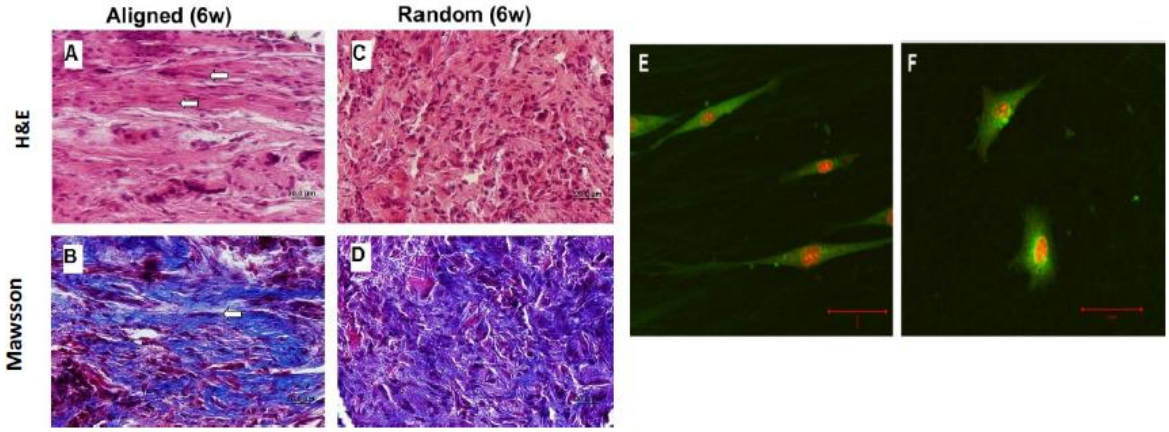

Figure 2-5 Effects of nano-fibre alignment on human tendon stem/progenitor cells (hTSPCs) orientation and morphology: Well-orientated stem cells in an aligned nano-fibre matrix at week 6 shown by H&E (hematoxylin and eosin) staining in (A) and Masson (Masson trichrome) staining in (B); random orientation of cells on a non-aligned (random) nano-fibre matrix shown by H&E staining in (C) and Massion staining in (D); (E) stretched CFDA-stained hTSPCs on the aligned nano-fibres in (E); and spread-like morphology of hTSPCs on the randomly-oriented matrix in (F). Scale bars : 20 µm (A-D) and 50 µm (E&F) – (Reprinted from (55) with permission)

2.4.1.1.3 PLGA

PLGA is a biocompatible and biodegradable linear copolymer that can be prepared at different ratios between its constituent monomers lactic and glycolic acid. PLGA offers superior control on its degradation by varying the ratio between its monomers (56). PLGA nano-fibrous matrices have been used to culture MSCs and ESCs (57,58).

PLGA nano-fibres promote stem cell attachment and growth compared to 2D culture systems.

MSCs were seeded onto PLGA nano-fibres and supplemented with normal medium (without any differentiating supplements) for 14 days. Live/dead assays showed stem cells remained viable after 2 weeks. Progressive cell numbers in a DNA quantification assay revealed the ability of PLGA nano-fibres to accommodate stem cell proliferation (59,60). SEM and confocal images suggested that MSCs were attached to nano-fibres but they have the same elongated shape after 14 days as that in 2D culture. These stem cells retained their ability to differentiate into chondrogenic or osteogenic lineage after 7 and 14 days indicated by histological staining (61).

Hybrid nano-micro-fibrous PLGA matrices were compared to knitted micro-fibrous PLGA. Hybrid nano-micro-fibrous matrices were prepared by electrospinning PLGA nano-fibres onto the surfaces of the knitted matrices. MSC seeding efficacy was slightly higher for knitted matrices and cell attachment was comparable. However cell proliferation was faster for hybrid matrices as cell population increased by 92% between days 2 to 7, while 21% for knitted matrices (62). More morphological structures of PLGA matrices have been examined for cell attachment, including nano-fibrous, micro-fibres, aligned micro-fibres and PLGA films. The C-17.2 NSCs were attached more on the surface of PLGA nano-fibrous matrices (63).

PLGA nano-fibrous matrices have also been explored for culturing bone marrow-derived hematopoietic stem cells (BM-HSCs). BM-HSCs are conventionally cultured in suspension special spinner flasks or stirred bioreactors since their non-adherent property. Therefore, due to the lack of close cell–cell and cell–matrix interaction, this culture system could not maintain cell localization to specific environment (64). Electrospinning

technique was employed for fabricating nano-fibre matrices with PLGA blended with collagen type I. The matrices were further coated with E-selectin, a critical adhesive biomolecule. BM-HSC capture efficiency significantly increased from 23.40% to 67.41% within 30 min and from 29.44% to 70.19% within 60 min of incubation at room temperature after blended nano-fibre matrices were coated with E-selectin (65).

2.4.1.1.4 Other synthetic polymers

Other synthetic polymers have also been explored for stem cell expansion. Polyurethane (PU) nano-fibres have been fabricated and integrated into the microfluidic chips to mimic vascularised tissues embedded in ECM nano-fibres due to their strong mechanical properties. MSCs attached and expanded on PU nano-fibres. The cell adhesion and proliferation was further enhanced by acrylic acid grafting to PU nano-fibres to decrease the PU surface hydrophobicity (66). However, non-biodegradability is a big obstacle to use PU in tissue engineering.

3D nano-fibrillar organization of polyamide nano-fibres resembles the ECM/basement membrane. Proliferation and self-renewal of mouse ESCs on this nano-fibrillar surface were greatly enhanced in comparison with tissue culture surfaces without nano-fibres. In addition, stem cells cultured on the 3D nano-fibrillar surface maintained their differentiation ability in the presence of differentiating factors (67).

Surface-aminated polyethersulfone (PES) nano-fibres were found to enhance the expansion rate of hematopoietic stem/progenitor cells (HSPCs) from human umbilical cord blood. HSPCs are multipotent cells which can proliferate and differentiate into all blood cell types 1 and 2. However, achievable HSPCs from umbilical cords are very low because of the small volume of blood and it restrains direct transplantation of HSPCs to patients. PES nano-fibres have been demonstrated to be one approach to expand HSPCs. SEM images revealed that cell colonies were formed on nano-fibres (68) and the chain length of the grafted amines have an impact on the proliferation rate of HPSCs (69).

2.4.1.1.5 Natural polymers

Natural polymers contain essential components of natural ECM and they have been fabricated into nano-fibres for culturing stem cells. For example, collagen is found in abundance in natural ECMs. Type I collagen nano-fibres by electrospin technology have been prepared for examining the morphology, growth, adhesion, cell motility, and osteogenic differentiation of human bone marrow-derived MSCs. MSCs grown on 500 – 1,000 nm nano-fibres showed significantly higher cell viability than 2D surface (70). Silk is another popular natural polymer to synthesize nano-fibres. Silk nano-fibrous mats with fibroin diameter 700±50 nm were found to support extensive MSC proliferation and matrix coverage (71,72).

2.4.1.1.6 Copolymers / blends

Great efforts have been made to modify the polymeric nano-fibres using copolymer electrospinning or blending with other polymeric materials in order to improve processability of polymers for nano-fibre manufacturing, to resemble the natural ECM as much as possible, and to promote the stem cell interactions with matrices.

Aligned poly (L-lactic-*co*-*ε*-caprolactone) [P (LLA-CL)] co-polymer nano-fibres were electrospun for growth of human coronary artery smooth muscle cells (SMCs). Cells adhesion to the copolymer nano-fibres was quite similar to 2D surface while SMCs proliferation rate on nano-fibrous matrices was 2 times faster than 2D surface in 7 days (73). Poly (ethylene oxide terephthalate)–poly (butylene terephthalate) (PEOT/PBT) nano-fibres were also explored for culturing stem cells due to their adjustable surface energies (74). Higher surface energy (hydrophilic) material leads to a higher cell attachment with a spread out and spindle-like shape and a lower surface energy (hydrophobic) material results in lower attached cells and a rounded morphology (75,76). Recently Moroni et al. found that nano-porous PEOT/PBT micro-fibres promoted MSC spread, attachment and proliferation, while smooth micro-fibres without nano-pores led to rounded aggregated cells (77).

Blending nano-fibres with different polymer supports can form a 3D network and help cell migration. An aligned nano-fibrous mesh essentially behaves as a 2D sheet on which cells can only migrate along the surface, rather than a 3D matrix in which cells are capable of infiltration. To overcome this problem, a novel 3D unwoven macro-porous nano-fibrous (MNF) matrix was manufactured from PLLA and PCL (w/w 9:1) using an electrospinning-based yarn assembly technique. Human MSCs derived from ESCs were seeded onto the MNF matrix and a much higher cell proliferation was observed (78).

Blending with natural polymers is another attractive strategy to mimic natural ECM. Stem cell responses to the blending matrices have been extensively studied through a hybrid nano and micro-fibrous matrices produced by blending starch and PCL (30/70 wt %). Micro-fibres were impregnated, as much as possible, with electrospun nano-fibres. Bone marrow MSCs growing on the hybrid matrices presented a different morphology being able to bridge between micro-fibres. Cells along the nano-fibres showed a much-stretched morphology. When the cells stretch themselves, the receptors are stretched and activated as well which leads to gene expressions different from un-stretched cells. Increasing metabolic activity and proliferation rates were seen for cells on hybrid matrices. When the diameter of the fibres is lower than the cells, they can adhere well around the fibres and organize themselves. In addition, filling large spaces of the micro-fibre meshes with nano-fibres will results in higher cell seeding efficiency because they could retain more cells inside the structure (79).

2.4.1.1.7 Self-assembled peptides

Self-assembly is to fabricate nano-fibres through weak non-covalent interactions from small molecules, proteins, peptides, and nucleic acids (34). Several peptides such as short fibrillizing peptides, β-hairpins, peptide-amphiphiles, and peptide derivatives self-assemble to form networks of β-sheet-rich nano-fibres which further merge to build supra-molecular hydrogel architectures for tissue engineering application.

For example, the peptide RADA16-I (AcN-RADARADARADARADA-CONH2) which is an alternating 16-residue peptide with basic arginine, hydrophobic alanine and aspartic acid, can undergo spontaneous assembly into well-ordered interwoven nano-fibres in water

and rapidly form hydrogels with ~10 nm fibre diameter, 5–200 nm pore size and >99% water content under physiological conditions, which is similar to the structure of natural ECM. This mild cross-linking chemistry allows yielding viable encapsulated cells for 3-D culture. This self-assembled peptide and its several different functional motifs with other short peptide sequences have been used as well-defined microenvironment for stem cells. Mouse ESCs encapsulated in RAD16 showed undifferentiated stem cell maintenance (80). Functionalizing peptide mixtures RAD /SKP (Ac-(RADA)4GGSKPPGTSS-CONH2), RAD/FHR (Ac-(RADA)4GGFHRRIKA-CONH2) and RAD/PRGD (Ac-(RADA)4GPRGDSGYRGDS-CONH2) onto 3-D matrices have been demonstrated to control human adipose stem cell (hASC) behaviours *in vitro* (81). Modified RADA16 with Bone Marrow Homing Peptides (BMHPs) has also been successfully applied to NSCs (82). Multidomain peptides (MDPs) are a type of amphiphilic self-assembling peptides with a modular ABA block design in which the amphiphilic B block drives self-assembly while the side A blocks, which are electrostatically charged, control the conditions of assembly procedure. Galler et al. synthesized a range of multidomain peptides for fabricating nano-fibres. The peptides were modified with enzymatic cleavage and supplement of cell adhesion motifs (RGD). Combination of these items came to an increase in MSC viability and proliferation and encouraged cell migration within the matrix (83).

Peptide-amphiphiles (PAs) are oligo-peptides including a hydrophobic N-terminal alkyl tail, a β-sheet-forming segment in the middle, and a hydrophilic C-terminal functional segment for increasing cell adhesion. (38). These molecules generally self-assemble into high aspect ratio rods/cylinders with a hydrophobic core and a hydrophilic region on the exterior of the fibre for cell interaction. The exterior region can be tailored to provoke desired chemical and biological responses, such as cell adhesive ligands and cell-mediated degradable sites to control cellular behaviours (84). MSCs (85-87) and NSCs (84) have been incorporated into the PA nano-fibres for proliferation and differentiation.

2.4.1.2 Nano-composites

Although nano-fibres have gained wide applications to support attachment and proliferation of stem cells, macro-porous structure and weak mechanical property are key limiting factors for specific tissue regeneration. The nano-fibres can be blended with nanoparticles, nano-rods, nano-tubes, and micro-fibres to form nano-composites. Examples of these materials described here and have been summarized in table 2-2. The nano-composites in the biological tissues provide a guideline for fabricating the nano-composite matrices for tissue engineering. For example, bone tissue is composed of rigid hydroxyapatite (HAp) nano-crystals (tens of nano-meters in length and width, 2-3 nm in depth) precipitated into collagen fibres (50-70 nm in diameter). HAp crystals are one of the main constituents of bone tissues to provide compressive strength. To manufacture nano-composites including HAp and nano-fibres, Chen et al. prepared HAp nano-rods with an average diameter of ~7 nm and length of ~27 nm and then the nano-rods were blending with poly (vinyl pyrolidone) (PVP) to form composite nano-fibres by electrospinning. MSCs were attached well to the HAp fabric substrates after culture for 24 h (88). The same approach has been used to electrospin aligned nano-fibrous PCL/PLLA/nHAp (nano-hydroxyapatite) composites and human unrestricted somatic stem cells (USSCs) were seeded into the nano-composites. Results showed that stem cells were viable in the matrices (89). However, higher HAp content in the poly (3-hydroxybutyrate-co-3-hydroxyvalerate) (PHBV)/HAp nano-composites decreased MSC proliferation rate (90), while a blend of PLGA, collagen and HAp nanoparticles was electrospun for fabricating nano-fibres which supported MSC adhesion and spreading (91). Composites consisting of nanoparticles of 20% Hap and 80% β-tricalcium phosphate (TCP) and PCL were fabricated to demonstrate cell proliferation was inversely proportional to the nano-fibre roughness (92).

Multi-walled carbon nano-tubes (MWNTs) have also been explored to form nano-composites. MWNTs were encapsulated into PLLA nano-fibres to provide three specific enhancements to fibrous tissue matrices: modified fibre size, electrical conductivity, and increased mechanical strength. Adipose-derived human MSCs were integrated into the PLA nano-fibres with 1 wt% MWNT and were viable after day 14. The proliferation rate

of the hMSCs increased drastically by day 14 and MWNTs in the nano-composites promoted MSC proliferation (93).

Except from nano-fibrous nano-composites, nano-composites can also be made from incorporation of nanoparticles or nano-fibres into micro-porous hydrogels or macro-porous sponges. The thixotropic polyethylene glycol (PEG)–silica gel was prepared by combining multi-arm PEG with hydrolysed tetraethoxysilane (TEOS). The viscosity of thixotropic nano-composites decreases under stress and returns to their original situation after stress removal. Good nutrients delivery and gases through the matrix improved MSCs proliferation and viability over three weeks (94).

Electronspun nano-fibres can also serve as fillers in the macro-porous structure to form new type of nano-composites. Poly (glycolic acid) (PGA) nano-fibres were formed as a sheet and added as a layer within the collagen sponge. The sheets noticeably improved the compressive strength of the collagen sponge. More cardiac stem cells (CSCs) were adhered to the collagen sponge with PGA nano-fibres than that sponge alone. Nano-fibres promoted the cell proliferation as well (95).

2.4.1.3 Surface-modified nano-structures

Introducing nano-featured elements such as nano-tubes or ultrathin layers on the surfaces or modifying their topography using nano-patterning techniques are other applications of nanotechnology in stem cell 3-D culture (Table 2-2).

Nano-patterned surfaces with different topographies can be achieved through synthesis methods or introduction of nano-structures to the surfaces. For example, di-block copolymers of polystyrene and poly-2-vinylpyrindine or poly-4-vinylpyrindine formed dot-like (6 nm) or wormlike (3 nm) surface nano-topography, respectively, via controlled microphase separation. The worm-like surfaces supported greater human mesenchymal progenitor cell proliferation. More elongated cells and thicker ECM deposits were found on the worm-like surfaces (96).

Nano-topography of the surfaces can be changed by coating nano-materials onto the surfaces. Nano-tubes on the matrix surface improved cellular tracking, sensing of

microenvironments, delivering of transfection agents along with scaffold enhancement (97). Carbon nano-tubes provided the needed structural reinforcement for tissue scaffolding (98-101) and mimicked some ECM fibres (102). Nano-tubes were placed in an array to simulate neural networks (103) and high electrical conductivity of carbon nano-tubes was be beneficial for directing cell growth (104). Carbon nano-tubes can also be functionalized to release bioactive factors. It has been shown that such factors, for example glucose oxidase, can be attached to nano-tubes without losing the enzymatic activity (105).

Titanium oxide nano-tubes are also demonstrated to affect human MSC behaviours. Dramatic change in MSC responses was found to when they were exposed to various ranges of nano-tube dimensions. Small (~30 nm diameter) nano-tubes enhanced attachment without noticeable differentiation, while larger (~70- 100 nm diameter) nano-tubes stimulated a dramatic stem cell elongation (~10 fold increase), which generated cytoskeletal stress and resulted in differentiation of MSCs into osteoblast-like cells (106).

The surface properties such as wettability can be tuned through surface modification. Introducing a thin layer of thermoresponsive polymers, poly(N-isopropylacrylamide) (PNIPAAm), imparts tuneable hydrophobic/hydrophilic characteristics to the surface which could be interchanged by temperature (107). The thickness of the layer was found to play an important role in cell adhesion. The optimum thickness of the polymer on the surface was determined to be 15 nm. Beyond this thickness, the hydrophobic environments in its vicinity no longer promoted the dehydration and shrinkage of the PNIPAAm chains and were no longer suitable for cell adhesion (108,109).

Table 2-2- Nano-composites and surface modified nano-structures for stem cells expansion

Category	Nanomaterial	Stem Cell	Significance/Result (s)	Reference
Nano-composites	HAp[a] nanorods/PVP[b] nano-fibre composite	MSC[c]	Nano-rods in nano-fibres - cells were attached	(88)
	PCL[d]/PLLA[e]/nHAp[f] nano-fibres composite	SSC[g]	nanoparticles in nano-fibres - not cytotoxic	(89)
	PHBV[h]/nHAp nano-fibre composite	MSC	nanoparticles in nano-fibres- proliferation lower than PHBV nano-fibres	(90)
	PLGA[i]/Collagen/nHAp nano-fibre composite	MSC	nanoparticles in nano-fibres - good adhesion and spreading	(91)
	PCL/nHAp/TCP[j] nano-fibre composite	MSC	nanoparticles in nano-fibres - cell proliferation is inversely proportional to nano-fibre roughness	(92)
	PEG[k]/Silica nanoparticles	MSC	nanoparticles in gel- cells are alive and good proliferation	(94)
	muti-welled carbon nano-tubes in PLLA	MSC	Nano-tube in nano-fibre - cells are alive, attached and proliferation is higher -make conductive fibres	(93)
	PGA[l] nano-fibre sheet/Collagen	CSC[m]	Nano-sheet in sponge - enhanced cell attachment and proliferation	(95)
Surface-modified nano-structures	titanium oxide nano-tube	MSC	Nano-tubes on surface - promote cell adhesion and proliferation without differentiation	(106)
	(PS-b-P2VP)/(PS-b-P4VP) [n]nano-patterned surface	MSC	Nano-patterned surface - effect of nano-topography	(96)
	nanolayer of PNIPAAm[o]	–	Nano-scale layer on surface - optimum cell adhesion and detachment depends on thickness of layer	(108)

a: Hydroxyapatite , b: poly (vinyl pyrolidone) , c: Mesenchymal Stem Cell , d: Poly (ε -caprolactone) , e: Poly (L-lactic acid) , f: nano-Hydroxyapatite , g: Somatic Stem Cell , h: poly (3-hydroxybutyrate-co-3-hydroxyvalerate) , i: Poly (D, L-lactide-co-glycolide) , j: β -tricalcium phosphate , k: poly (ethylene glycol) , l: Poly (glycolic acid) , m: Carcinoma Stem Cell , n: poly(styrene)-block-poly(2-vinylpyrindine) diblock copolymer / poly(styrene)-block-poly(4-vinylpyrindine) diblock copolymer , o: poly(N-isopropylacrylamide)

2.5 Matrices for cartilage tissue engineering

After stem cells are proliferated to reach a high cell density, stem cells are then differentiated into chondrocytes for generating neocartilage in an appropriate microenvironment. Matrices are the important component for such a microenvironment. Among the general aforementioned requirements of matrices, other features of matrices are also required in cartilage tissue engineering. It has been demonstrated that culturing the chondrocyte cells in a 2D culture may lead to phenotype transition of cells to fibroblast tissues and they will not be able to produce cartilage ECM (111). This phenomenon is lessened in a 3D environment and matrices should provide chondrocytes with such a suitable 3D microenvironment. From clinical point of view, the matrices should be integrated into the host tissue and fill the defect site properly with minimal invasive implantation procedure.

Potential biomaterials as matrices or scaffolds include metals, ceramics or polymers. Metals and ceramics are less attractive because they are not biodegradable and their processability is very limited (112). Therefore, polymers are the most appealing. They can be divided into two major categories: natural and synthetic polymers.

Natural polymers consist of decellularized ECM (small intestinal submucosa (SIS), dermis, and urinary bladder matrix); purified ECM components (collagen, elastin, gelatin, fibrin, keratin, hyalorunan, sulphated GAGs); other natural polymers (silk, chitin, chitosan, alginate, agarose, carrageenan, starch, cellulose, soy protein, pectin); and polyhydroxyalkanoates (PHA) (9, 113-115). These polymers except PHA belong to either proteins or polysaccharides. This group of polymers usually provides good immune and biological recognition, embedded structural and functional molecules, suitable surface chemistry for cell attachment, growth and differentiation (116). For example, decellularized ECM is composed of many structural proteins and bioactive factors. However, these polymers suffer from non-controllable degradation rate, potential to provoke immune responses (116), pathogen transmissions (9), batch-to-batch variations, poor mechanical properties and insolubility in physiological conditions such as collagen and chitin (112).

On the other hand, synthetic polymers are prepared artificially from synthetic or natural monomers and building blocks. The most common synthetic polymers are polyglycolide acid (PGA), polylactide acid (PLA), poly lactide-co-glycolide acid (PLGA), poly(ethylene glycol) (PEG), poly(hydroxyl butyrate) (PHB), polycaprolactones (PCL), polyorthoesters, polyanhydrides, poly(vinyl alcohol) (PVA), poly(amido-amine)s (PAAs), polycarbonates, poly(fumarate)s, poly(urethane)s (PU), poly(phosphazene)s, poly(glycerol sebacate) (PGS), peptide-based, and DNA-based (9, 114, 117, 118). Synthetic polymers can be chemically synthesized at large scales with reproducible and predictable properties. The mechanical and degradation properties of synthetic polymers can be tailored by co-polymerization, blending and controlling the molecular weight of these polymers (9). Less immune response is another advantage of synthetic polymers (114). Most synthetic polymers are degraded through chemical hydrolysis, rather than enzymatic, leading to less patient-to-patient variations (112). Although synthetic materials expand scaffold design capabilities, they do not have an intrinsic mechanism of cell-matrix interactions. The polymer or its degradation products might be toxic or stimulate inflammatory responses (9, 114). Synthetic polymers have been modified to improve their bioactivity. For example, incorporation of cell adhesive peptides such as RGD elicited to enhance cell attachment properties. Peptides sensitive to cleavage by enzymes such as metalloproteinases and plasmin have also been introduced to the structure of polymers, in order to regulate their degradability rate (4, 8, 9).

Matrices have been used for cartilage scaffolds in the forms of sponge, fibrous meshes and hydrogels (119). As cartilage contains 80% interstitial fluid, hydrogels are considred to be appropriate in mimicking the hydrated structure in cartilages. Various hydrogels in cartilage tissue engineering are reviewed. Then the review was narrowed to thermoresponsive hydrogels followed by chitosan-based thermoresponsive hydrogels in which I will use in my thesis.

2.5.1 Hydrogels

Hydrogels are three-dimensional networks, made from cross-linked polymer chains. The hydrophilic structure of hydrogels exhibits outstanding swelling behaviour in the presence

of water (120). Cross-linking might be through chemical bonds or physical interactions (121). Hydrogels have received a lot of attention in tissue engineering due to their ability to fill the defect site, excellent nutrient transfer, high cell seeding efficiency, homogeneous cell distribution, and easy modification with cell adhesion ligands, good biocompatibility, low interfacial tension, and minimal mechanical and frictional irritation (122). Various scaffold forms have been used in 3D cell expansion and tissue engineering based on the tissue type and their requirements. Many of them have been examined for cartilage regeneration as well. Among them, hydrogels are one of the most suitable scaffolds for 3D chondrogenic differentiation of stem cells in cartilage tissue engineering due to their similarity to the natural ECM of cartilages which is highly hydrated tissue (over 80% of ECM is water) (123). Various biomaterials have been used to form hydrogels as a scaffold for cartilages, including fibrin, agarose, alginate, collagen, chitosan, hyaluronan and self-assembling peptides as naturally derived hydrogels and PVA, PEG, and oligo (poly(ethylene glycol) fumarate) (OPF) as synthesized hydrogels (124, 125). Of all hydrogels, stimuli-responsive hydrogels are more attractive due to their capbility for good cell distribution, injectability and bioactive molecules release. This hydrogel exhibits dramatic changes in their swelling behavior, network structure and/or mechanical characteristics in response to various environmental stimuli (126). A class of these smart materials converts from solution to gel during a process called sol-gel transition (121), which might be reversible or irreversible, based on the nature of cross-linking. The stimuli-responsiveness occurs in response to environment stimuli in a controllable and predictable manner such as temperature, pH, ionic strength, light, and magnetism, electrical or mechanical stimulus (158,127-129). Stimuli-responsive hydrogels with sol-gel transition behaviour can be used as injectable matrices for minimally invasive procedures in cartilage tissue engineering. In this approach, cell and polymer solution are mixed well and administered easily to the defective site by a syringe (e.g. knee cartilage). The polymer solution becomes gel within the cavity in response to a physiological stimulus such as temperature. It provides a 3D microenvironment for cells to regenerate cartilage. In addition, essential bioactive molecules such as growth factors can be encapsulated in

scaffolds. Then the bioactive molecule is released by stimulus and delivered to cells in a sustained manner.

2.5.2 Thermoresponsive hydrogels

Thermo-responsive or thermoresponsive polymers exhibit a response such as gelation, phase separation or shrinkage due to a change in temperature. For polymer solutions, if the gelation or phase separation happens above a temperature upon heating, the threshold is lower critical solution temperature (LCST), while if the gelation or phase separation takes place below a certain temperature upon cooling, the polymer has an upper critical solution temperature (UCST) (130). In case of cross-linked hydrogels, the system may swell or collapse at the transition temperature which is called volume phase transition temperature (VPTT) (131). Some natural polymers such as cellulose derivatives, gelatin, agarose, amylase, amylopectin, xyloglucan, carrgeenans, gellans (132) and chitosan associated with polyol salts (133) showed thermo-responsiveness. Moreover, poly(N-Isopropylacrylamide) (PNIPAAm), poly (ethylene oxide) / poly(propylene oxide) block copolymers (or Pluronic or poloxamers), PEG/biodegradable polyester block copolymers(130,134), and other combinations of PEG as the hydrophilic moiety with polymers can result in thermo-responsiveness (135). For instance, PEG grafted poly(phosphazenes) (136) and chitosan (137) have been reported as thermoresponsive biomaterials. In addition, poly (1,2-propylene phosphate) in the presence of calcium ion forms a temperature-sensitive hydrogel (138).

Thermoresponsive hydrogels are gaining interests for cartilage regeneration because they can be injected in the liquid form at room temperature and then they are converted into the gel form at the body temperature. Therefore, the hydrogels can avoid heavy surgical procedures for implants and they are minimally invasive. However, their lack of mechanical strength has not been completely solved yet (139).

2.5.3 Chitosan-based thermoresponsive hydrogels

Chitosan is an aminopolysccharide consisting of β (1 → 4) linked glucosamine with randomly located N-acetyl-glucosamine groups derived from alkaline deacetylation of chitin (140). The percentage of deacetylation is termed as degree of deacetylation (DDA). Chitin is one of the main components of fungal cell walls and exoskeletons of arthropods such as shrimps and crabs. Depending on the source of the chitin and preparation process, molecular weight of the product chitosan can vary between 50 to 1000 kDa with a DDA of 30% to 95%. Chitosan is considered as a pH-sensitive material because it is insoluble in aqueous solutions above pH 7 due to its stability and crystalline structure, but it is soluble in acidic solutions under pH 6 through protonation of the amino groups leading to a decrease in its crystallinity. It has been rated as a fascinating candidate for biomedical applications including tissue engineering because of its unique properties such as excellent biocompatibility, tunable biodegradability, cell adhesion ability (141,142), antimicrobial (143,144), wound healing (145), physiological inertness, remarkable affinity to proteins, haemostatic, antitumoral and anticholesteremic properties. In addition, chitosan structure is quite similar to some ECM components such as glycosaminoglycans (GAGs). Chitosan is degradable *in vivo* by enzymatic hydrolysis and the degradation rate is tunable by its DDA. Highly deacetylated chitosan presents a higher crystallinity and thus a lower degradation rate. Its antibacterial properties come from attaching its cationic amino groups to the anions on bacterial cell wall, which leads to suppressing biosynthesis, and disrupting the mass transport across the wall of the bacteria which causes the bacteria cell death. Chitosan also exhibits wound healing properties because chitosan and some of its degraded products could be involved in the synthesis of extracellular matrix components such as chondroitin, chondroitin sulphate, dermatane-sulphate, keratan-sulphate and hyaluronic acid. Furthermore, as a natural polymer, its renewable source makes it an attractive choice for medical applications. Its ability to form porous scaffolds by freezing, lyophilizing and internal bubbling is another advantage of chitosan. Chitosan is a cationic pH-dependent polymer that makes it a significant polycation to prepare insoluble ionic complexes with biological polyanions such as GAGs, PGs and DNA. The charge density of these complexes is pH-dependent. Negatively charged polymers can be partially released in physiological pH. This property becomes more important when some cytokines/growth

factors are bounded and modulated by GAGs including heparin and heparin sulphate. Mechanical, physical and chemical properties of chitosan can be easily modified by side group attachment through reactions with amino groups as well as primary and secondary hydroxyl groups. Poor mechanical properties and insolubility at physiological pH (146) can be improved by grafting with other synthetic or natural materials.

Chitosan-based thermoresponsive hydrogels have promising applications in cartilage tissue engineering. Chitosan is not a thermoresponsive hydrogel by itself but it is possible to make it thermoresponsive, in association with other chemicals or by grafting with other polymers.

Cho et al. prepared poly(N-isopropylacrylamide) and chitosan copolymer as a scaffold for chondrogenic differentiation of MSCs (154). PNIPAAm is well known for its phase transition behaviour with LCST of 32 – 33 ºC that makes it an attractive material in bioengineering and biotechnology. This transition occurs as a result of the H-bonding forces between amide-water and amide-amide groups. Homopolymer of NIPAAm has no functional groups to form chemically incorporated bioconjugate with other biomacromolecules. Therefore, it is usually used as a copolymer with other polymers (148). Gene expression as well as histological and immunohistochemical studies on PNIPAAm-grafted chitosan indicated encouraging results (154). However, more biochemical assays need to be conducted to verify the results.

Chitosan/β-glycerol phosphate (β-GP) was also used as a thermoresponsive injectable scaffold for cartilage repair (147,150). In another work, chitosan–pluronic was prepared as a thermoresponsive hydrogel to improve stability, mechanical strength and biocompatibility for cartilage tissue engineering (139). Dang et al. demonstrated that hydroxybutyl chitosan was soluble and thermoresponsive (151). It was nontoxic for MSCs, but it was not applied to cartilage regeneration. PEG grafted chitosan was reported as a water soluble thermoresponsive hydrogel when an appropriate amount of PEG was used (152). However, its suitability for cartilage tissue engineering has not been yet determined. Chitosan / carboxymethyl cellulose (CMC) complex was assumed to be appropriate for tissue engineering due to its polyelectrolyte properties. Chitosan is a polycation and CMC is a weak polyanion. The complex revealed thermo-responsiveness at physiological pH.

Morphological examinations of the cultured chondrocytes and *in vivo* evaluations showed that this complex can be potentially used as a scaffold for cartilage regeneration (153). However cartilage specific ECM formation needs to be confirmed.

2.6 Cells for cartilage tissue engineering

Various cell types and sources have been exploited for cartilage tissue engineering. Cells can be isolated from the same tissue of the patient (autologous) or another person (allogenic) or another animal (xenogenic). Chondrocytes (adult, neonatal or fetal) as cartilage-specific differentiated cells have been extensively utilized. Multipotent stem cells such as umbilical cord blood stem cells or adult stem cells including mesenchymal stem cells (MSCs), adipose-derived stem cells (ADSCs) and synovial-derived stem cells (SDSCs) are another category of cells with chondrogenic capabilities. Embryonic stem cells (ESCs) and induced pluripotent stem cells (iPSCs) have been also reported as pluripotent stem cells for cartilage regeneration (149). MSCs are considered as an attractive candidate for cartilage tissue engineering because of their ease of isolation, *in vitro* expansion, high proliferation rate and strong chondrogenic differentiation potential (149,155). These cells easily expand in monolayer culture and have the ability to differentiate into various cell types, including chondrocytes. Moreover, they have the potential to deposit extracellular matrix with properties mimicking closely the healthy hyaline joint cartilage. Besides, they can differentiate into multiple lineages including osteoblasts, adipocytes and fibroblasts. MSCs can be isolated from bone marrow, adipose, skin, cord blood, and articular cartilage and MSCs from each source may have different advantages and disadvantages (156).

2.7 Conclusions

Graft copolymer of chitosan and PNIPAAm showed promising preliminary results as a thermoresponsive hydrogel for cartilage tissue engineering (154). However, its solution and gel properties need to be manipulated for desired applications. Synthesis conditions

can be optimized to control the properties. In addition, the zonal structure of the engineered cartilage as one of the essential requirements has not been met. Finding a way to use thermoresponsive hydrogels along with microengineering technologies might be a solution. On the other hand, non-grafted chitosan/PNIPAAm hybrid scaffolds could be another potential alternative to enhance cell proliferation and chondrogenic differentiation. In that case, the possible influence of PNIPAAm molecular weight on cytotoxicity of the matrix needs to be determined. In this thesis, we will try to address these gaps and examine the hypotheses by designing various experiments and assays.

2.8 References

1. Cartilage. In: Cowin SC, Doty SB, editors. Tissue Mechanics: Springer New York; 2007. p. 471-505.

2. Flik KR, Verma N, Cole BJ, Bach BR. Articular Cartilage-Structure, Biology, and Function. In: Williams RJ, editor. Cartilage Repair Strategies: Humana Press; 2007. p. 1-12.

3. Mow VC, Wang CC-B. Some Bioengineering Considerations for Tissue Engineering of Articular Cartilage. Clinical Orthopaedics and Related Research. 1999;367:S204-S23.

4. Zhang Z, Gupte MJ, Ma PX. Biomaterials and stem cells for tissue engineering. Expert opinion on biological therapy. 2013;13(4):527-40.

5. Kock L, van Donkelaar CC, Ito K. Tissue engineering of functional articular cartilage: the current status. Cell and Tissue Research. 2012;347(3):613-27.

6. Frenkel SR, Di Cesare PE. Scaffolds for Articular Cartilage Repair. Annals of Biomedical Engineering. 2004;32(1):26-34.

7. Butler DL, Goldstein SA, Guldberg RE, Guo XE, Kamm R, Laurencin CT, et al. The Impact of Biomechanics in Tissue Engineering and Regenerative Medicine. TISSUE ENGINEERING: Part B. 2009;15(4):477-84.

8. Keane TJ, Badylak SF, editors. Biomaterials for tissue engineering applications. Seminars in Pediatric Surgery; 2014: Elsevier.

9. Chan G, Mooney DJ. New materials for tissue engineering: towards greater control over the biological response. Trends in biotechnology. 2008;26(7):382-92.

10. Goldberg M, Langer R, Jia X. Nanostructured materials for applications in drug delivery and tissue engineering. Journal of Biomaterials Science, Polymer Edition. 2007;18(3):241-68.

11. Ramalingam M, Jabbari E, Ramakrishna S, Khademhosseini A. Micro and Nanotechnologies in Engineering Stem Cells and Tissues: John Wiley & Sons; 2013.

12. Sun T, Norton D, Vickers N, L McArthur S, Neil SM, Ryan AJ, et al. Development of a bioreactor for evaluating novel nerve conduits. Biotechnol Bioeng. 2008;99(5):1250-60.

13. Sun T, Mai S, Norton D, Haycock JW, Ryan AJ, Macneil S. Self-organization of skin cells in three-dimensional electrospun polystyrene scaffolds. Tissue Eng. 2005;11(7-8):1023-33.

14. Blackwood KA, McKean R, Canton I, Freeman CO, Franklin KL, Cole D, et al. Development of biodegradable electrospun scaffolds for dermal replacement. Biomaterials. 2008;29(21):3091-104.

15. Haycock JW. 3D cell culture: a review of current approaches and techniques. 3D Cell Culture: Springer; 2011. p. 1-15.

16. Lee J, Cuddihy MJ, Kotov NA. Three-dimensional cell culture matrices: state of the art. Tissue Engineering Part B: Reviews. 2008;14(1):61-86.

17. Hutmacher DW, Schantz T, Zein I, Ng KW, Teoh SH, Tan KC. Mechanical properties and cell cultural response of polycaprolactone scaffolds designed and fabricated via fused deposition modeling. J Biomed Mater Res. 2001;55(2):203-16.

18. Woodfield TBF, Malda J, de Wijn J, Peters F, Riesle J, van Blitterswijk CA. Design of porous scaffolds for cartilage tissue engineering using a three-dimensional fiber-deposition technique. Biomaterials. 2004;25(18):4149-61.

19. Andersson H, Van Den Berg A. Microfabrication and microfluidics for tissue engineering: state of the art and future opportunities. Lab Chip. 2004;4(2):98-103.

20. Khademhosseini A, Langer R, Borenstein J, Vacanti JP. Microscale technologies for tissue engineering and biology. Proceedings of the National Academy of Sciences of the United States of America. 2006;103(8):2480-7.

21. Khademhosseini A, Langer R. Microengineered hydrogels for tissue engineering. Biomaterials. 2007;28(34):5087-92.

22. Borenstein J, Terai H, King K, Weinberg EJ, Kaazempur-Mofrad MR, Vacanti JP. Microfabrication Technology for Vascularized Tissue Engineering. Biomedical Microdevices. 2002 2002/07/01;4(3):167-75.

23. Fidkowski C, Kaazempur-Mofrad MR, Borenstein J, Vacanti JP, Langer R, Wang Y. Endothelialized microvasculature based on a biodegradable elastomer. TISSUE ENGINEERING. 2005;11(1-2):302-9.

24. Ling Y, Rubin J, Deng Y, Huang C, Demirci U, Karp JM, et al. A cell-laden microfluidic hydrogel. Lab on a Chip. 2007;7(6):756-62.

25. Du Y, Ghodousi M, Qi H, Haas N, Xiao W, Khademhosseini A. Sequential assembly of cell-laden hydrogel constructs to engineer vascular-like microchannels. Biotechnology and Bioengineering. 2011;108(7):1693-703.

26. Du Y, Lo E, Ali S, Khademhosseini A. Directed assembly of cell-laden microgels for fabrication of 3D tissue constructs. Proceedings of the National Academy of Sciences. 2008 July 15, 2008;105(28):9522-7.

27. Annabi N, Nichol JW, Zhong X, Ji C, Koshy S, Khademhosseini A, et al. Controlling the porosity and microarchitecture of hydrogels for tissue engineering. Tissue Engineering Part B: Reviews. 2010;16(4):371-83.

28. Norman JJ, Desai TA. Methods for fabrication of nanoscale topography for tissue engineering scaffolds. Annals of Biomedical Engineering. 2006;34(1):89-101.

29. Popat KC, Leary Swan EE, Mukhatyar V, Chatvanichkul K-I, Mor GK, Grimes CA, et al. Influence of nanoporous alumina membranes on long-term osteoblast response. Biomaterials. 2005;26(22):4516-22.

30. Desai TA, West T, Cohen M, Boiarski T, Rampersaud A. Nanoporous microsystems for islet cell replacement. Advanced Drug Delivery Reviews. 2004;56(11):1661-73.

31. Almeida R, Gama A, Vueva Y. Bioactive sol–gel scaffolds with dual porosity for tissue engineering. Journal of sol-gel science and technology. 2011;57(3):336-42.

32. Jones JR, Ehrenfried LM, Hench LL. Optimising bioactive glass scaffolds for bone tissue engineering. Biomaterials. 2006;27(7):964-73.

33. A. Mellati and H. Zhang. Expansion of stem cells by nanotissue engineering, in Stem-cell nanoengineering (eds H. Baharvand and N. Aghdami), 2015, John Wiley & Sons Inc., Hoboken, NJ. DOI: 10.1002/9781118540640.ch14

34. Prakash S, Khan A, Paul A. Nanoscaffold based stem cell regeneration therapy: recent advancement and future potential. Expert Opinion on Biological Therapy. 2010;10(12):1649-61.

35. Zhang H, Dai S, Bi J, Liu K-K. Biomimetic three-dimensional microenvironment for controlling stem cell fate. Interface Focus. 2011;1(5):792-803.

37. Goldberg M, Langer R, Jia X. Nanostructured materials for applications in drug delivery and tissue engineering. J Biomater Sci Polym Ed. 2007;18(3):241-68.

39. Ruckh TT, Kumar K, Kipper MJ, Popat KC. Osteogenic differentiation of bone marrow stromal cells on poly(ε-caprolactone) nanofiber scaffolds. Acta Biomater. 2010;6(8):2949-59.

38. Dahlin RL, Kasper FK, Mikos AG. Polymeric nanofibers in tissue engineering. Tissue Engineering, Part B: Reviews. 2011;17(5):349-64.

40. Yoshimoto H, Shin YM, Terai H, Vacanti JP. A biodegradable nanofiber scaffold by electrospinning and its potential for bone tissue engineering. Biomaterials. 2003;24(12):2077-82.

41. Ghasemi-Mobarakeh L MM, Karbalaie K. The thickness of electrospun poly (e-caprolactone) nanofibrous scaffolds influences cell proliferation. nternational Journal of Artificial Organs. 2009;23(3):150-8.

42. Marletta G, Ciapetti G, Satriano C, Perut F, Salerno M, Baldini N. Improved osteogenic differentiation of human marrow stromal cells cultured on ion-induced chemically structured poly-ε-caprolactone. Biomaterials. 2007;28(6):1132-40.

43. Xie J, Willerth SM, Li X, Macewan MR, Rader A, Sakiyama-Elbert SE, et al. The differentiation of embryonic stem cells seeded on electrospun nanofibers into neural lineages. Biomaterials. 2009;30(3):354-62.

44. Hashemi SM, Soleimani M, Zargarian SS, Haddadi-Asl V, Ahmadbeigi N, Soudi S, et al. In vitro Differentiation of Human Cord Blood-Derived Unrestricted Somatic Stem Cells into Hepatocyte-Like Cells on Poly(ε-Caprolactone) Nanofiber Scaffolds. Cells Tissues Organs. 2009;190(3):135-49.

45. Pham QP, Sharma U, Mikos AG. Electrospun Poly(ε-caprolactone) Microfiber and Multilayer Nanofiber/Microfiber Scaffolds: Characterization of Scaffolds and Measurement of Cellular Infiltration. Biomacromolecules. 2006;7(10):2796-805.

46. Kim G, Son J, Park S, Kim W. Hybrid Process for Fabricating 3D Hierarchical Scaffolds Combining Rapid Prototyping and Electrospinning. Macromol Rapid Commun. 2008;29(19):1577-81.

47. Yoon H, Ahn S, Kim G. Three-Dimensional Polycaprolactone Hierarchical Scaffolds Supplemented with Natural Biomaterials to Enhance Mesenchymal Stem Cell Proliferation. Macromol Rapid Commun. 2009;30(19):1632-7.

48. Rasal RM, Janorkar AV, Hirt DE. Poly(lactic acid) modifications. Prog Polym Sci. 2010;35(3):338-56.

49. Yang F, Murugan R, Ramakrishna S, Wang X, Ma YX, Wang S. Fabrication of nano-structured porous PLLA scaffold intended for nerve tissue engineering. Biomaterials. 2004;25(10):1891-900.

50. Yang F, Xu CY, Kotaki M, Wang S, Ramakrishna S. Characterization of neural stem cells on electrospun poly(L-lactic acid) nanofibrous scaffold. J Biomater Sci Polym Ed. 2004;15(12):1483-97.

51. Yang F, Murugan R, Wang S, Ramakrishna S. Electrospinning of nano/micro scale poly(l-lactic acid) aligned fibers and their potential in neural tissue engineering. Biomaterials. 2005;26(15):2603-10.

52. Lampin M, Warocquier-Clérout R, Legris C, Degrange M, Sigot-Luizard MF. Correlation between substratum roughness and wettability, cell adhesion, and cell migration. J Biomed Mater Res. 1997;36(1):99-108.

53. Thapa A, Webster TJ, Haberstroh KM. Polymers with nano-dimensional surface features enhance bladder smooth muscle cell adhesion. Journal of Biomedical Materials Research Part A. 2003;67A(4):1374-83.

54. Shanmugasundaram S, Chaudhry H, Arinzeh TL. Microscale versus nanoscale scaffold architecture for mesenchymal stem cell chondrogenesis. Tissue Engineering Part A. 2010;17(5-6):831-40.

55. Yin Z, Chen X, Chen JL, Shen WL, Hieu Nguyen TM, Gao L, et al. The regulation of tendon stem cell differentiation by the alignment of nanofibers. Biomaterials. 2010;31(8):2163-75.

56. Lanao RPF, Jonker AM, Wolke JG, Jansen JA, van Hest JC, Leeuwenburgh SC. Physicochemical Properties and Applications of Poly (lactic-co-glycolic acid) for Use in Bone Regeneration. Tissue Engineering Part B: Reviews. 2013.

57. Massumi M, Abasi M, Babaloo H, Terraf P, Safi M, Saeed M, et al. The effect of topography on differentiation fates of matrigel-coated mouse embryonic stem cells cultured on PLGA nanofibrous scaffolds. Tissue Engineering Part A. 2011;18(5-6):609-20.

58. Meade KA, White KJ, Pickford CE, Holley RJ, Marson A, Tillotson D, et al. Immobilization of Heparan Sulfate on Electrospun Meshes to Support Embryonic Stem Cell Culture and Differentiation. J Biol Chem. 2013;288(8):5530-8.

59. Alhadlaq A, Mao JJ. Mesenchymal stem cells: isolation and therapeutics. Stem cells and development. 2004;13(4):436-48.

60. Parker GC, Anastassova-Kristeva M, Eisenberg LM, Rao MS, Williams MA, Sanberg PR, et al. Stem cells: shibboleths of development, part II: toward a functional definition. Stem cells and development. 2005;14(5):463-9.

61. Xin X, Hussain M, Mao JJ. Continuing differentiation of human mesenchymal stem cells and induced chondrogenic and osteogenic lineages in electrospun PLGA nanofiber scaffold. Biomaterials. 2007;28(2):316-25.

62. Goh JC-H. Characterization of a Novel Polymeric Scaffold for Potential Application in Tendon/Ligament Tissue Engineering. Tissue Eng. 2006;12(1):91-9.

63. Bini TB, Gao S, Wang S, Ramakrishna S. Poly(l-lactide-co-glycolide) biodegradable microfibers and electrospun nanofibers for nerve tissue engineering: an in vitro study. Journal of Materials Science. 2006;41(19):6453-9.

64. Cabrita GJ, Ferreira BS, Da Silva CL, Goncalves R, Almeida-Porada G, Cabral JM. Hematopoietic stem cells: from the bone to the bioreactor. Trends Biotechnol. 2003;21(5):233-40.

65. Ma K, Chan CK, Liao S, Hwang WYK, Feng Q, Ramakrishna S. Electrospun nanofiber scaffolds for rapid and rich capture of bone marrow-derived hematopoietic stem cells. Biomaterials. 2008;29(13):2096-103.

66. Lee KH, Kwon GH, Shin SJ, Baek JY, Han DK, Park Y, et al. Hydrophilic electrospun polyurethane nanofiber matrices for hMSC culture in a microfluidic cell chip. Journal of Biomedical Materials Research Part A. 2009;90(2):619-28.

67. Nur-E-Kamal A, Ahmed I, Kamal J, Schindler M, Meiners S. Three-Dimensional Nanofibrillar Surfaces Promote Self-Renewal in Mouse Embryonic Stem Cells. Stem Cells. 2006;24(2):426-33.

68. Chua K-N, Chai C, Lee P-C, Tang Y-N, Ramakrishna S, Leong KW, et al. Surface-aminated electrospun nanofibers enhance adhesion and expansion of human umbilical cord blood hematopoietic stem/progenitor cells. Biomaterials. 2006;27(36):6043-51.

69. Chua K-N, Chai C, Lee P-C, Ramakrishna S, Leong KW, Mao H-Q. Functional nanofiber scaffolds with different spacers modulate adhesion and expansion of cryopreserved umbilical cord blood hematopoietic stem/progenitor cells. Exp Hematol. 2007;35(5):771-81.

70. Shih YRV, Chen CN, Tsai SW, Wang YJ, Lee OK. Growth of mesenchymal stem cells on electrospun type I collagen nanofibers. Stem Cells. 2006;24(11):2391-7.

71. Jin H-J, Chen J, Karageorgiou V, Altman GH, Kaplan DL. Human bone marrow stromal cell responses on electrospun silk fibroin mats. Biomaterials. 2004;25(6):1039-47.

72. Li C, Vepari C, Jin H-J, Kim HJ, Kaplan DL. Electrospun silk-BMP-2 scaffolds for bone tissue engineering. Biomaterials. 2006;27(16):3115-24.

73. Xu CY, Inai R, Kotaki M, Ramakrishna S. Aligned biodegradable nanofibrous structure: a potential scaffold for blood vessel engineering. Biomaterials. 2004;25(5):877-86.

74. Deschamps AA, Claase MB, Sleijster WJ, de Bruijn JD, Grijpma DW, Feijen J. Design of segmented poly (ether ester) materials and structures for the tissue engineering of bone. J Controlled Release. 2002;78(1):175-86.

75. Mahmood TA, de Jong R, Riesle J, Langer R, van Blitterswijk CA. Adhesion-mediated signal transduction in human articular chondrocytes: the influence of biomaterial chemistry and tenascin-C. Exp Cell Res. 2004;301(2):179-88.

76. Jansen EJ, Sladek RE, Bahar H, Yaffe A, Gijbels MJ, Kuijer R, et al. Hydrophobicity as a design criterion for polymer scaffolds in bone tissue engineering. Biomaterials. 2005;26(21):4423-31.

77. Moroni L, Licht R, de Boer J, de Wijn JR, van Blitterswijk CA. Fiber diameter and texture of electrospun PEOT/PBT scaffolds influence human mesenchymal stem cell proliferation and morphology, and the release of incorporated compounds. Biomaterials. 2006;27(28):4911-22.

78. Cai Y-Z, Zhang G-R, Wang L-L, Jiang Y-Z, Ouyang H-W, Zou X-H. Novel biodegradable three-dimensional macroporous scaffold using aligned electrospun nanofibrous yarns for bone tissue engineering. Journal of Biomedical Materials Research Part A. 2012;100A(5):1187-94.

79. Tuzlakoglu K, Bolgen N, Salgado AJ, Gomes ME, Piskin E, Reis RL. Nano- and micro-fiber combined scaffolds: A new architecture for bone tissue engineering. J Mater Sci Mater Med. 2005 2005/12/01;16(12):1099-104.

80. Garreta E, Genové E, Borrós S, Semino CE. Osteogenic differentiation of mouse embryonic stem cells and mouse embryonic fibroblasts in a three-dimensional self-assembling peptide scaffold. Tissue Eng. 2006;12(8-15):2215-27.

81. Liu X, Wang X, Wang X, Ren H, He J, Qiao L, et al. Functionalized self-assembling peptide nanofiber hydrogels mimic stem cell niche to control human adipose stem cell behavior in vitro. Acta Biomater. 2013(0).

82. Gelain F, Bottai D, Vescovi A, Zhang S. Designer self-assembling peptide nanofiber scaffolds for adult mouse neural stem cell 3-dimensional cultures. PloS one. 2006;1(1):e119.

83. Galler KM, Aulisa L, Regan KR, D'Souza RN, Hartgerink JD. Self-Assembling Multidomain Peptide Hydrogels: Designed Susceptibility to Enzymatic Cleavage Allows Enhanced Cell Migration and Spreading. J Am Chem Soc. 2010 2010/03/10;132(9):3217-23.

84. Jun H-W, Paramonov SE, Dong H, Forraz N, McGuckin C, Hartgerink JD. Tuning the mechanical and bioresponsive properties of peptide-amphiphile nanofiber networks. J Biomater Sci Polym Ed. 2008;19(5):665-76.

85. Webber MJ, Tongers J, Renault M-A, Roncalli JG, Losordo DW, Stupp SI. Development of bioactive peptide amphiphiles for therapeutic cell delivery. Acta Biomater. 2010;6(1):3-11.

86. Lee J-Y, Choo J-E, Choi Y-S, Suh J-S, Lee S-J, Chung C-P, et al. Osteoblastic differentiation of human bone marrow stromal cells in self-assembled BMP-2 receptor-binding peptide-amphiphiles. Biomaterials. 2009;30(21):3532-41.

87. Hosseinkhani H, Hosseinkhani M, Kobayashi H. Proliferation and differentiation of mesenchymal stem cells using self-assembled peptide amphiphile nanofibers. Biomedical Materials. 2006;1(1):8-15.

88. Chen F, Tang Q-L, Zhu Y-J, Wang K-W, Zhang M-L, Zhai W-Y, et al. Hydroxyapatite nanorods/poly(vinyl pyrolidone) composite nanofibers, arrays and three-dimensional fabrics: Electrospun preparation and transformation to hydroxyapatite nanostructures. Acta Biomater. 2010;6(8):3013-20.

89. Bakhshandeh B, Soleimani M, Ghaemi N, Shabani I. Effective combination of aligned nanocomposite nanofibers and human unrestricted somatic stem cells for bone tissue engineering. Acta pharmacologica Sinica. 2011;32(5):626-36.

90. Lü L-X, Zhang X-F, Wang Y-Y, Ortiz L, Mao X, Jiang Z-L, et al. Effects of Hydroxyapatite-Containing Composite Nanofibers on Osteogenesis of Mesenchymal Stem Cells In vitro and Bone Regeneration In vivo. ACS Applied Materials & Interfaces. 2012 2013/01/23;5(2):319-30.

91. Jose MV, Thomas V, Xu Y, Bellis S, Nyairo E, Dean D. Aligned Bioactive Multi-Component Nanofibrous Nanocomposite Scaffolds for Bone Tissue Engineering. Macromol Biosci. 2010;10(4):433-44.

92. Patlolla A, Collins G, Livingston Arinzeh T. Solvent-dependent properties of electrospun fibrous composites for bone tissue regeneration. Acta Biomater. 2010;6(1):90-101.

93. McCullen SD, Stevens DR, Roberts WA, Clarke LI, Bernacki SH, Gorga RE, et al. Characterization of electrospun nanocomposite scaffolds and biocompatibility with adipose-derived human mesenchymal stem cells. International journal of nanomedicine. 2007;2(2):253-63.

94. Pek YS, Wan AC, Shekaran A, Zhuo L, Ying JY. A thixotropic nanocomposite gel for three-dimensional cell culture. Nature nanotechnology. 2008;3(11):671-5.

95. Hosseinkhani H, Hosseinkhani M, Hattori S, Matsuoka R, Kawaguchi N. Micro and nano-scale in vitro 3D culture system for cardiac stem cells. Journal of Biomedical Materials Research Part A. 2010;94(1):1-8.

96. Khor HL, Kuan Y, Kukula H, Tamada K, Knoll W, Moeller M, et al. Response of Cells on Surface-Induced Nanopatterns: Fibroblasts and Mesenchymal Progenitor Cells. Biomacromolecules. 2007 2007/05/01;8(5):1530-40.

97. Harrison BS, Atala A. Carbon nanotube applications for tissue engineering. Biomaterials. 2007;28(2):344-53.

98. Wang SF, Shen L, Zhang WD, Tong YJ. Preparation and mechanical properties of chitosan/carbon nanotubes composites. Biomacromolecules. 2005;6(6):3067-72.

99. MacDonald RA, Laurenzi BF, Viswanathan G, Ajayan PM, Stegemann JP. Collagen–carbon nanotube composite materials as scaffolds in tissue engineering. Journal of Biomedical Materials Research Part A. 2005;74A(3):489-96.

100. Correa-Duarte MA, Wagner N, Rojas-Chapana J, Morsczeck C, Thie M, Giersig M. Fabrication and biocompatibility of carbon nanotube-based 3D networks as scaffolds for cell seeding and growth. Nano Lett. 2004;4(11):2233-6.

101. Abarrategi A, Gutiérrez MC, Moreno-Vicente C, Hortigüela MJ, Ramos V, López-Lacomba JL, et al. Multiwall carbon nanotube scaffolds for tissue engineering purposes. Biomaterials. 2008;29(1):94-102.

102. Hu H, Ni Y, Montana V, Haddon RC, Parpura V. Chemically functionalized carbon nanotubes as substrates for neuronal growth. Nano Lett. 2004;4(3):507-11.

103. Gabay T, Jakobs E, Ben-Jacob E, Hanein Y. Engineered self-organization of neural networks using carbon nanotube clusters. Physica A: Statistical Mechanics and its Applications. 2005;350(2-4):611-21.

104. Supronowicz PR, Ajayan PM, Ullmann KR, Arulanandam BP, Metzger DW, Bizios R. Novel current-conducting composite substrates for exposing osteoblasts to alternating current stimulation. J Biomed Mater Res. 2002;59(3):499-506.

105. Besteman K, Lee JO, Wiertz FGM, Heering HA, Dekker C. Enzyme-coated carbon nanotubes as single-molecule biosensors. Nano Lett. 2003;3(6):727-30.

106. Oh S, Brammer KS, Li YJ, Teng D, Engler AJ, Chien S, et al. Stem cell fate dictated solely by altered nanotube dimension. Proceedings of the National Academy of Sciences. 2009;106(7):2130-5.

107. Fukumori K, Akiyama Y, Yamato M, Kobayashi J, Sakai K, Okano T. Temperature-responsive glass coverslips with an ultrathin poly (N-isopropylacrylamide) layer. Acta Biomater. [Article]. 2009 Jan;5(1):470-6.

108. Akiyama Y, Kikuchi A, Yamato M, Okano T. Ultrathin poly (N-isopropylacrylamide) grafted layer on polystyrene surfaces for cell adhesion/detachment control. Langmuir. 2004;20(13):5506-11.

109. Kikuchi A, Okano T. Nanostructured designs of biomedical materials: applications of cell sheet engineering to functional regenerative tissues and organs. J Controlled Release. 2005;101(1–3):69-84.

110. Horne MK, Nisbet DR, Forsythe JS, Parish CL. Three-dimensional nanofibrous scaffolds incorporating immobilized BDNF promote proliferation and differentiation of cortical neural stem cells. Stem cells and development. 2009;19(6):843-52.

111. Huang X, Zhang Y, Donahue HJ, Lowe TL. Porous Thermoresponsive-co-Biodegradable Hydrogels as Tissue-Engineering Scaffolds for 3-Dimensional In Vitro Culture of Chondrocytes. TISSUE ENGINEERING. 2007;13(11):2645 - 52.

112. Yang S, Leong K-F, Du Z, Chua C-K. The design of scaffolds for use in tissue engineering. Part I. Traditional factors. TISSUE ENGINEERING. 2001;7(6):679-89.

113. Gomes M, Azevedo H, Malafaya P, Silva S, Oliveira J, Silva G, et al. 16 Natural Polymers in Tissue Engineering Applications. Handbook of Biopolymers and Biodegradable Plastics: Properties, Processing and Applications. 2012:385.

114. Kim MS, Kim JH, Min BH, Chun HJ, Han DK, Lee HB. Polymeric scaffolds for regenerative medicine. Polymer Reviews. 2011;51(1):23-52.

115. Migliaresi C, Motta A. Scaffolds for Tissue Engineering: Biological Design, Materials, and Fabrication: CRC Press; 2014.

116. Mikos AG, Herring SW, Ochareon P, Elisseeff J, Lu HH, Kandel R, et al. Engineering complex tissues. TISSUE ENGINEERING. 2006;12(12):3307-39.

117. Chen G, Ushida T, Tateishi T. Scaffold design for tissue engineering. Macromolecular Bioscience. 2002;2(2):67-77.

118. Guo B, Ma PX. Synthetic biodegradable functional polymers for tissue engineering: a brief review. Science China Chemistry. 2014;57(4):490-500.

119. Kim IL, Mauck RL, Burdick JA. Hydrogel design for cartilage tissue engineering: A case study with hyaluronic acid. Biomaterials. 2011;32(34):8771-82.

120. Seliktar D. Designing cell-compatible hydrogels for biomedical applications. Science. 2012;336(6085):1124-8.

121. Fedorovich NE, Alblas J, Wijin JR, Hennink WE, Verbout AJ, Dhert WJA. Hydrogels as Extracellular Matrices for Skeletal Tissue Engineering: State-of-the-Art and Novel Application in Organ Printing. TISSUE ENGINEERING. 2007;13(8):1905-25.

122. Baroli B. Hydrogels for tissue engineering and delivery of tissue-inducing substances. Journal of Pharmaceutical Sciences. 2007;96(9):2197-223.

123. Drury JL, Mooney DJ. Hydrogels for tissue engineering: scaffold design variables and applications. Biomaterials. 2003;24(24):4337-51.

124. Spiller KL, Maher SA, Lowman AM. Hydrogels for the Repair of Articular Cartilage Defects. Tissue Engineering Part B: Reviews. 2011;17(4):281-99.

125. Reddi AH, Becerra J, Andrades JA. Nanomaterials and hydrogel scaffolds for articular cartilage regeneration. Tissue Engineering Part B: Reviews. 2011;17(5):301-5.

126. El-Sherbiny IM, Yacoub MH. Hydrogel scaffolds for tissue engineering: Progress and challenges. Global cardiology science & practice. 2013;2013(3):316.

127. de las Heras Alarcón C, Pennadam S, Alexander C. Stimuli responsive polymers for biomedical applications. Chemical Society Reviews. 2005;34(3):276-85.

128. Mano JF. Stimuli‐Responsive Polymeric Systems for Biomedical Applications. Advanced Engineering Materials. 2008;10(6):515-27.

129. Imran AB, Seki T, Takeoka Y. Recent advances in hydrogels in terms of fast stimuli responsiveness and superior mechanical performance. Polymer journal. 2010;42(11):839-51.
130. Klouda L, Mikos AG. Thermoresponsive hydrogels in biomedical applications. European Journal of Pharmaceutics and Biopharmaceutics. 2008;68(1):34-45.
131. Constantin M, Cristea M, Ascenzi P, Fundueanu G. Lower critical solution temperature versus volume phase transition temperature in thermoresponsive drug delivery systems. Express Polym Lett. 2011;5(10):839-48.
132. Jain S, Sandhu PS, Malvi R, Gupta B. Cellulose Derivatives as Thermoresponsive Polymer: An Overview. Journal of Applied Pharmaceutical Science Vol. 2013;3(12):139-44.
133. Supper S, Anton N, Seidel N, Riemenschnitter M, Curdy C, Vandamme T. Thermoresponsive chitosan/glycerophosphate-based hydrogel and its derivatives in pharmaceutical and biomedical applications. Expert opinion on drug delivery. 2014;11(2):249-67.
134. Jeong B, Kim SW, Bae YH. Thermoresponsive sol–gel reversible hydrogels. Advanced Drug Delivery Reviews. 2002;54(1):37-51.
135. Ko DY, Shinde UP, Yeon B, Jeong B. Recent progress of in situ formed gels for biomedical applications. Progress in Polymer Science. 2013;38(3):672-701.
136. Song S-C, Lee SB, Jin J-I, Sohn YS. A new class of biodegradable thermoresponsive polymers. I. Synthesis and characterization of poly (organophosphazenes) with methoxy-poly (ethylene glycol) and amino acid esters as side groups. Macromolecules. 1999;32(7):2188-93.
137. Bhattarai N, Matsen FA, Zhang M. PEG‐Grafted Chitosan as an Injectable Thermoreversible Hydrogel. Macromolecular Bioscience. 2005;5(2):107-11.
138. Wang J, Sun D, Leong K, editors. Injectable polyphosphate hydrogel. Proc Int Symp Control Rel Bioact Mater; 2003.

139. Park KM, Lee SY, Joung YK, Na JS, Lee MC, Park KD. Thermoresponsive chitosan–Pluronic hydrogel as an injectable cell delivery carrier for cartilage regeneration. Acta Biomaterialia. 2009;5(6):1956-65.

140. Di Martino A, Sittinger M, Risbud MV. Chitosan: a versatile biopolymer for orthopaedic tissue-engineering. Biomaterials. 2005;26(30):5983-90.

141. Hirano S, Tsuchida H, Nagao N. N-acetylation in chitosan and the rate of its enzymic hydrolysis. Biomaterials. 1989;10(8):574-6.

142. Freier T, Koh HS, Kazazian K, Shoichet MS. Controlling cell adhesion and degradation of chitosan films by N-acetylation. Biomaterials. 2005;26(29):5872-8.

143. Rabea EI, Badawy ME-T, Stevens CV, Smagghe G, Steurbaut W. Chitosan as antimicrobial agent: applications and mode of action. Biomacromolecules. 2003;4(6):1457-65.

144. Zheng LY, Zhu JF. Study on antimicrobial activity of chitosan with different molecular weights. Carbohydrate Polymers. 2003;54(4):527-30.

145. Ueno H, Mori T, Fujinaga T. Topical formulations and wound healing applications of chitosan. Advanced Drug Delivery Reviews. 2001;52(2):105-15.

146. Oliveira JT, Reis R. Polysaccharide‐based materials for cartilage tissue engineering applications. Journal of tissue engineering and regenerative medicine. 2011;5(6):421-36.

147. Ruel-Gariépy E, Leroux J-C. In situ-forming hydrogels—review of temperature-sensitive systems. European Journal of Pharmaceutics and Biopharmaceutics. 2004;58(2):409-26.

148. Rzaev ZMO, Dinçer S, Pişkin E. Functional copolymers of N-isopropylacrylamide for bioengineering applications. Progress in Polymer Science. 2007;32(5):534-95.

149. Keeney M, Lai JH, Yang F. Recent progress in cartilage tissue engineering. Current opinion in biotechnology. 2011;22(5):734-40.

150. Chenite A, Chaput C, Wang D, Combes C, Buschmann MD, Hoemann CD, et al. Novel injectable neutral solutions of chitosan form biodegradable gels in situ. Biomaterials. 2000;21(21):2155-61.

151. Dang JM, Sun DDN, Shin-Ya Y, Sieber AN, Kostuik JP, Leong KW. Temperature-responsive hydroxybutyl chitosan for the culture of mesenchymal stem cells and intervertebral disk cells. Biomaterials. 2006;27(3):406-18.
152. Bhattarai N, Matsen FA, Zhang M. PEG-Grafted Chitosan as an Injectable Thermoreversible Hydrogel. Macromolecular Bioscience. 2005;5(2):107-11.
153. Huangqin C, Mingwen F. Novel Thermally Sensitive pH-dependent Chitosan/ Carboxymethyl Cellulose Hydrogels. Journal of Bioactive and Compatible Polymers. 2008;23(1):38-48.
154. Cho JH, Kim S-H, Park KD, Jung MC, Yang WI, Han SW, et al. Chondrogenic differentiation of human mesenchymal stem cells using a thermoresponsive poly(N-isopropylacrylamide) and water-soluble chitosan copolymer. Biomaterials. 2004;25(26):5743-51.
155. Galle J, Bader A, Hepp P, Grill W, Fuchs B, Kas J, et al. Mesenchymal stem cells in cartilage repair: state of the art and methods to monitor cell growth, differentiation and cartilage regeneration. Current medicinal chemistry. 2010;17(21):2274-91.
156. Lanza R, Longer R, Vacanti J, editors. Principles of Tissue Engineering. 3 ed: Elsevier Academic Press; 2007.
157. Lee SJ, Atala A. Scaffold technologies for controlling cell behavior in tissue engineering. Biomedical Materials. 2013;8(1):010201.
158. Liu F, Urban MW. Recent advances and challenges in designing stimuli-responsive polymers. Progress in Polymer Science. 2010;35(1):3-23.

CHAPTER THREE

3. A Biodegradable Thermoresponsive Hydrogel with Tunable Properties for Mimicking Three-Dimensional Microenvironments of Stem Cells

A Biodegradable Thermoresponsive Hydrogel with Tuneable Properties for Mimicking Three-Dimensional Microenvironments of Stem Cells

Amir Mellati[a], Sheng Dai[a], Jingxiu Bi[a], Bo Jin[a], Hu Zhang[a]*

[a]School of Chemical Engineering, The University of Adelaide, Adelaide SA5005, Australia

*Corresponding author
E-mail: hu.zhang@adelaide.edu.au
Tel: + 61 8 8313 3810

Published in: RSC Advances, 2014, 4(109): 63951-63961. DOI: 10.1039/C4RA12215A

3.1 Abstract

Employing stem cells in therapeutic applications strongly depends on the extracellular three-dimensional (3D) microenvironment and cell carrier properties. In this work, chitosan-*g*-poly(N-isopropylacrylamide) (CS-*g*-PNIPAAm) was synthesized as stem cell mimicking microenvironment. The influence of various polymerization conditions, such as acid concentration, reaction temperature and monomer feed, on the grafting parameters of this thermo-responsive hydrogel, was systematically investigated. We found that the resulting copolymers with a small amount of long poly(N-isopropylacrylamide) (PNIPAAm) side chains are low-soluble at low temperatures, but can form stronger hydrogels (almost 5 folds) at high temperatures, whereas copolymers with a high amount of short PNIPAAm side chains are more soluble at low temperatures, however, they cannot form strong hydrogels at high temperatures. In a physiological pH, optimized balance between the solubility (as the pre-requirement for cell dispersion and injectability) of copolymers at ambient temperature and enhanced gel mechanical strength (as the essential parameter of stem cell microenvironments) at body temperature can be achieved through controlled reaction conditions. Mesenchymal stem cells (MSCs) were cultured in the CS-g-PNIPAAm hydrogels. Further analysis of confocal images confirms MSCs can maintain their viability and increase the cellular biomass inside hydrogels. Sectional analysis demonstrates cells are uniformly distributed within the hydrogels. Our results confirm that the CS-g-PNIPAAm with manipulated properties could provide a potential 3D microenvironment for stem cell culture, differentiation and *in vivo* injection.

3.2 Introduction

The remarkable potential of stem cells in clinical applications is being increasingly revealed. However, the success in their biomedical applications highly depends on the creation of a microenviroment to provide chemical, mechanical and topological cues inside a 3D archicture in a precisely controlled, temporal and spatial manner, which are essential for regulating stem cell proliferation, differentiation and migration (1). The microenvironment is often realised through the elegant design of biomaterials. Among

different types of biomaterials, hydrogels are more appealing than conventional porous scaffolds. Highly hydrated polymeric networks of hydrogels result in a soft and elastic 3D structure which could resemble natural living tissues, especially soft tissues (2). In addition, hydrogels are great materials for efficient entrapment of viable cells (3). They can facilitate sufficient nutrient and oxygen transport, and metabolic waste removal. They usually show excellent biocompatibility as well as great potential to be easily modified with cell adhesion ligands (4). Furthermore, their low interfacial tension and minimal mechanical and frictional irritations (5) make them a superb choice for 3D cell culture. Hydrogels can also be tailored to meet the requirements of stem cell microenvironment by adjusting physio-chemical and mechanical properties.

Living systems contain macromolecules such as polysaccharides and proteins which respond to their environment in a non-linear manner and undergo a drastic change around a given critical point. Therefore, stimuli-responsive hydrogels that can respond to external stimuli, such as temperature, pH, ionic strength, light, magnetism, electrical or mechanical stimulus in a controllable and predictable manner, are considered as biomimetic systems (6-8).

Thermoresponsive hydrogels are such biomimetic polymers. These polymers can be prepared as a solution or cross-linked network. The solution (or cross-linked swollen) form of these polymers can be converted to hydrogels (or shrunken hydrogels) by temperature change (9). The solution form of the copolymer can show a reversible or irreversible thermo-responsive sol-gel transition behaviour. For most applications, a good solubility at room temperature and neutral pH, and tuneable mechanical strength at physiological temperature are required. Good solubility can facilitate effective cell dispersion inside the polymer solution which leads to a homogeneous cell distribution within the hydrogel to form a uniform product. In addition, when the injectability of cell/polymer is desired, the cell-laden hydrogel solution can be administered to fill any shape of a defect site in a minimally invasive manner and then converted into hydrogels to retain cells inside the 3D hydrogel constructs (3, 10-13). The hydrogels with reversibility in their sol-gel transition behaviour are also suitable for 3D cell culture to acquire a sufficient number of cells while preserving their cellular functions and phenotype in a 3D microenvironement. Cell harvest

can be simply achieved by liquifying the gel at a low temperature and no enzyme such as trypsin to detach the adherent cells is required. In this way, cells can be detached without trypsinization which may inversely affect cell functionality (14, 15). On the other hand, tuneable mechanical properties of the gel could provide a competent tool to regulate stem cell fate.

Chitosan-based thermoresponsive hydrogels have a great potential to construct a biomimetic microenvironment. Chitosan (CS) is a linear polysaccharide composed of β (1,4)-linked glucosamine and N-acetyl glucosamine subunits (16). It has excellent biocompatibility, tuneable biodegradability and cell adhesion ability (17, 18), antimicrobial (19, 20) and wound healing (21) properties. In addition, the chitosan structure is quite similar to some extracellular matrix components such as glycosaminoglycans (GAGs). Therefore, chitosan was extensively chosen as the backbone for cell support. As a thermoresponsive moiety, PNIPAAm could be introduced to the chitosan via a variety of chemical approaches. PNIPAAm undergoes a reversible phase transition in an aqueous solution at a temperature called "lower critical solution temperature (LCST)". The LCST of PNIPAAm is around 31 ˚C which is close to the body temperature. This fact has made PNIPAAm as one of the most studied thermoresponsive polymers. The simple structure of PNIPAAm which does not contain functional groups to interact with other biomolecules has limited its applications (22). Therefore, it is usually utilized in conjunction with other moieties to improve its functionalities.

PNIPAAm has been introduced to chitosan by different research groups in various ways, including interpenetrating polymer networks (IPN) (23, 24), semi-IPN (24, 25), surface grafted membranes (26), chemically cross-linked hydrogels in forms of discs (27-29), films (29, 30) , nanoparticles (31-35) and solutions (36-41). However, to the best of our knowledge, there is no systematic investigation on polymerization conditions which can regulate the key features (solubility and mechanical strength) of this copolymer as a sol-gel thermoreversible hydrogel. Rheological bahaviour of the copolymer at physiological pH and its correlation to grafting parameters need to be addressed. Moreover, few biological applications within a 3D CS-g-PNIPAAm hydrogel have been studied.

In this study, chitosan-g-poly(N-isopropylacrylamide) was synthesized through free radical graft polymerization. We investigated essential physical and mechanical properties of this copolymer for intended biomedical applications which can be precisely manipulated by polymerization conditions. Biomimetic microenvironments were created from the resulting hydrogel. Viability, proliferation, distribution and morphology of mesenchymal stem cells were also evaluated.

3.3 Materials and methods

3.3.1 Materials

N-Isopropylacrylamide (NIPAAm, 97 %, Sigma-Aldrich) was purified by recrystallization in *n*-hexane. Ammonium cerium (IV) nitrate (CAN) and chitosan (MW of 200-300 kDa) were purchased from Acros Organic (New Jersey). Dulbecco's Modified Eagle's Medium (DMEM), trypsin-EDTA, penicillin-streptomycin and fetal bovine serum (FBS) were from Gibco-BRL (Grand Island). 3-(4,5-Dimethylthiazol-2-yl)-2,5-diphenyltetrazolium bromide (MTT), Live/Dead® viability/cytotoxicity kit (L3224) and Press-to-Seal™ silicone isolators (P24741) were ordered from Molecular Probes (Oregon). All other chemicals not mentioned were of analytical grades and used directly without further purification.

3.3.2 Synthesis of chitosan-g-PNIPAAm

Chitosan-g-PNIPAAm was synthesized by free radical grafting polymerization. In detail, chitosan was dissolved in 30 mL aqueous acetic acid to make a 1 wt% solution. 2.0 g purified NIPAAm monomer was dissolved in 10 mL Milli-Q water, and then mixed with the above chitosan solution in a three-neck flask fitted with a condenser and gas inlet/outlet. The mixed solution was bubbled with nitrogen for 30 min, and 3 mL CAN solution was injected into the flask to initiate polymerization. The reaction was carried out for 24 h under nitrogen atmosphere.

After polymerization, the solution was condensed and precipitated in an excess amount of THF/hexane (4:1). The crude products were obtained by centrifugation and dried under

vacuum at room temperature. The polymer was further purified by methanol soxhelet extraction for 48 h to remove PNIPAAm homopolymer and other reaction residues. The purified product was dried under vacuum. Grafting ratio (GR) and percentage of homopolymerization (PoH) were calculated using Equations 1 and 2:

$$\text{Grafting Ratio (GR)} = \frac{\text{W2-W1}}{\text{W1}} \times 100\% \quad \textbf{(1)}$$

$$\boldsymbol{Percentage\ of\ Homopolymerisation\ (PoH) = \frac{W4-W2}{W3} \times 100\%} \quad \textbf{(2)}$$

where W1, W2, W3 and W4 are the weights of initial chitosan loaded, PNIPAAm grafted chitosan after soxhelet extraction, NIPAAm monomer feed and the crude product of grafted chitosan with NIPAAm before soxhelet extraction, respectively.

3.3.3 Conductometric and potentiometric titration

The amount of free amino groups on chitosan before and after grafting polymerization was quantified by conductometric and potentiometric titration. Typically, a solution of 35 mg copolymer in 70 ml Milli-Q water was prepared and a small amount of HCl was added to adjust pH to 3.5. The solution was then back-titrated using a 0.1 M NaOH. After each addition, the conductivity and pH were measured using a H18733 conductivity meter (Hana Instrument, USA) and a pre-calibrated pH/mV meter (smartCHEM-pH, TPS Australia). The degree of substitution (DS%) was calculated according to Equation 3:

$$\textbf{Degree of Substitution (DS)} = \frac{free\ amino\ groups\ of\ chitosan\ after\ polymerisation}{free\ amino\ groups\ of\ initial\ chitosan} \times 100\% \quad \textbf{(3)}$$

3.3.4 FTIR spectroscopy

The dry powders of grafting copolymers and chitosan were examined using Fourier Transformed Infrared (FTIR), where the spectra were recorded over a wave number range of 600-3000 cm^{-1} using a Nicolet 6700 FTIR spectrometer (Thermo Electron, USA) at room temperature.

3.3.5 Rheological characterization

The rheological properties of concentrated copolymer solutions were investigated using a SR5 controlled stress rheometer (Rheometric Scientific, USA) equipped with a cone and plate geometry fixture (diameter: 40 mm; actual gap: 0.0483 mm; actual angle: 0.0398 rad). Experimental temperature was controlled by a peltier system connected to a water bath, and silicone oil was used to prevent solvent evaporation. Grafting copolymer solutions were prepared in phosphate buffered saline (PBS, pH ~ 7.4). Stress sweeps were first performed to determine linear viscoelastic regions for each sample. Within the linear viscoelastic regime and under a fixed stress and frequency, the storage (G') and loss (G") modules were measured over a temperature range of 25 to 45°C.

3.3.6 Solubility

To investigate the solubility of grafting copolymers, 0.44 mg mL^{-1} solutions of copolymers in 0.2 wt% acetic acid were first prepared. A small amount of 2.5 M NaOH was used to adjust pH while recording their absorbance as a function of pH at 600 nm using a UV-1601 UV/Vis spectrophotometer (Shimadzu, Japan).

3.3.7 Hydrogel morphology

A hydrogel prepared from 35 mg mL^{-1} of the copolymer in PBS at 37°C was instantly immersed in liquid nitrogen and then dried in a ALPHA 1-2LD plus freeze-dryer (CHRIST, Germany) for 48 h. The dried samples were gold coated and their morphologies were observed by a Philips XL 30 FEG scanning electron microscope (SEM) (FEI, USA).

3.3.8 Cell culture

A stem cell line, murine embryonic mesenchymal progenitor cell (C3H/10T1/2) from Riken Cell Bank (Japan), was cultured in DMEM supplemented with 10 % FBS, 100 U

mL^{-1} of penicillin, 100 mg mL^{-1} of streptomycin and 2 mM L^{-1} L-glutamine. The cells were incubated at 37°C in a humidified atmosphere in the presence of 5% CO_2.

3.3.9 3D cell culture

MSCs were trypsinized from flasks and resuspended in a fresh culture medium. A polymer solution (CS-NI-2) of 31.5 mg mL^{-1} in PBS was prepared (pH of 7.4) and sterilized by autoclave. Cell suspension and copolymer solution were mixed to prepare a mixture of cell and polymer at a cell concentration of 1.0 x 10^6 cells mL^{-1} and a final polymer concentration of 30 mg mL^{-1}. 0.5 mL of the cell/polymer mixture was transferred to each well on a 24-well plate and incubated for 1 h at 37˚C to form mixed hydrogels. The same cell concentrations were prepared by mixing cells and PBS without copolymer as a control. 2.0 mL of fresh growth medium was topped up to each well and kept in a humidified incubator at 37˚C and 5% CO_2. Medium was replaced with fresh medium once every other day.

3.3.10 MTT assay

Cell viability and proliferation inside the mixed hydrogels were examined using the MTT assay. At each time point, 0.5 mL of MTT (5 mg/ml in PBS) was added to each well, including both test and control, and then incubated for 4 h at 37˚C. All the liquid was removed from the top of the hydrogels and 1 mL dimethyl sulfoxide (DMSO) was added to each well to ensure complete solubilization of formazan crystals. After 1 h further incubation, all of the well content was transferred to an eppendorf tube, vortexed briefly and centrifuged at 10,000 rpm for 5 min. Finally, 200 µL of supernatant were transferred to a 96-well plate and the absorbance was read using a microplate reader (ELx808, BioTek, USA) at 595 nm. Triplicates of every time point were used.

3.3.11 Confocal Laser Scanning Microscopy

Live/dead cytotoxicity/viability kit was used to stain live and dead cells. 1 μM of acetomethoxy derivate of calcein (calcein AM) and 2.5 μM of ethidium homodimer-1 (EthD-1) working solutions were prepared freshly according to the manufacturer's protocol. At days 1 and 7, the growth medium was removed and mixed hydrogels were washed with 1.0 mL prewarmed PBS (37˚C). The PBS was replaced with 1.0 mL of fresh prewarmed PBS and left in the incubator at 37˚C. The liquid was replaced with 2 mL of dye working solution and further incubated at 37˚C for 45 min. The dye solution was removed and hydrogel was washed twice with 1.0 mL prewarmed PBS. All the liquid was removed and hydrogel was then transferred carefully to a chamber made from coverslips and Press-to-Seal™ silicone isolators. To make the 3D structure more stable and to prevent disolution, the extra liquid was absorbed from the hydrogel by gently touching its surface with a piece of tissue paper so that the gel got highly concentrated (semi-dried). The cultured cells in the hydrogels were observed under a Leica SP5 spectral scanning confocal microscope (Leica Microsystems, Germany) equipped with a temperature controlled stage to keep the thermoresponsive hydrogels at 37˚C. Excitation wavelengths were set to 494 and 528 nm and emission wavelengths were at 517 and 617 nm for live (green) and dead (red) cells, respectively.

3.4 Results and discussion

3.4.1 Synthesis and characterization of chitosan-g-PNIPAAm

Chitosan-g-PNIPAAm copolymers were synthesized in various reaction conditions, as detailed in Table 1. Chitosan is a natural biodegradable and biocompatable polymer, which is a promising material in biomedical applications. In order to make chitosan thermoresponsive as well as more soluble at physiological pH 7.4, we introduced the thermoresponsive moieties of poly(N-isopropylacrylamide) to chitosan backbone through graft copolymerization. The schematic of synthesis outline is shown in Sceme 1. The success of graft copolymerization was confirmed by the characteristic bands of NIPAAm in the FTIR spectra of copolymer (Figure S1, Supporting information), where the peaks at

Table 1. Reaction optimization for the graft polymerization of NIPAAm onto chitosan

Sample Name	CAN (mmol)	Acetic Acid (wt %)	Temperature(°C)
CS-NI-1	0.09	10	25
CS-NI-2	0.18	10	25
CS-NI-3	0.27	10	25
CS-NI-4	0.36	10	25
CS-NI-5	0.18	5	25
CS-NI-6	0.18	15	25
CS-NI-7	0.18	20	25
CS-NI-8	0.18	10	32
CS-NI-9	0.18	10	45
CS-NI-10	0.18	10	60

All reactions were carried out for 24 hrs. Chitosan free amino groups and NIPAAm monomer were 1.6 and 17.7 mmol in feed.

2970 and 1456 cm^{-1} correspond to the C-H stretching and CH_3 bending deformation. In addition, the peak at 1385 cm^{-1} can be assigned to the methyl in isopropyl groups. Absorption bands of amide I and amide II are strengthened at 1626 and 1529 cm^{-1}, respectively, while the weak bands at 1586 cm^{-1} are attributed to -NH_2 scissoring of chitosan.

Grafting and homopolymerization parameters were determined by gravimetric, potentiometric and conductometric measurements as summarized in Figure 1 and Table 2, where the amount of un-grafted amino groups along chitosan backbone was measured from potentiometric and condutometric titrations (Figur S2, Supporting information). For the titration of chitosan and chitosan-g-PNIPAAm, a slight excess of HCl was added to ensure the complete protonation of all amimo groups. After gradual addition of alkali, the conductivity first decreases rapidly (descending leg) as the excess HCl is neutralized. After a transition point, a buffering zone is observed. In this buffering range, the conductivity

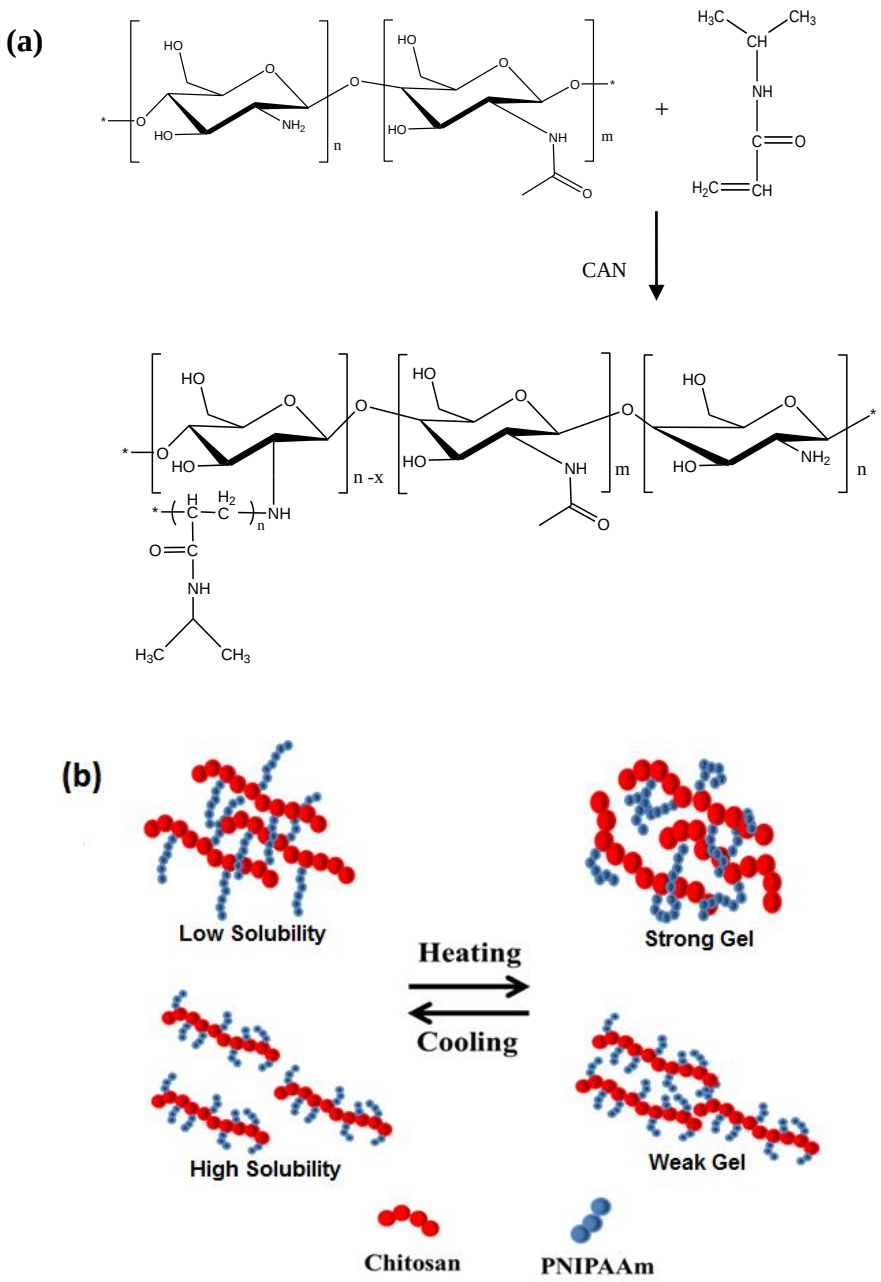

Scheme 1. (a) Outline of the synthesis of chitosan-*g*-PNIPAAm; (b) Schematic description on solubility and gelation behaviour of chitosan-*g*-PNIPAAm: Copolymers with long side chains are viscous and less-soluble at low temperatures, but can form strong hydrogels at high temperatures, whereas copolymers with short side chains are more soluble at low temperatures. However, they cannot form strong hydrogels at high temperatures.

increases slowly with the alkali addition, as a consequence of the neutralization of the protonated free amino groups. Therefore, this range can be used for the quantification of the PNIPAAm side chains on chitosan backbone as they have substituted amino groups on chitosan (39). A narrower buffering zone corresponds to the less availability of free $-NH_2$ groups and more grafts on chitosan. After the second transition point, the conductivity increases (ascending leg), indicating the introduction of excess NaOH. Similar steps are distinguishable in potentiometric titration curves. The degrees of substitution were calculated for each sample from the values of reacted and un-reacted functional groups (free amino groups in this case) using Equation 3 (14, 39). The mechanisms for initiation, propagation and termination of grafting polymerization are as follows:

Initiation:

$$CS+Ce^{4+} \leftrightarrow \text{Complex} \rightarrow CS\cdot + Ce^{3+} + H^{+} \quad (4)$$

$$M+Ce^{4+} \rightarrow M\cdot + Ce^{3+} + H^{+} \quad (5)$$

$$CS\cdot + M \rightarrow CSM\cdot \quad (6)$$

Propagation:

$$CSM\cdot + nM \rightarrow CSM\cdot_{n+1} \quad (7)$$

$$M\cdot + nM \rightarrow M\cdot_{n+1} \quad (8)$$

Termination:

$$CSM\cdot_n + M\cdot_m \rightarrow CSM_{n+m} \quad (9)$$

$$M\cdot_n + M\cdot_m \rightarrow M_{n+m} \quad (10)$$

$$CSM\cdot_n + CSM\cdot_m \rightarrow CSM_n\text{-}CSM_m \quad (11)$$

$$CSM\cdot_n + Ce^{4+} \rightarrow CSM_n + Ce^{3+} + H^{+} \quad (12)$$

$$M\cdot_n + Ce^{4+} \rightarrow M_n + Ce^{3+} + H^{+} \quad (13)$$

$$CSM\cdot_n + M \rightarrow CSM_n + M\cdot \quad (14)$$

$$CSM\cdot_n + P \rightarrow CSM_n + P\cdot \quad (15)$$

where CS, M, Ce and P represent chitosan, NIPAAm monomer, ceric ion and propagating polymers, respectively.

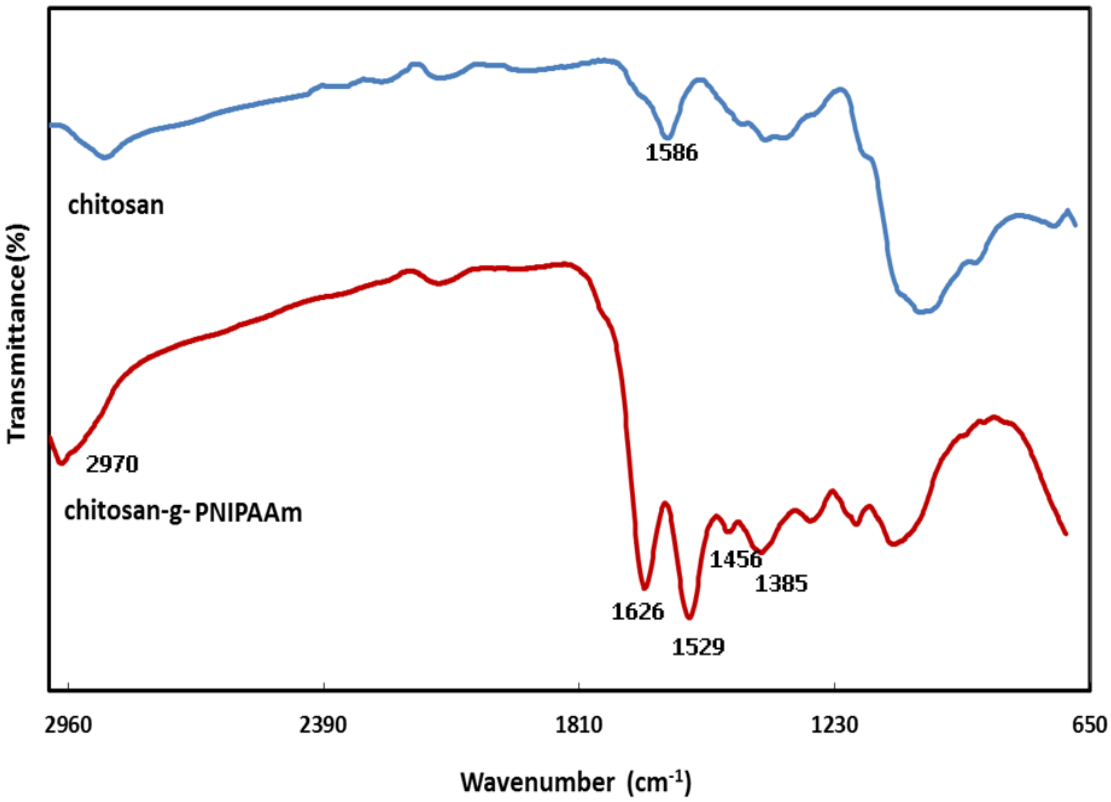

Figure S1. FTIR spectra of chitosan and chitosan-g-PNIPAAm (CS-NI-2)

Table 2. Summary of products synthesized at different reaction conditions

Parameter	Sample name	Percentage of homo-polymerization (%)[a]	Yield (%)[a]	Gelation[b]
Acid concentration	CS-NI-5	6	20	NO
	CS-NI-2	27	61	Yes
	CS-NI-6	27	66	Yes
	CS-NI-7	28	73	Yes
Temperature	CS-NI-2	27	61	Yes
	CS-NI-8	44	71	Yes
	CS-NI-9	40	65	Yes
	CS-NI-10	30	56	Yes
Initiator concentration	CS-NI-1	9	20	NO
	CS-NI-2	27	61	Yes
	CS-NI-3	43	78	Yes
	CS-NI-4	80	96	Yes

[a] Calculated from gravimetric measurements and Equation 1.

[b] Visually verified (Yes: gelation occurs with temperature rise, No: no gelation with temperature rise).

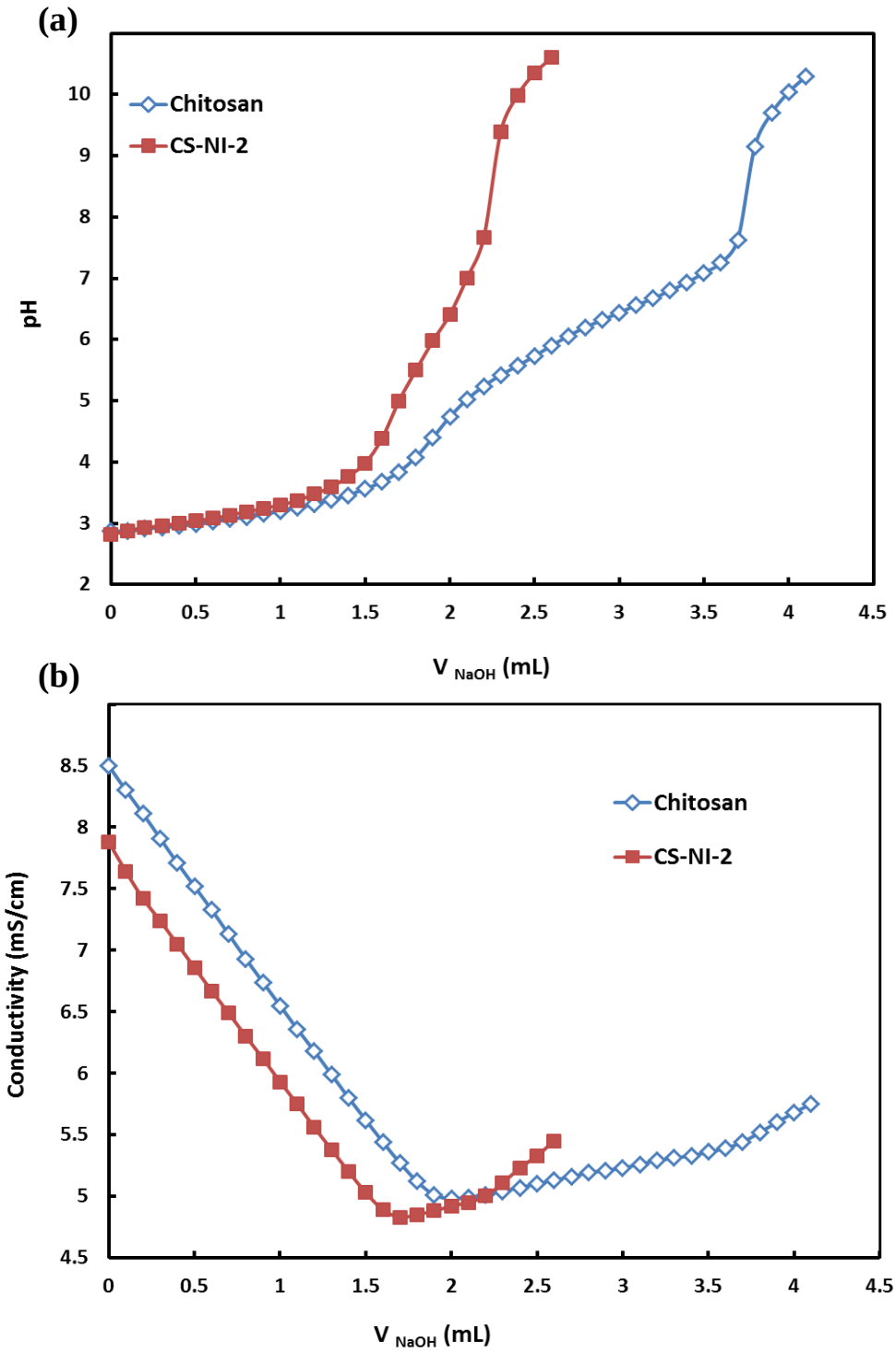

Figure S2. Potentiometric (a) and conductometric (b) titration curves for 0.5 mg/mL chitosan and CS-NI-2

3.4.1.1 Effect of initiator concentration

Based on Equations 4, 6 and 7, it is expected that grafting ratio and degree of substitution increase by increasing initiator concentration. To investigate the influence of initiator feed on grafting parameters, a range of polymerizations at various CAN concentrations from 0.09 to 0.36 mmol has been carried out. The results are shown in Figure 1a and Table 2. The degree of substitution increases continuously with increasing the amount of CAN initiator. It is expected that the more the initiator is fed, the more the free radical can be formed on chitosan backbone, leading to more side graft chains (Equations 4 & 6). At a low concentration of initiator (0.09 mmol), no grafting occurs and only the homopolymerization of NIPAAm is found. The grafting ratio increases with the increment of initiator concentration up to 0.18 mmol. On the other hand, the percentage of homopolymer is increased simultaneously. Beyond this concentration, a further increase in CAN lead to a slight drop in grafting ratios. That could be due to the increase in formation of free radicals on chitosan, leading to more termination reactions by coupling these radicals according to Equations 9,11,12,14 and 15 (36, 42, 43), while homopolymerization increment is continued as a competitor reaction (Equations 5 & 8). Similar experimental trend has also been observed by Lee et al. (36).

3.4.1.2 Effect of reaction temperature

Effect of reaction temperature on polymerization parameters was investigated between 25 to 60 □C. As shown in Figure 1b and Table 2, the grafting ratio gradually decreases, but the degree of substitution drastically increases with the increase of temperature. In addition, it is observed that the percentage of homopolymerization increases with the increament of temperature below the LCST, while it decreases when temperature keeps rising above the LCST. At a low temperature below the LCST of PNIPAAm, the initiator is less active and therefore offer less free radicals on chitosan amino groups and in solution. However, the fully homogeneous system allows monomers to access to and react with these free radicals easily. As a result, less grafts are found on the backbone, while thier chain length are long. By increasing the temperature, the initiator is more active,

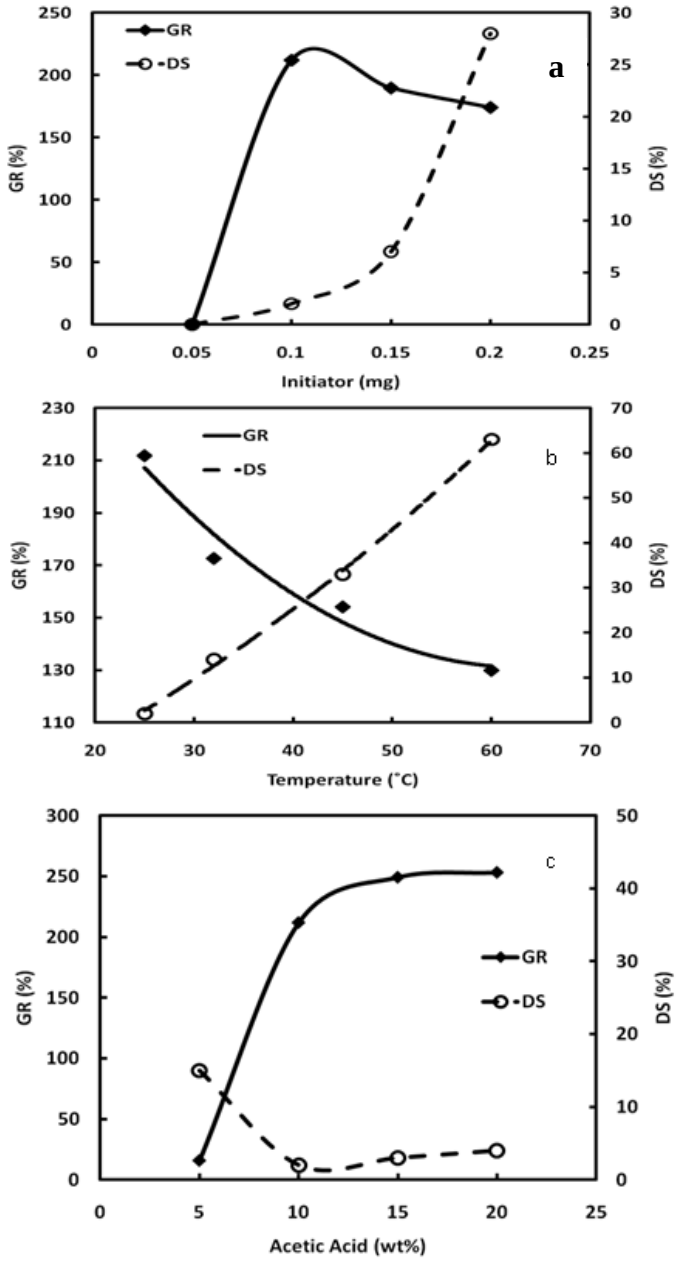

Figure 1. Effect of reaction parameters on grafting properties of chitosan-g-NIPAAM, where filled squares indicate GR% and open circles show the DS%. (a) Initiator concentration [acid concentration:10 wt%; reaction temperature: 25° C and reaction time: 24 h] ; (b) reaction temperature [initiator concentration: 0.1 mg; acid concentration:10 wt% and reaction time: 24 h]; (c) acetic acid concentration [initiator concentration: 0.1 mg; reaction temperature: 25° C and reaction time: 24 h].

leading to more substitutions and homopolymers. However, the increased rate of termination reduces the grafting ratio. When the temperature is close or over the LCST, thermo-reversible phase transition of grafted chains and homopolymers occurs. The solution turns from a water-soluble hydrophilic state to a water-insoluble hydrophobic state. Thus, the system is likely heterogeneous which ultimately affects the penetration and diffusion of NIPAAm monomers into the active sites on the chitosan and homopolymer radicals (43). Therefore, more substitution and less grafting ratio on chitosan backbone together with low percentage of hopolymer are expected.

3.4.1.3 Effect of acetic acid concentration

During the synthesis, it is also found that the amount of acetic acid applied to prepare chitosan aqueous solution in the reaction system has significant effect on grafting parameters. Therefore, this effect was systematically studied at different acetic acid concentrations ranging from 5 to 20 wt% with experimental results shown in Figure 1c and Table 2.

Initially, an increase in acetic acid concentration from 5 to 10 wt% results in increasing both the grafted and homopolymerized NIPAAm. The degree of substitution shows a significant drop over this acid concentration range. By further increasing acetic acid concentration, no significant effect on grafting parameters is observed. At low H^+ concentrations, a high degree of substitution and a low grafting ratio suggest more grafts with shorter chain lengths. It is attributed to the initiation Equations of 4 and 5, which are more favorable at low H^+ concentrations (42). At a higher acid concentration, high H^+ concentration leads to less initiation and subsequently less growing chains on chitosan backbone. Simultaneously, termination reactions get less favorable (Equations 12 & 13), which promote longer chain formation.

3.4.2 Solubility

Although the solubility of an injectable hydrogel is an important parameter, no comprehensive study has been reported on the solubility of chitosan-g-PNIPAAm yet. The

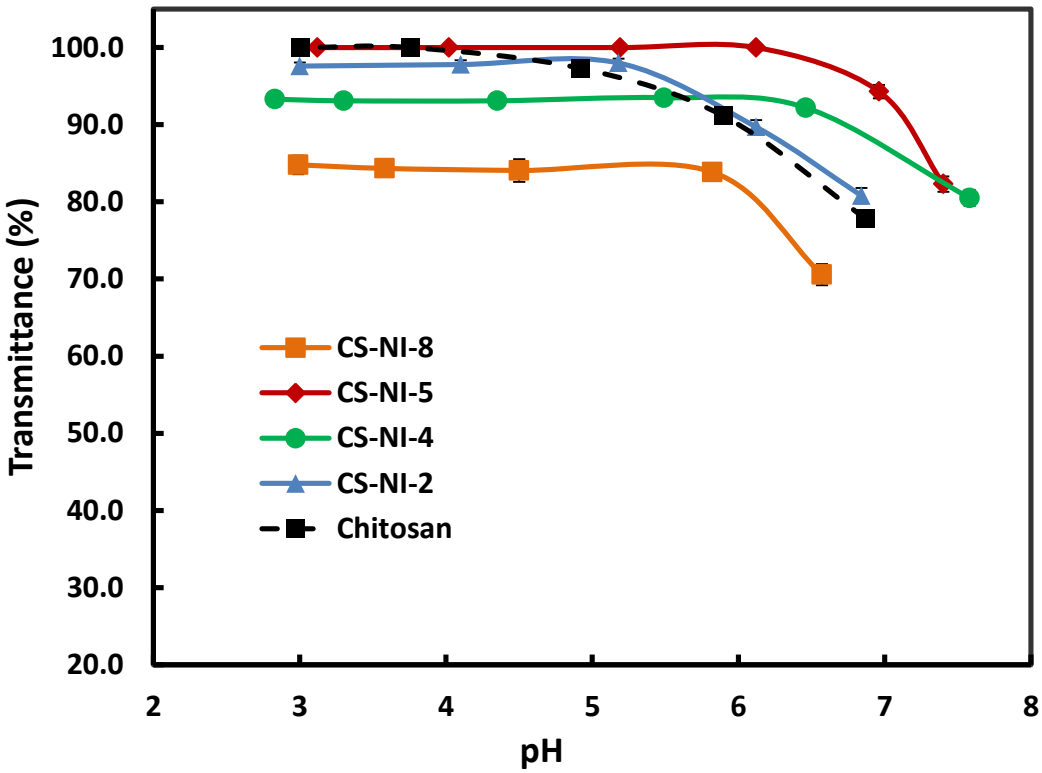

Figure 2. Solubility of chitosan and various chitosan-g-PNIPAAm samples at different pHs as measured by the turbidity of 0.44 mg mL^{-1} polymer solutions at 600 nm.

solubility of various copolymers was investigated by measuring the turbidity of polymer solutions against pH. Figure 2 demonstrates the pH-responsiveness of the grafting copolymers in comparison with chitosan. At low pH, all samples showed no significant change in their solubilities. However, the turbidity of each solution dropped dramatically at a certain pH, which indicates phase separation.

The plot reveals that by increasing the initiator concentration from 0.18 mmol for CS-NI-2 to 0.36 mmol for CS-NI-4, the pH-solubility profile is extended and the precipitation points elevate from pH ≈ 5.2 to pH ≈ 6.5. The solubility of chitosan in aqueous solution is governed by two main factors: protonation of free amino groups which results in interruption of intermolecular hydrogen bonds and hence improves solubility; and inter-

chain crystallinity which reduces the solubility. An increase in the initiator leads to a higher degree of substitution and results in less free amino groups along chitosan backbone (See section 3.4.1.1). As a result, the remaining amino groups need less protons for protonation, which could be provided at higher pHs. Moreover, these grafts can destroy the crystallinity and further improve water solubility.

Reducing the acetic acid concentration in the reaction solution for CS-NI-5 (5 wt%) results in a broader solubility window with an onset at pH ≈ 6.1 in comparison with CS-NI-2 (10 wt%), which is due to its higher degree of substitution (See section 3.4.1.3).

Precipitation at higher pHs was observed for the CS-NI-8 synthesized at 32 °C compared to CS-NI-2 (prepared at 25°C), which is in agreement with its higher graft numbers (See section 3.4.1.2). A decrease in turbidity of the stable phase (low pH) might be attributed to the non-homogeneous reaction condition that the polymerization temperature close to the LCST of PNIPAAm. More growing side chains on the chitosan backbones result in higher chance of self-crosslinking.

3.4.3 Rheological measurements

Mechanical properties of stem cells niche are known to modulate their fates along with the chemical and biophysical properties of the microenvironement. Cell mechano-sensitive pathways translate these cues into biochemical signals that guide the cell to a specific lineage or behaviour (44-46). Therefore, it is extremely important to control the mechanical properties such as elasticity when designing a biomaterial to mimic the 3D microenvironement for stem cells.

To investigate the viscoelastic characteristics of chitosan-g-PNIPAAm solution at different temperatures before and after gelation, we have conducted dynamic mechanical analysis. At low temperatures (20-30˚C), loss modulus (G") dominates the flow property and the value of storage modulus (G') is too small to be accurately measured, as shown in Figure 3b. This corresponds to the solution state of the samples. In this temperature range, the loss modulus decreases slightly with an increase in the temperature due to thermal movement

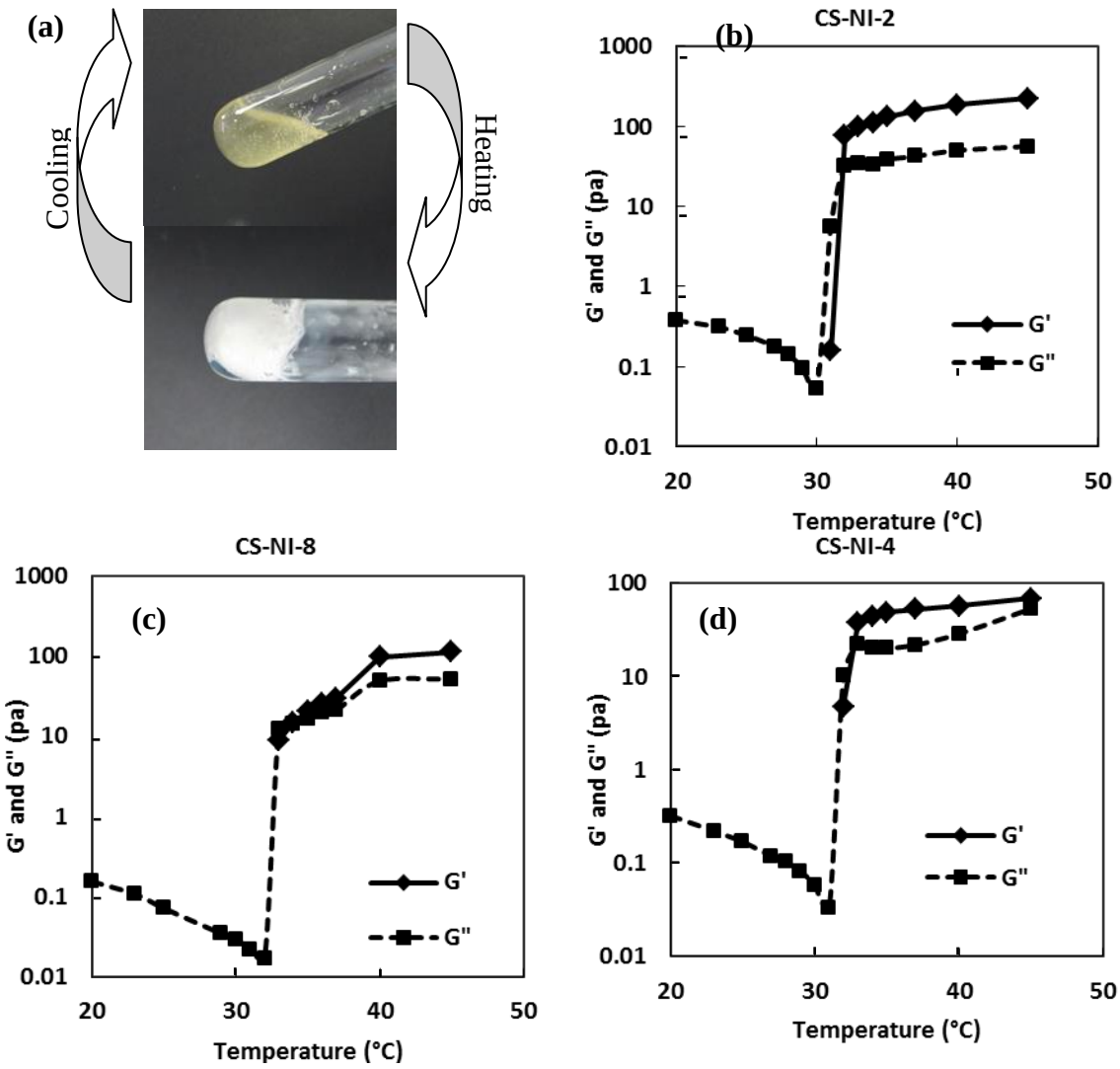

Figure 3. (a) Phase transition of chitosan-g-PNIPAAm upon heating and cooling; (b-d) Dynamic temperature sweeps of 36 mg/ml of chitosan-g-PNIPAAm copolymers in PBS (pH=7.4) at 1 rad/s.

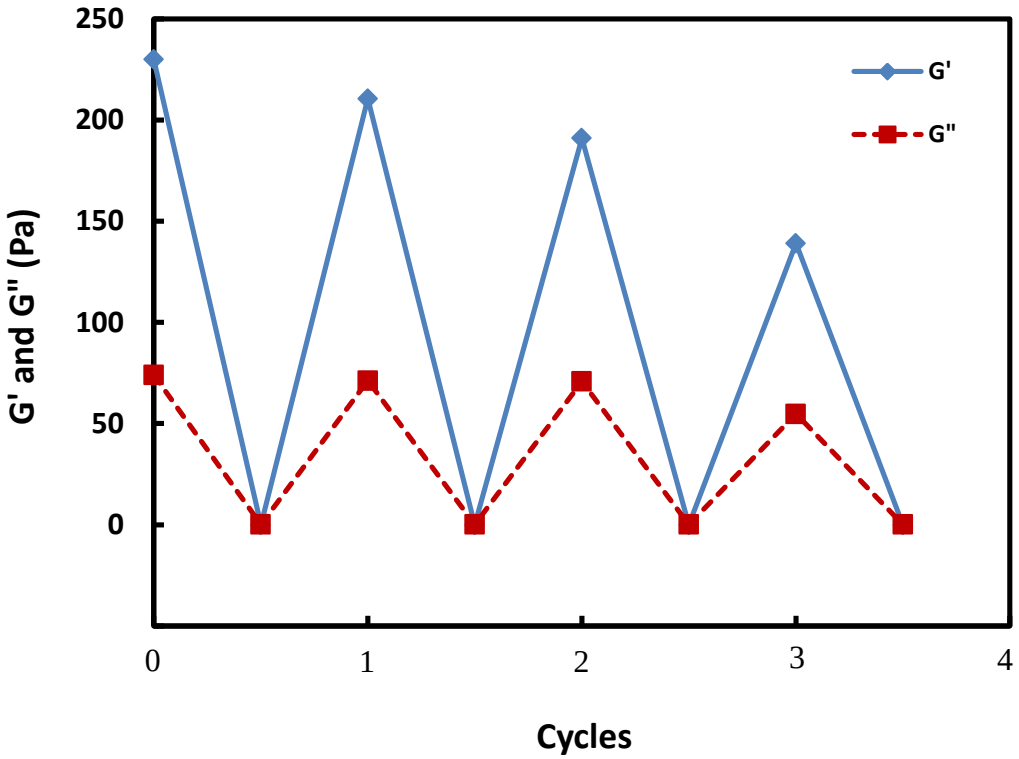

Figure 4. Storage and loss moduli of CS-NI-2 in stepwise periodic changes of temperature between 25 and 37° C at 1 rad/s.

of polymer chains leading to a lower viscosity (Arrhenius model). Beyond this temperature range, a sharp increase in both G' and G" is observed and after a cross-over between two lines, storage modulus, G', starts to become higher than loss modulus, G", indicating the formation of hydrogel (Figure 3b), which is evidenced by Figure 3a. The cross-over between G' and G" lines is considered as the gelation point and the corresponding temperature is termed as the gelation temperature (T_{gel}) which is close to the LCST of the copolymer.

Storage modulus which represent the mechanical strength of gels are 155 and 52 Pa at 37 °C for CS-NI-2 and CS-NI-4, respectively (Figures 3b and d). The drop could be explained by less degree of substitution and higher grafting ratio of CS-NI-2 in comparison to CS-NI-4 as a consequence of increasing initiator concentration (Figure 1a). It means longer

side chain lengths on chitosan backbone in CS-NI-2 could improve polymer chain entanglements and hence make the gels stronger.

Sample CS-NI-5 synthesized in 5 wt% acid does not show a phase transition with rise in temperature (Table 2). However, CS-NI-2 synthesized at 10 wt% acid undergoes a sol-gel transition and forms a relatively strong gel. It happens due to the very low grafting ratio and high degree of substitution (Figure 1c), which results in very short side chain lengths in CS-NI-5.

An increment in reaction temperature from 25 °C (CS-NI-2) to 32°C (CS-NI-8) results in the decrease in gel mechanical strength from 155 Pa to 30 Pa at 37 °C (Figures 3b and c). GR and DS in Figure 1b can be used to explain the decrease of mechanical strength. Increasing the reaction temperature makes more, but shorter PNIPAAm side chains on chitosan and consequencely gels are weaker.

To examine the reversibility of the sol-gel transition behaviour, several cycles of stepwise temperature change between 25 and 37˚C were applied and the mechanical modulus were monitored. As shown in Figure 4, the copolymer reveals a thermo-reversible behaviour. However, the storage modulus slightly decreases over cycles. After cooling the hydrogel, without any stirring, the solution is not a homogeneous liquid as it was before the first gelation. Therefore, when the solution is warmed up again, the structure could not regain a uniform network of hydrogel, resulting in a weaker hydrogel at further cycles.

3.4.4 Morphological studies

The microstructure of the hydrogel was studied using a scanning electron microscopy. Figure 5 presents the SEM micrographs of the hydrogel cross-sections. These images demonstrate the interconnected porous structure of the hydrogel which provides adequate space for nutrient delivery to cells and waste removal from their microenvironment as well as supports cell proliferation and migration.

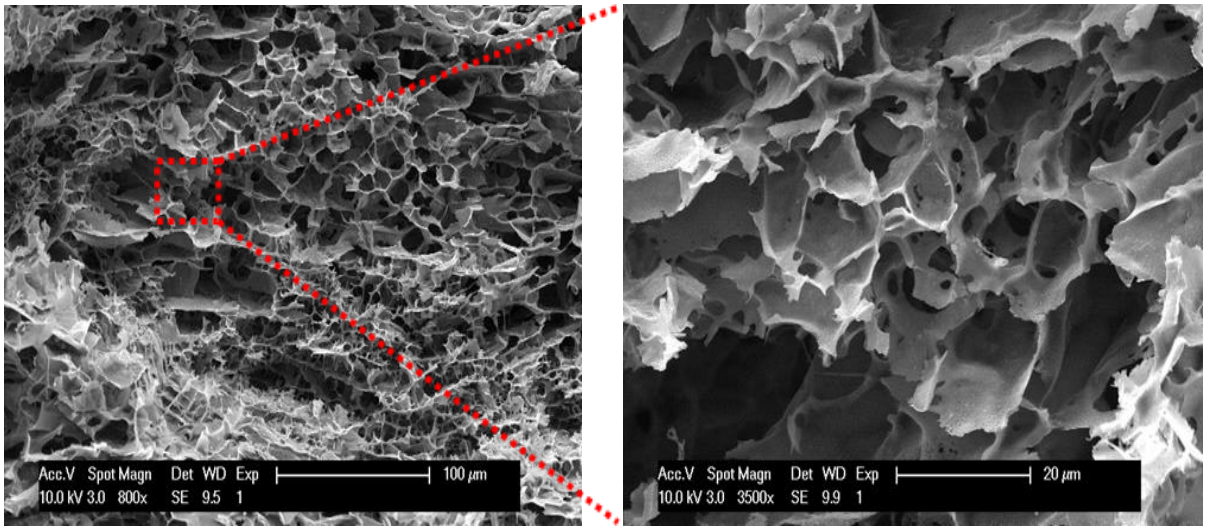

Figure 5. SEM micrograph of (a) chitosan-g-PNIPAAM (CS-NI-2) hydrogel and (b) the enlarged section of marked area in a.

3.4.5 *In vitro* three-dimensional cell culture

To investigate the interactions between MSCs and the hydrogel microenvironment, the MTT assays were employed. Cell viability was monitored over a 14 day period. Figure 6 shows the optical densities obtained from the MTT assays, which represent the number of viable cells. The results reveal that cells retain their biological activities and gradually proliferate inside the hydrogel during the first 7 days of cultivation, and after that, the cell number ceases to increase. However, cells remain metabolically active at day 14 as evidenced by the optical density, which is nearby the same as day 7. When cells are cultured in a 3D microenvironment, the cell viability and metabolic activity depend on several parameters including cell type, cell-seeding density and the surrounding material. Cardiac cells showed a constant number of viable cells within alginate hydrogel regardless of seeding density while proliferated significantly on 2D culture dishes (47). The same trend has been reported for the viability of osteoblasts encapsulated in Arg-Gly-Asp

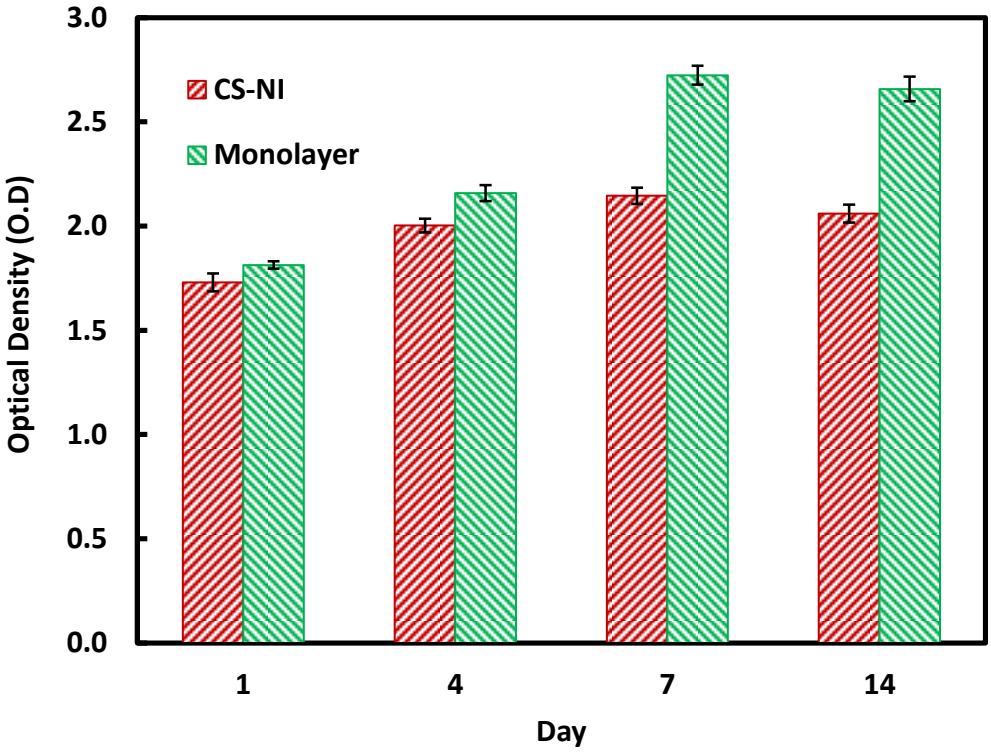

Figure 6. MSCs proliferation cultured in chitosan-g-PNIPAAm (CS-NI-2) hydrogels (red bars) and monolayers (green bars) measured by MTT assays. (n=3, *Mean± SE)*

(RGD)-modified poly (ethylene glycol) hydrogels (48). Hepatocytes entrapped in alginate scaffolds lost 66% of their metabolic activity within 7 days when seeded at the cell density of $0.28x10^6$ cells.cm^{-3} scaffold. However, they maintained their viability when cultured at an initial seeding density of $18.2x10^6$ cells.cm^{-3} after a 25% decrease within the first 24h (49). MSC metabolic activity decreased up to day 3 when cultured within chitosan/alginate polyelectrolyte complex-based scaffolds and then showed an slight increase until day 14 (50). In comparison with 2D cell culture, the number of MSCs is less in the 3D chitosan-g-PNIPAAm hydrogel. However, cell proliferation is observed from Figure 6 and the cellular biomass reaches a plateau after 7 days. The dynamic balance of cell number inside the hydrogel is due to insufficient oxygen and nutrient supplied to cells and lack of space when a certain cell density is reached. The cell survival is significantly improved through

manipulation of hydrogel properties; while the decreased cell viability of osteoblasts (36) and MSCs (37) have been reported when cells were cultured within the same hydrogel without manipulation. The retaining of cell viability is essential for downstream processing steps. For example, in the *in vivo* injection of cell-laden hydrogels to cure tissue damages, cells must be able to survive in human body environment so that cells can play their therapeutic roles. In tissue engineering applications using stem cells and hydrogels, cells need to keep viable during cell differentiation process. The preliminary results have demonstrated that the synthesized chitosan-g-PNIPAAm hydrogel with manipulated properties can support cell proliferation and retain cell viability for up to 14 days.

Figure 7 shows confocal laser scanning images of cells inside the hydrogel. Live and dead cells were stained in green and red, respectively. An increase in green intensity from day 1 (a-c) to day 7 (d-f) corresponds to cell number increment and also cell spread morphology. It verifies cell viability and proliferation during the seven-day period. However, the higher green intensity is not just implied by cell number. It is also partially due to cells' elongation and even some aggregations (48). These results are consistent with the MTT values. At day 1, more dead cells (red spots) could be observed in comparison with day 7 and the cell death at day 1 may be explained as a consequence of the first shock when cells adapting them with a new culture microenvironment. In order to determine cell distribution inside the hydrogel, images were taken at the different heights of 40, 80 and 120 μm above the bottom of the microwell plate, and images c & f, b & e and a & d (in Figure 7) were corresponding to three scans respectively. The images demonstrate that cells retained their viability and well distributed within the hydrogel, all through the different depths of the hydrogel inside the microwell, not on the top of the gel or at the bottom of the wells. Cell morphology at day 1 **(**Figure 7g) and day 7 (Figure 7h) can be observed from high-magnification (60×) images. Cells appear to be in a round shape at day 1 (Figure 7g), when there are still not strong cell-matrix interactions. In contrast, at day 7, cells lose their spherical shape and change to a spread or elongated structure in a 3D manner. This change might be due to cellular adaptation to the porous and interconnected microenvironment which encourages cells to attach to the surface of the pores and conform to the shape of the available lacuna. Cells start to grow and remain close to each other to impart cell-cell

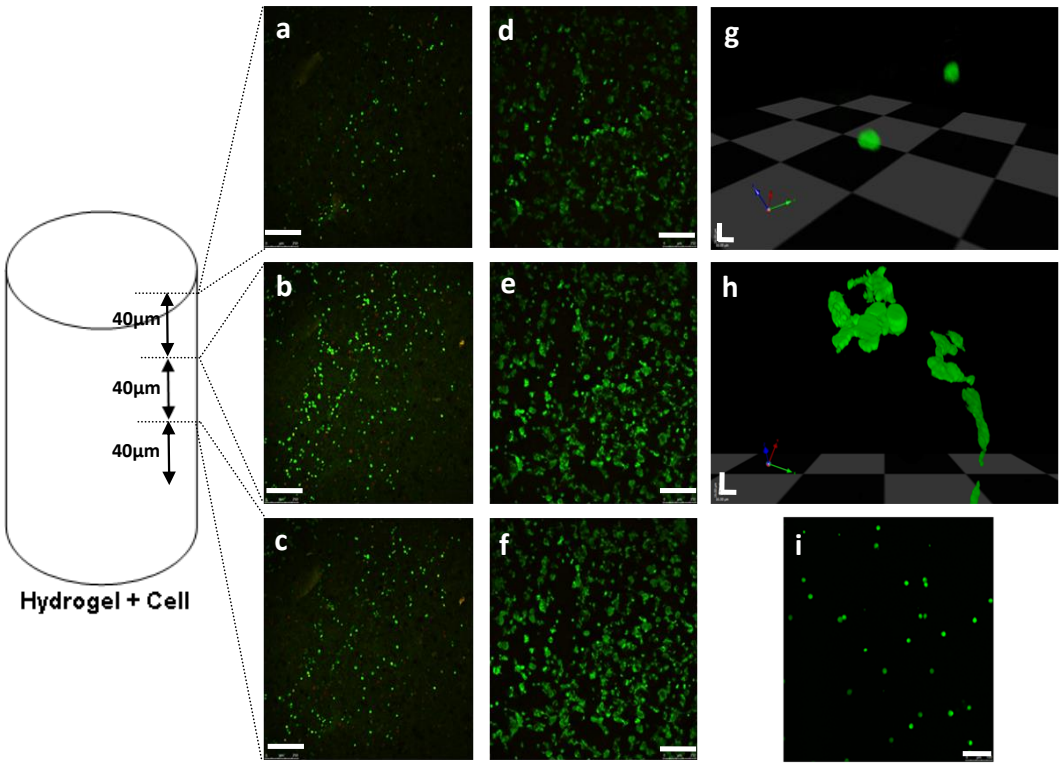

Figure 7. Confocal laser scanning images of MSCs cultured in chitosan-g-PNIPAAm (CS-NI-2) hydrogels:

(a-f): Comparison on cell densities at day 1 (a-c) and day 7 (d-f). Images were taken at different distances (a, d = 120 µm; b, e = 80 µm and c, f = 40 µm) from the bottom of the samples. 10X oil immersion objective. Scale bars are 250 µm.

(g, h): Z-series of images captured at high magnification (63X oil immersion objective) and converted to 3D images using the Volocity ™ software, at day 1 (g) and 7(h). Scale bars are 16 µm.

(i): Harvested cells after melting down the mixed hydrogels at day 7. 20X oil immersion objective. Scale bar is 100 µm.

interactions. They overlap inside the pore structure and individual cells are not easily distinguishable. However, spherical individual cells can be observed to be resuspended in the solution when the hydrogel converts to solution after reducing the temperature to an ambient one, which is shown in Figure 7i. The recovered cells can be re-cultured onto the 2D rigid surface, which means the cells are viable and can retain their migration capacity as well.

3.5 Conclusions

In this study, chitosan-g-poly(N-isopropylacrylamide) was synthesized as a thermo-responsive hydrogel. The synthesized polymer showed a thermo-reversible sol-gel transition behaviour at around 32˚C. It has been demonstrated that the solubility of copolymer aqueous solutions and mechanical strength of their gels could be manipulated by the number and length of PNIPAAm grafts which have been substituted with free amino groups on chitosan backbone. To control the graft ratio and chain length, the effect of polymerization conditions, including acid concentration, reaction temperature and initiator concentration on the degree of substitution and grafting ratio have been systematically investigated. SEM observations revealed the porous structure of the hydrogel which can facilitate oxygen and nutrient delivery to cells and cell growth. Mesenchymal stem cells were cultured in CS-g-PNIPAAm hydrogels. Cell viability and proliferation were evaluated by the MTT assay. It was demonstrated that cells retained their biological activities. Confocal images confirmed the cell viability and proliferation and uniform distribution inside the hydrogel while their phenotypic morphology was preserved. These results reinforce the suitability of chitosan-g-poly(N-isopropylacrylamide) copolymer as a well-controlled microenvironement for cells, especially stem cells and its potential applications in 3D cell culture, tissue engineering and regenerative medicine.

3.6 References

1. Zhang H, Dai S, Bi J, Liu KK. Biomimetic three-dimensional microenvironment for controlling stem cell fate. Interface Focus. 2011;1(5):792-803.
2. Van Vlierberghe S, Dubruel P, Schacht E. Biopolymer-based hydrogels as scaffolds for tissue engineering applications: a review. Biomacromolecules. 2011;12(5):1387-408.
3. Drury JL, Mooney DJ. Hydrogels for tissue engineering: scaffold design variables and applications. Biomaterials. 2003;24(24):4337-51.
4. Hoffman AS. Hydrogels for biomedical applications. Adv Drug Del Rev. 2002;54(1):3-12.
5. Baroli B. Hydrogels for tissue engineering and delivery of tissue-inducing substances. J Pharm Sci. 2007;96(9):2197-223.
6. Liu F, Urban MW. Recent advances and challenges in designing stimuli-responsive polymers. Prog Polym Sci. 2010;35(1):3-23.
7. Mano JF. Stimuli-Responsive Polymeric Systems for Biomedical Applications. Adv Eng Mater. 2008;10(6):515-27.
8. Alarcon CdlH, Pennadam S, Alexander C. Stimuli responsive polymers for biomedical applications. Chem Soc Rev. [10.1039/B406727D]. 2005;34(3):276-85.
9. Klouda L, Mikos AG. Thermoresponsive hydrogels in biomedical applications. European Journal of Pharmaceutics and Biopharmaceutics. 2008;68(1):34-45.
10. Yu L, Ding J. Injectable hydrogels as unique biomedical materials. Chem Soc Rev. 2008;37(8):1473-81.
11. Jeong B, Kim SW, Bae YH. Thermoresponsive sol–gel reversible hydrogels. Adv Drug Del Rev. 2012.
12. Fedorovich NE, Alblas J, de Wijn JR, Hennink WE, Verbout AJ, Dhert WJ. Hydrogels as extracellular matrices for skeletal tissue engineering: state-of-the-art and novel application in organ printing. Tissue Eng. 2007;13(8):1905-25.
13. Gutowska A, Jeong B, Jasionowski M. Injectable gels for tissue engineering. The Anatomical Record. 2001;263(4):342-9.

14. Shen Z, Bi J, Shi B, Nguyen D, Xian CJ, Zhang H, et al. Exploring thermal reversible hydrogels for stem cell expansion in three-dimensions. Soft Matter. 2012;8(27):7250-7.

15. Shen Z, Mellati A, Bi J, Zhang H, Dai S. A thermally responsive cationic nanogel-based platform for three-dimensional cell culture and recovery. RSC Advances. 2014;4(55):29146-56.

16. Di Martino A, Sittinger M, Risbud MV. Chitosan: A versatile biopolymer for orthopaedic tissue-engineering. Biomaterials. 2005;26(30):5983-90.

17. Hirano S, Tsuchida H, Nagao N. N-acetylation in chitosan and the rate of its enzymic hydrolysis. Biomaterials. 1989;10(8):574-6.

18. Freier T, Koh HS, Kazazian K, Shoichet MS. Controlling cell adhesion and degradation of chitosan films by N-acetylation. Biomaterials. 2005;26(29):5872-8.

19. Rabea EI, Badawy ME-T, Stevens CV, Smagghe G, Steurbaut W. Chitosan as antimicrobial agent: applications and mode of action. Biomacromolecules. 2003;4(6):1457-65.

20. Zheng LY, Zhu JF. Study on antimicrobial activity of chitosan with different molecular weights. Carbohydr Polym. 2003;54(4):527-30.

21. Ueno H, Mori T, Fujinaga T. Topical formulations and wound healing applications of chitosan. Adv Drug Del Rev. 2001;52(2):105-15.

22. Rzaev ZM, Dincer S, Pişkin E. Functional copolymers of N-isopropylacrylamide for bioengineering applications. Prog Polym Sci. 2007;32(5):534-95.

23. Kim SY, Cho SM, Lee YM, Kim SJ. Thermo‐and pH‐responsive behaviors of graft copolymer and blend based on chitosan and N‐isopropylacrylamide. J Appl Polym Sci. 2000;78(7):1381-91.

24. Lee WF, Chen YJ. Studies on preparation and swelling properties of the N‐isopropylacrylamide/chitosan semi‐IPN and IPN hydrogels. J Appl Polym Sci. 2001;82(10):2487-96.

25. Chen X, Song H, Fang T, Bai J, Xiong J, Ying H. Preparation, characterization, and drug‐release properties of pH/temperature‐responsive poly

(N‐isopropylacrylamide)/chitosan semi‐IPN hydrogel particles. J Appl Polym Sci. 2010;116(3):1342-7.

26. da Silva RM, López‐Pérez PM, Elvira C, Mano JF, Román JS, Reis RL. Poly (N‐isopropylacrylamide) surface‐grafted chitosan membranes as a new substrate for cell sheet engineering and manipulation. Biotechnol Bioeng. 2008;101(6):1321-31.

27. Wang J, Chen L, Zhao Y, Guo G, Zhang R. Cell adhesion and accelerated detachment on the surface of temperature-sensitive chitosan and poly (N-isopropylacrylamide) hydrogels. J Mater Sci Mater Med. 2009;20(2):583-90.

28. Don TM, Chou SC, Cheng LP, Tai HY. Cellular compatibility of copolymer hydrogels based on site‐selectively‐modified chitosan with poly (N‐isopropyl acrylamide). J Appl Polym Sci. 2011;120(1):1-12.

29. Lee SB, Ha DI, Cho SK, Kim SJ, Lee YM. Temperature/pH‐sensitive comb‐type graft hydrogels composed of chitosan and poly (N‐isopropylacrylamide). J Appl Polym Sci. 2004;92(4):2612-20.

30. Don T-M, Chen H-R. Synthesis and characterization of AB-crosslinked graft copolymers based on maleilated chitosan and N-isopropylacrylamide. Carbohydr Polym. 2005;61(3):334-47.

31. Chuang CY, Don TM, Chiu WY. Preparation of environmental-responsive chitosan-based nanoparticles by self-assembly method. Carbohydr Polym. 2011;84(2):765-9.

32. Sanoj Rejinold N, Sreerekha P, Chennazhi K, Nair S, Jayakumar R. Biocompatible, biodegradable and thermo-sensitive chitosan-g-poly (N-isopropylacrylamide) nanocarrier for curcumin drug delivery. Int J Biol Macromol. 2011;49(2):161-72.

33. Sundaresan V, Menon JU, Rahimi M, Nguyen KT, Wadajkar AS. Dual-responsive polymer-coated iron oxide nanoparticles for drug delivery and imaging applications. Int J Pharm. 2014;466(1):1-7.

34. Gui R, Wang Y, Sun J. Embedding fluorescent mesoporous silica nanoparticles into biocompatible nanogels for tumor cell imaging and thermo/pH-sensitive in vitro drug release. Colloids Surf B Biointerfaces. 2014;116:518-25.

35. Wang Y, Wang J, Ge L, Liu Q, Jiang L, Zhu J, et al. Synthesis, properties and self‐assembly of intelligent core‐shell nanoparticles based on chitosan with different molecular weight and N‐isopropylacrylamide. J Appl Polym Sci. 2013;127(5):3749-59.

36. Lee J, Jung M, Park H, Park K, Ryu G. Synthesis and characterization of thermoresponsive chitosan copolymer as a novel biomaterial. Journal of Biomaterials Science, Polymer Edition. 2004;15(8):1065-79.

37. Cho JH, Kim S-H, Park KD, Jung MC, Yang WI, Han SW, et al. Chondrogenic differentiation of human mesenchymal stem cells using a thermoresponsive poly (N-isopropylacrylamide) and water-soluble chitosan copolymer. Biomaterials. 2004;25(26):5743-51.

38. Cao Y, Zhang C, Shen W, Cheng Z, Yu LL, Ping Q. Poly (N-isopropylacrylamide)–chitosan as thermoresponsive in situ gel-forming system for ocular drug delivery. J Controlled Release. 2007;120(3):186-94.

39. Recillas M, Silva LL, Peniche C, Goycoolea FM, Rinaudo M, Argu□elles-Monal WM. Thermoresponsive behavior of chitosan-g-N-isopropylacrylamide copolymer solutions. Biomacromolecules. 2009;10(6):1633-41.

40. Chen JP, Cheng TH. Thermo‐Responsive Chitosan‐graft‐poly (N‐isopropylacrylamide) Injectable Hydrogel for Cultivation of Chondrocytes and Meniscus Cells. Macromol Biosci. 2006;6(12):1026-39.

41. Chen C, Liu M, Gao C, Lü S, Chen J, Yu X, et al. A convenient way to synthesize comb-shaped chitosan-graft-poly (N-isopropylacrylamide) copolymer. Carbohydr Polym. 2013;92(1):621-8.

42. McDowall D, Gupta B, Stannett V. Grafting of vinyl monomers to cellulose by ceric ion initiation. Prog Polym Sci. 1984;10(1):1-50.

43. Gupta K, Khandekar K. Temperature-responsive cellulose by ceric (IV) ion-initiated graft copolymerization of N-isopropylacrylamide. Biomacromolecules. 2003;4(3):758-65.

44. Reilly GC, Engler AJ. Intrinsic extracellular matrix properties regulate stem cell differentiation. J Biomech. 2010;43(1):55-62.

45. Engler AJ, Sen S, Sweeney HL, Discher DE. Matrix Elasticity Directs Stem Cell Lineage Specification. Cell. 2006;126(4):677-89.

46. Discher DE, Mooney DJ, Zandstra PW. Growth Factors, Matrices, and Forces Combine and Control Stem Cells. Science. 2009 June 26, 2009;324(5935):1673-7.

47. Dar A, Shachar M, Leor J, Cohen S. Optimization of cardiac cell seeding and distribution in 3D porous alginate scaffolds. Biotechnol Bioeng. 2002;80(3):305-12.

48. Burdick JA, Anseth KS. Photoencapsulation of osteoblasts in injectable RGD-modified PEG hydrogels for bone tissue engineering. Biomaterials. 2002;23(22):4315-23.

49. Dvir-Ginzberg M, Gamlieli-Bonshtein I, Agbaria R, Cohen S. Liver tissue engineering within alginate scaffolds: effects of cell-seeding density on hepatocyte viability, morphology, and function. Tissue Eng. 2003;9(4):757-66.

50. Ceccaldi C, Bushkalova R, Alfarano C, Lairez O, Calise D, Bourin P, et al. Evaluation of polyelectrolyte complex-based scaffolds for mesenchymal stem cell therapy in cardiac ischemia treatment. Acta Biomater. 2014;10(2):901-11.

CHAPTER FOUR

4. Microengineered 3D Cell-laden Thermoresponsive Hydrogels as a Platform for Bi-zonal Cartilage Tissue Engineering Using Mesenchymal Stem Cells

Microengineered 3D cell-laden thermoresponsive hydrogels as a platform for bi-zonal cartilage tissue engineering using mesenchymal stem cells

Amir Mellati[a], Chia-ming Fan[b], Ali Tamayol[c], Sheng Dai[a], Jingxiu Bi[a], Bo Jin[a], Cory Xian[b], Ali Khademhosseini[c,d,e], Hu Zhang[a]*

[a]School of Chemical Engineering, the University of Adelaide, Adelaide SA 5005, Australia

[b] Sansom Institute for Health Research, School of Pharmacy and Medical Sciences, University of South Australia, Adelaide, SA 5001, Australia

[c] Center for Biomedical Engineering, Department of Medicine, Brigham and Women's Hospital, Harvard Medical School, Boston, MA 02139, USA

[d] Harvard-MIT Division of Health Sciences and Technology, Massachusetts Institute of Technology, Cambridge, MA 02139, USA

[e] Wyss Institute for Biologically Inspired Engineering, Harvard University, Boston, MA 02115, USA

*Corresponding author

E-mail: hu.zhang@adelaide.edu.au

Tel: + 61 8 8313 3810

4.1 Abstract

Engineering the articular cartilage with the same zonal organization as the native tissue remains a great challenge for tissue engineering. In this study, we employed a micropatterning technique to mimic the cellular shape and orientation within the superficial and middle zone of the natural cartilage. Chitosan-g-poly(N-isopropylacrylamide) (CS-g-PNIPAAm) was synthesized as a thermresponsive copolymer and mesenchymal stem cells were incoporated within the CS-g-PNIPAAm hydrogel. Biochemical assays show 6 and 7 fold increment in glycosaminoglycans and total collagen at 28 day incubation in chondrogenic medium, respectively. Chondrogenic differentiation was also verified qualitatively by histological and immunohistochemical assessments. Three-dimensional micropatterned cell-laden hydrogels were fabricated using poly(ethylene glycol) dimethacrylate micromolds. Within the 50 μm wide microconstructs, 75 ± 6% of cells are oriented with an aspect ratio of 2.075 ± 0.161 at day 5, which is the highest level of cell alignment and elongation, and much greater than those (12 ± 7% alignment and a shape index of 1.202 ± 0.07) of the unpatterned constructs. The highly oriented microconstruct was used for mimicing the cell shape and organization in the superficial zone cartilage while the unpatterned one for middle zone. Our results suggest that micropatterning of 3D cell-laden thermoresponsive hydrogels is a promising platform for multi-zonal cartilage tissue engineering.

4.2 Introduction

Articular cartilage is a thin layer of hyaline cartilage covering the bone heads of articulating joints that permits smooth motion between adjoining bony segments (1). It is a multiphasic tissue consisting of chondrocyte cells, interstitial fluid and extracellular matrix (ECM) mainly composed of collagen fibres and proteoglycans (PG) (2). Three important zones or layers are distinguishable in articular cartilage as shown in Scheme 1a (3). The closest layer to the cartilage surface is termed as superficial zone where chondrocytes are ellipsoidal and parallel to the surface. The middle or transitional zone is laid under the superficial zone. Chondrocytes are rounder in comparison to the superficial zone and they are randomly aligned. The deep zone is below the middle layer. Chondrocytes are spherical in shape and are aligned columnar and perpendicular to the tidemark (4-6). Each layer has its specific mechanical properties and biochemical composition.

Cartilage-related diseases such as arthritis are the most common reasons for giving rise to disabilities around the world (7). Daily accidents may also damage this soft tissue. Unfortunately, articular cartilage has limited self-repair potential (8). Among various therapeutic strategies to repair a damaged articular cartilage, tissue engineering is one of the most appealing approaches. However, many challenges remain to be resolved in this technique, including selecting an appropriate cell source and a matrix as well as recreating the zonal organisation. Various cell sources can be used in cartilage tissue engineering, including chondrocytes as cartilage-specific adult cells, embryonic stem cells (ESCs), induced pluripotent stem cells (iPS) or adult stem cells such as mesenchymal stem cells (MSCs) (9). MSCs are considered as an attractive candidate because of their ease of isolation, *in vitro* expansion, and differentiation into cartilage (10). Interestingly, MSCs can be differentiated to zonal chondrocytes in a suitable microenvironment (11). A variety of artificial matrices have been explored for cartilage tissue engineering, and hydrogels are one of the most suitable choices due to their similarity to the natural ECM of the cartilage which is a highly hydrated tissue (12). Chitosan-based hydrogels have great potential to enhance chondrogenesis and to modulate the chondrocyte morphology, differentiation and

function because of its structure similar to glycosaminoglycans (GAGs) and hyaluronic acid in PGs of native articular cartilages (13-16).

Recreating the aforementioned spatially-zoning organization of the native articular cartilage is the most challenging. This complex zonal organization supports cartilage functions within body joints (17). Various strategies (i.e cell-, matrix-, bioreactor- and bioactive molecule-based) have been employed by researchers to mimic the layered articular cartilage. In cell-based approaches, incorporation of different zonal chondrocytes in a depth-dependent fashion within either a single layer (18) or multilayered hydrogel of the same material (19, 20) was found to have a potential to recreate biomimetic zones. Furthermore, Bhumiratana et al. showed that condensed mesenchymal cell bodies and their fusion into homogeneous cellular aggregates (21) resulted in a stratified structure of the articular cartilage. Matrices have also been manunipulated to recapitulate the organized zonal architecture of the native cartilage. Encapsulation of MSCs (22, 23) or chondrocytes (24, 25) in a layered hydrogel made of the same material (26) or in the spatially composition-varying matrix displayed encouraging results. Other matrix-based strategies include depth-dependent regulation of the physical and mechanical properties by altering gel concentration (27), degradability (28), pore size through bioprinting (29), nanofiber size and orientation (6, 17), nanoparticle concentration (30) or combinatorial scaffold morphologies (e.g. electrospun poly(caprolactone) (PCL) fibers on top and porous PCL scaffold in bottom) (31). Bioreactors have also been exploited to stimulate the cell-seeded constructs by mechanical or chemical gradients (32-35). Gradient delivery of bioactive molecules or nutrients such as oxygen (36) and glucose (37) is the fourth approach. In addition, the combination of various approaches may enhance the zonal variation similar to the inhomogeneity of the native cartilage. Thorpe et al. reported that manipulation of oxygen tension and mechanical cues over the depth of cell-laden constructs to mimic the zones of the cartilage by controlling MSC differentiation (38). Zonal chondrocytes in poly (ethylene glycol)-based (PEG) hydrogels containing exogenous type I collagen, hyaluronic acid (HA), or chondroitin sulfate (CS) at different layers demonstrated zone-dependent cellular responses (39). While some of these sterategies have been focous on regenerating the zone-specific ECM biochemical composition at a molecular level, or on mimicking the

zone-specific mechanical properties, other efforts have been made to resemble the layered physical microarchitecture of the native cartilage, such as celluralr shape and arrangement. Micropatterning might be potentially an alternative apporoach for mimicking the microstructural organisation of cartilage zones. Micropatterning is a microfabrication method based on soft lithography. It has been demonstrated that micropatterning is an effective method for cell alignment and elongation in 2D or 3D (40). As zonal chondrocytes were required to be kept in a 3D microenvironment to preserve or restore their zone-specific characteristics (41), thus a 3D micropatterned construct would be needed for engineering different zones of the cartilage. Although UV curing of photocrosslinkable hydrogels is the most popular approach in microfabrication of 3D cell-encapsulated patterned constructs, UV irradiation as well as UV-induced free radicals during the crosslinking process can potentially bring damage to the cells inside the constructs (42, 43) or alter cell characteristics and functionalities. Cell viability is highly dependent on UV exposure time and photoinitiator concentration (43) which are critical parameters in regulation of gel physical and mechanical properties as well. As a consequence, preparation of such constructs with optimum properties might be sacrificed by reduced cell viability. Thermoresponsive hydrogels can be an alternative to form the constructs with temperature change rather than UV curing. Thermoresponsive polymers have attracted a lot of interest in 3D cell culture and differentiation due to ease of cell distribution and instant cell release. These polymers have been also widely used to prepare thermo-responsive microengineered platforms which could be exploited for 2D patterned cell culture and co-culture (44), co-cultured cell sheets (45), patterned cell layers (46) and cell aggregates from responsive microwells (47). These constructs were prepared through the modified thermoresponsive surface of the substrates and templates. Switchable and dynamic properties of these constructs can facilitate cultivation and detachment of cells and microtissues. However, there are few reported studies on 3D constructs based on thermoresponsive polymers. In one recent report, thermoresponsive polymers were used for fabricating micromolds and cell-embedded agarose was cast in the micromolds for sequential micropatterns (48).

In this study, we first diferentiated mesenchymal stem cells into chondrocytes in a thermoresponsive polymer structure in 3D based on chitosan-g-poly(N-isopropylacrylamide) (CS-g-PNIPAAm). The cell-laden copolymer was then cast into micropatterns generated from PEG-DMA as a template to mimic cellular morphology and orientation within the superficial zone of the native articular cartilage. Our results suggest that the microengineered 3D cell-laden CS-g-PNIPAAm can offer great promise in bi-zonal cartilage tissue engineering.

4.3 Materials and methods

4.3.1 CS-g-PNIPAAm synthesis and characterization

CS-g-PNIPAAm was synthesized by free radical grafting polymerization as described in our recent work (49). Briefly, *N*-Isopropylacrylamide (NIPAAm) (Sigma-Aldrich, MO, USA) was purified by recrystallization in *n*-hexane, and then 1 wt% chitosan (MW of 200-300 kDa) (Acros Organic, NJ, USA) in 30 mL aqueous acetic acid (10 wt%) was mixed with 17.7 mmol purified NIPAAm monomer and the mixture was degassed. Polymerization was initiated by adding 0.18 mmol ammonium cerium (IV) nitrate (CAN) (Acros Organic, NJ, USA) and reaction was carried out for 24 h under nitrogen atmosphere. The solution was condensed and precipitated in an excess amount of tetrahydrofuran/hexane (4:1). The precipitate was further purified by methanol soxhelet extraction for 48 h. The purified product was dried under vacuum. Two products (CS-NI-1 and CS-NI-2) with different properties were obtained at the polymerisation temperature of 60 °C and 25 °C, respectively. Rheological measurement was conducted using a SR5 controlled stress rheometer (Rheometric Scientific, USA) as described before (49).

4.3.2 3D cell culture in hydrogel

Mesenchymal stem cells (MSCs) (murine, 10T1/2, RIKEN cell bank, Japan) were cultured in Dulbecco's Modified Eagle's Medium (DMEM) supplemented with 10 % fetal bovine

serum (FBS), 100 U/mL of penicillin, 100 mg/mL of streptomycin and 2 mM/L L-glutamine (All from Gibco, NY, USA) and incubated at 37°C in a humidified atmosphere with 5% CO_2. MSCs were detatched by trypsine-EDTA (Gibco, NY, USA) and resuspended in a fresh growth medium for further use.

In a typical 3D cell culture experiment, the polymer sample was dissolved in PBS to prepare a polymer solution of 31.5 mg/mL (pH of 7.4) and sterilized by autoclave. Cell suspension and copolymer solution were mixed to prepare a cell/polymer mixture at a final cell concentration of 1.0 x 10^6 cells/mL and a final polymer concentration of 30 mg/mL. A 300 µL of the cell/polymer mixture was transferred to each well on a 24-well plate and incubated for 1 h at 37˚C to form cell-laden hydrogels. The same cell concentrations were prepared by mixing cells and PBS without copolymer and served as a negative control. Fresh growth medium (2 mL) was topped up to each well and further incubated in an incubator at 37˚C and 5% CO_2 for 7 days. Medium was replaced with fresh medium once every other day. Two hydrogel samples were used to compare the cell performance and the best sample was further employed for invetigating the influence of polymer concentration on cell proliferation. The same procedure was repeated using 20, 25 and 30 mg/mL solutions of the selected polymer sample.

4.3.3 The MTT assay

Cell viability and proliferation within the cell-seeded hydrogels were evaluated using the MTT assay. At each time point, 0.5 mL of 3-(4,5-dimethylthiazol-2-yl)-2,5-diphenyltetrazolium bromide (MTT) (Molecular Probes, OR, USA) (5 mg/ml in PBS) was added to each well and then incubated for 4 h at 37˚C. All the liquid content was replaced with 1 mL dimethyl sulfoxide (DMSO) to make sure that formazan crystals were solubilized completely. After 1 h incubation, all of the well content (including liquid and gel) was transferred to an eppendorf tube, vortexed briefly and centrifuged at 10,000 rpm for 5 min. Finally, 200 µL of supernatant was transferred to a 96-well plate and the absorbance was read using a microplate reader (ELx808, BioTek, USA) at 595 nm. The absorbance of cell-free hydrogels (negative control) was deducted from cell-encapsulated

hydrogels to remove any inteference from hydrogel-MTT reaction. Triplicates for every time point were used.

4.3.4 3D MSC differentiation in hydrogel

The selected polymer sample from the previous experiment was mixed with MSC suspension so that the final cell seeding density was 1.0×10^7 cells/mL of hydrogel and the final polymer concentration was fixed at the optimised value obtained from the above experiment. Tranferable wells were prepared by mounting Press-To-Seal^{TM} silicone rubbers (Molecular Probes, OR, USA) on cover glasses and the wells were then sterilized. The cell-polymer solution (300 μL) was added to the wells and incubated at 37°C to acheive cell-embedded hydrogels. Rubber-made wells were tranferred to each well on a 6-well plate. Five mL of chondrogenic medium was added to each well, contating high glucose-DMEM, 1% insulin, transferrin, selenous acid (ITS)+Permix (BD Bioscience, MA, USA), 10^{-7} M dexamethasone (Sigma-Aldrich), 10 ng/mL transforming growth factor-beta 1 (TGF-β1) (Peprotech, NJ, USA), 50 μg/mL ascorbate-2-phosphate (Sigma-Aldrich), 100 U/mL of penicillin, 100 mg/mL of streptomycin and 2 mM/L L-glutamine. Constructs were kept in incubator at 37 °C and 5% CO_2 for continuous 28 days. The medium was being changed every day. Four wells at predefined sampling days were taken out for biochemical analysis (3 wells) and for histological and immunohistochemical staining (1 well).

4.3.5 Biochemical analysis

DNA, GAG and total collegen content were quantified by Hoechst 33258, DMMB and hydroxyproline assays as described previously (50, 51). At each time point, constructs were collected, rinsed with prewarmed PBS, freeze-dried for 48 h and digested by incubation in a papain (Sigma-Aldrich) solution (125 μg/mL) at 60 °C for 16 h. The supernatant of the papain-digested hydrogels was used for biochemical assessment.

DNA content was measured by the Hoechst 33258 assay. A 30 µL of the supernatant of the papain-digested constructs was added to 3 mL of 0.1 µg/mL Hoechst 33258 dye (Sigma-Aldrich) solution in TNE buffer and the intensity was read using a RF-5301PC fluorospectrometer (Shimadzu, Japan) at 360 nm excitation and 460 nm emission. The corresponding DNA amount was calculated based on a ds-calf Thymus DNA type I (Sigma-Aldrich) standard curve.

For GAG analysis, the supernatant was reacted with 1,9-dimethylmethylene blue (DMMB) (Sigma-Aldrich) in PBE buffer solution (46 µM) and absorbance was read at 525 nm by the spectrophotometer. Chondroitin sulphate (Sigma-Aldrich) was served to generate an standard curve.

Total collagen was evaluated by the hydroxyproline assay. Papain-digested supernatant was hydrolyzed in 6 N HCl for 18 h at 110 °C, then neutralized and combined with chloramine-T (Sigma-Aldrich) soultion (15.7 mg/mL) followed by incubation at room temperature for 20 min. The solution was mixed with Ehrlich's reagent, vortexed and further incubated for 30 min at 60 °C. Finally, the absorbance was read at 550 nm using the spectrophotometer and collagen content was computed according to the trans-4-hydroxy-L-proline (Sigma-Aldrich) standard curve. All values of biochemical assays were normalized to the dry weight of the constructs.

4.3.6 Histological and immunohistochemical staining

Cell-seeded hydrogels were transferred into cryomolds, embedded in Tissue-Tek® O.C.T™ coumpound (Sakura, The Netherlands), and then cryosectioned in 10 µm thickness. Sections were fixed in cold acetone for 10 min, air dried and washed in PBS. Cell-laden microconstructs were also fixed in 4% paraformaldehyde for 30 min. For GAG histological staining, sections were stained in 1% safranin O (Sigma-Aldrich) solution for 30 min. Sections were also immunohistochemically stained for collagen type II (a commonly used marker for chondrogenesis) (52). Sections were quenched in 3% hydrogen peroxide for 20 mins and treated with 1.0 µg/ml proteinase K for 20 mins for antigen retrieval. After being blocked for an hour with 5% rabbit serum (Sigma-Aldrich), sections were incubated with a

primary antibody (rat anti-collagen-II) (Santa Cruz Biotechnology, TX, USA) at 1:800 dilution overnight. Labelling was visualized with a rabbit anti-rat biotinylated IgG (Dako, Denmark) (1:600), streptavidin and biotin mix (Thermo Scientific, MA, USA) (1:700), and liquid diaminobenzidine (DAB+) (Dako, Denmark) substrate for colour development. Sections were then counterstained in haematoxylin (United Biosciences, QLD, Australia). Sections were obsereved by an Olympus BX41 microscope (Japan).

4.3.7 Micropatterning of CS-g-PNIPAAm

To prepare micropatterned templates, 0.5% (w/v) photoinitiator (2-hydroxy-1-(4-(hydroxyethoxy)phenyl)-2-methyl-1-propanone; Irgacur 2959) (CIBA Chemicals, NY, USA) was added to 20% solution of poly(ethylene glycol)$_{1000}$-dimethacrylate (PEG-DMA) (Polyscience,PA, USA) in PBS and vortexed. Then, 90 µL of the preheated solution was pipetted between an untreated glass and 3-(trimethoxysilyl)propyl methacrylate (TMSPMA) (Sigma-Aldrich) coated glass slide separated by a 150 µm spacer. The photomask was placed on top of the glass slide and exposed to 800 mW UV light (8 cm distance) for 120 s. After photocrosslinking, the glass slide was removed and washed gently with preheated PBS to remove unreacted solution. Unpatterned rectangular PEG-DMA hydrogels were prepared with the same method. The micropatterned and unpatterned PEG-DMA hydrogels were kept in PBS until use.

Then, 90 µL of aforementioned cell-laden CS-g-PNIPAAm solution (cell density: 1.0×10^7 cells/mL polymer solution, polymer concentration: 25 mg/mL) was placed on top of PEG-DMA micropatterned template, gently coverslipped and left in an incubator at 37 °C for 20 min to become gel. The coverslip was carefully taken off by sliding and any excess CS-g -PNIPAAm on PEG-DMA spacing was removed by sliding a sterile coverslip all over the micropatterned surface for several times. Micropatterned cell-laden CS-g-PNIPAAm hydrogel within PEG-DMA microchannels (hereinafter microconstructs) were transferred to a 6-well plate containing either preheated growth or chondrogenic medium and kept in a humidified incubator at 37˚C and 5% CO_2. Medium was replaced once every other day.

4.3.8 Live/dead cell staining

The LIVE/DEAD® cytotoxicity/viability kit (Molecular Probes, OR, USA) was used to stain live and dead cells. A working solution of 0.5 µL/mL of calcein acetotoxymethyl ester (calcein AM) and 2 µL/mL of ethidium homodimer-1 (EthD-1) in PBS were freshly prepared. At day 1 and 5, the growth medium was removed and microconstructs were washed with 5 mL prewarmed PBS (37˚C). After the PBS solution was removed, 0.5 mL of dye working solution was added on top of microconstructs and then incubated at 37˚C for 20 min. The dye solution was removed and the hydrogel was washed twice with 5 mL prewarmed PBS. All the liquid was removed and the extra liquid from the hydrogel was absorbed by gently touching its surface with a piece of tissue paper. As a result, the gel was made highly concentrated (semi-dried) to stabilize the structure of the thermoresponsive hydrogel at room temperature and prevent it from dissolution during handling. Embedded cells were observed under a flourescence microscope (Nikon TE 2000, Japan) equipped with a temperature controlled chamber to keep the temperature at 37 ˚C. Excitation wavelengths were set to 494 and 528 nm and emission wavelengths were at 517 and 617 nm for live (green) and dead (red) cells, respectively.

4.3.9 Quantification of cellular alignment and elongation

For F-actin staining, cell-seeded gels were fixed in paraformaldehyde (4%) for 30 min. The cells were then permeabilized in a Triton X-100 solution (0.1% w/v) in PBS for 20 min and blocked in bovine serum albumin (BSA) (1% w/v) for 1 h. The samples were then incubated in a solution of 1:40 ratio of Alexa Fluor-594 phalloidin (Invitrogen) in BSA (0.1%) for 45 min at room temperature to stain actin filaments of the cell cytoskeleton. Samples were rinsed in PBS and counterstained with 1 µL/mL of 4’,6-diamidino-2-phenylindole (DAPI) (Sigma-Aldrich) in PBS for 5 min in an incubator. Samples were washed with PBS and visualized using a Nikon TE 2000 fluorescence microscope (Japan), equipped with an environmental chamber. The nuclear shape index and alignment of DAPI stained nuclei were measured to quantitatively evaluate overall cell elongation and alignment as previously demonstrated (53, 54). The nuclear alignment angles, defined as

the orientation of the major axis of the best ellipse fit to the individual nuclei with respect to the horizontal axis, were measured using the built-in functions of the NIH ImageJ software. All nuclear alignment angles were then normalized to the respective preferred nuclear orientation defined as the mean orientation of all nuclei per sample. For analysis, alignment angles were subsequently grouped in 10° increments with respect to the preferred nuclear orientation, and all cells within less then 20° were considered to be aligned as previously described (53). Additionally, the shape index, the aspect ratio between the major elliptic axis and the minor elliptic axis of each individual cell nucleus, was used to determine the nuclear elongation and was calculated using the built-in functions of the NIH ImageJ software. A shape index of 1 representes a circle. The effects of channel width and culture time on cellular alignment and elongation were investigated by using micropatterned gels with a channel size of 50, 100 and 150 μm at different post-seeding time (1 and 5 days). For quantification, at least four images per sample and from three samples were used for each condition.

4.3.10 Multiphoton microscopy

After 21 days incubation in chondrogenic medium, micropatterned cell-laden microconstructs were rinsed twice in preheated PBS. All the liquid was removed and the exess liquid was extracted from the CS-g-PNIPAAm hydrogel by gently touching its surface with a piece of tissue paper until the semi-dried thermoresponsive hydrogel could not become solution anymore. The autofluorescence (AF) and second harmonic generation (SHG) signals were detected using a LaVision BioTec TriM Scope multiphoton microscope (Germany) with two-photon excitation at 840 nm using a Ti:Sa laser (Coherent, CA, USA) and emission bandwidths of 470-550 nm and 410-430 nm for autofluorescence and SHG, respectively.

4.3.11 Statistical analysis

All measurements were performed in triplicates for all measurment points unless otherwise stated. Data obtained from our experiments are represented as mean ± SD (standard deviation) or ± SE (standard error). Statistical significance was determined by application of student's t-test. The differences were considered to be significant when $P < 0.05$.

4.4 Results and discussion

4.4.1 Hydrogel optimization for 3D cell culture

CS-g-PNIPAAm hydrogels were first screened and optimised for 3D MSC culture and maintenance. A range of CS-g-PNIPAAm hydrogels with different grafting chractrestics and therefore different mechanical properties were prepared in our privous work (49).

Table 1. Summary for the graft polymerization of NIPAAm onto chitosan

Sample Name	T_{rxn} (ºC)[a]	GR (%)[b]	G' (pa) [c] at 37 ºC
CSNI-1	60	130	18 ± 3
CSNI-2	25	212	101 ± 9

[-NH2] : [CAN] : [NIPAAm] = 9:1:100 ; ($-NH_2$: chitosan free amino groups, CAN : initiator and NIPAAm : monomer in feed). Chitosan was dissolved in 10% acetic acid. All reactions were carried out for 24 hrs.

[a] T_{rxn} : Reaction temperature

[b] Grafting ratio (GR) was calculated as $(W_2-W_1)/W_1 \times 100\%$, where W_1 and W_2 are the weights of initial chitosan loaded and PNIPAAm-grafted chitosan after soxhelet extraction, respectively.

[c] Measured by a cone & plate rheometer for 30 mg/mL of CS-g-PNIPAAm copolymers in PBS (pH=7.4) at 1 rad/s. (n=3, ±SD)

Based on the solubility and mechanical strength results (49), we further selected the polymerisation temperature as a control variable to synthesize two different ploymer samples (CSNI-1 and CSNI-2) for evaluating the MSC performance. Table 1 summerizes the details of two samples. CSNI-1 was polymerised at 60˚C. The grafting ratio, representing number of PNIPAAm side chains grafted onto chitosan backbone, for this polymer was 130% and storage moduli, a mechnical parameter for evaluating gel strength, was 18±3 Pa at 37˚C. By reducing the reaction temperature to 25˚C, the grafting ratio increased to 212% and the gel became stronger with a storage moduli of 101±9 Pa. Figure 1a shows the MTT absorbance of MSCs cultured in these two polymers. Cell number was significantly higher in CSNI-2. The gel with a higher mechanical strength can provide a more suitable microenvironment for maintenance and growth of MSCs. It is well known that cells sense and respond to mechanical properties of their sorrounding environment by translating them to chemical signals (55). Mechanical cues can consequently affect cell fate and behaviours such as viability, proliferation, differentiation, migration and death (56). Therefore, CSNI-2 sample was employed for all subsequent studies.

The influence of polymer concentration on cellular viability was studied at three different polymer aqueous concentrations (20, 25 and 30 mg/mL) of the selected sample CSNI-2. Figure 1b indicates the optical density of the cell-laden hydrogels treated with the MTT reagents. Results revealed that the best cell growth can be achieved in the hydrogel formed at 25 mg/mL of polymer solution in PBS. Polymer concentration alters gel physical and mechanical properties which accordingly affect the cell behaviours (40, 57, 58). A low gel concentration results in weak gels which can not provide sufficient mechanical requirements of cell microenvironment. A high gel concentration may lead to a very dense structure with a small pore size and low interconnectivity (59) which hinders nutrient and oxygen delivery to cells and does not meet the cellular spatial demands for self-renewal and migration. The polymer concentration of 25 mg/mL was thus chosen for the subsequent experiments.

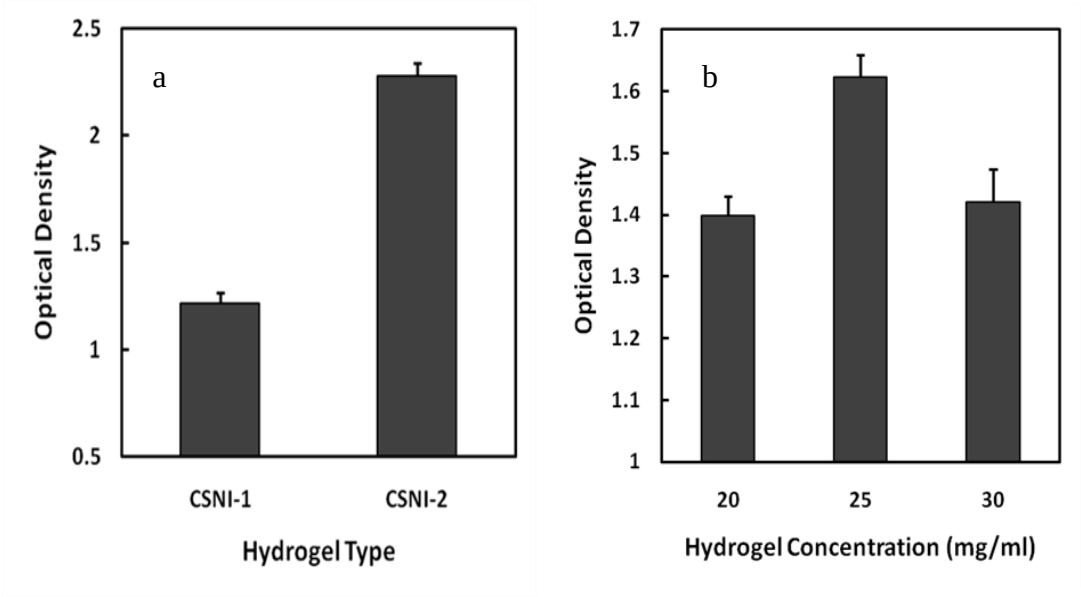

Figure 1. Optimisation of 3D cell culture conditions for MSCs. Absorbance of MTT after 7 days' incubation at different (a) CS-g-PNIPAAm hydrogels synthesized at different reaction temperatures which led to various grafting ratios and mechanical properties, and (b) CSNI-2 hydrogel concentrations. (n=3, mean±SE)

4.4.2 3D MSC differentiation in hydrogel

After hydrogel composition and its concentration were determined, we further applied the hydrogel for differentiating MSC into chondrocytes. By continuously culturing MSC in the differentiating medium for 28 days, cell proliferation and ECM (GAGs and collagen type II) production were monitored, and the constructs were histologically and immunohistologically examined at day 14 and 28 to confirm cartilage formation in the CS-g-PINAAM hydrogels.

Cell proliferation has been assessed by the Hoescht 33258 assay. The Hoescht assay results (Figure 2a) indicated that the cell number increases over culture time. Although, during the first 14 days, the proliferation rate was very slow, cells grew faster (almost 2 folds) during the following two weeks. The DMMB and hydroxyproline assays were employed to

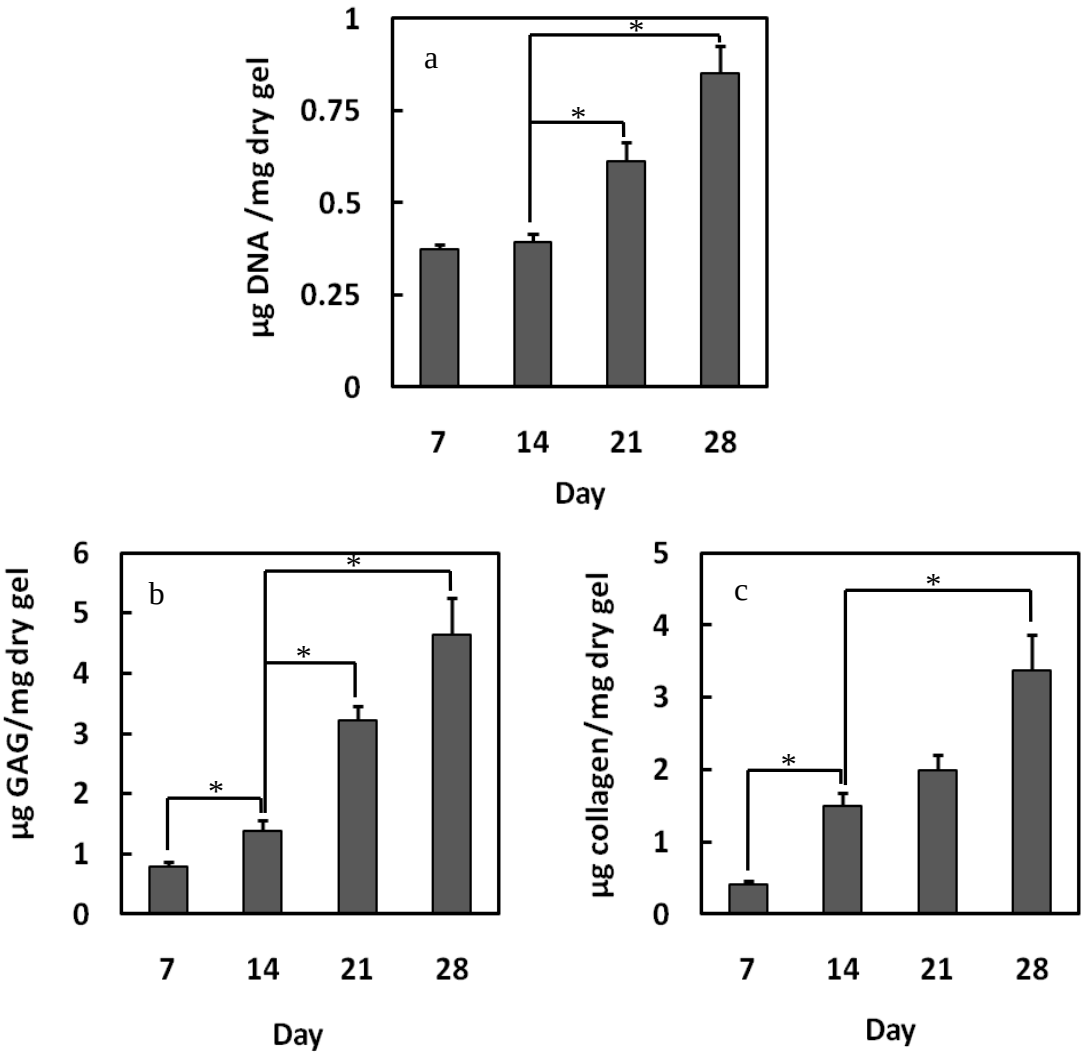

Figure 2. Quantification of (a) DNA, (b) GAG and (c) total collagen in cell-seeded CSNI-2 over 4 weeks. All values were normalized by the dry weight of the hydrogel (n=3, mean ± SE). * P< 0.05, ** P< 0.01

quantify GAGs and collagen deposition, respectively. The GAG level (Figure 2b) increased significantly from 0.8 µg/mg dry gel at day 7 to 4.8 µg/mg dry gel at day 28. Total collagen accumulation (Figure 2c) showed 7 fold increments during 28 days. GAGs and collagens are the main components of cartilagous tissues. Enhanced GAG and collagen

deposition revealed the successful chondrogenic differentiation of MSCs within the 3D microenvironment provided by CS-g-PNIPAAm. The ECM deposition rate was equivalent to or higher than those of other biomaterials which have been used for cartilage tissue engineering (60-63). These results suggest that CS-g-PNIPAAm is a promising hydrogel for this application.

We further confirmed the cartilage tissue formation by histological and immunohistochemical staining of constructs as shown in Figure 3. Figures 3a & b show low (4X) and high (10X) magnification micrographs of H&E staining. The black spots represent cells and all other components including ECM and hydrogel are stained red. This images revealed that cells were well distributed inside the structure while preserving their round morphology in the bulk hydrogel. The hydrogel surrounding the cells provided a 3D microenvironment so that the cells present in a round shape, which is very similar to the cell morphology in the middle zone of the cartilage. Figures 3c & d represent safranin O-stained sections where the presence of GAGs within ECM can be distinguished by pink colour. The intensity of positively stained pericellular regions was increased from day 14 (Figure 3c) to day 28 (Figure 3d). It confirmed continuous GAG secretion by cells and formation of sulfated proteoglycan-rich ECM which is seen in native articular cartilage tissues. Figures 3e & f show the distribution of collagen type II, a cartilage-specific ECM component, by immunohistochemical staining. Positive collagen type II was stained in brown color. The darker stained regions around the cells at day 28 (Figure 3f) than day 14 (Figure 3e) further supported the sustained collagen type II production over time as a specific marker of chondrogenesis.

Histological and immunohistochemical staining qualitatively verified the chondrogenic differentiation of MSCs encapsulated within CS-g-PNIPAAm hydrogels. The level of ECM deposition was visually identical to other comparable popular hydrogels such as agarose and gelatin loaded with MSCs, after 90 days of culture in chondrogenic medium (60).

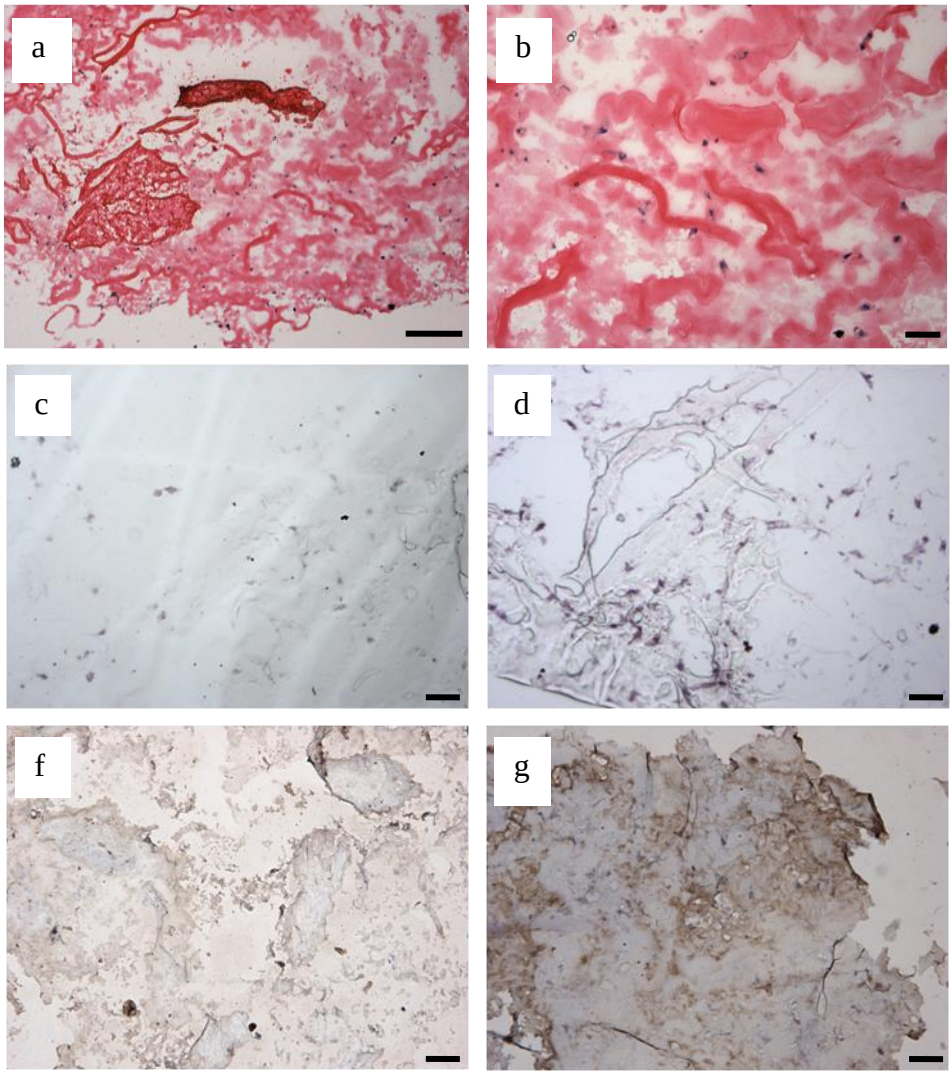

Figure 3. Histological and immunohistochemical staining of the cell-seeded hydrogels. (a-b) Sections were stained with H&E at day 14 (a) and day 28 (b); (c-d) sections were stained with Safranin O for GAGs after 14 days (c) and 28 days (d) of incubation; and (f-g) sections were immunohistochemically stained for collagen type II after 14 days (f) and 28 days (g) of incubation. (scale bar (a) =200 µm, 4× magnification; (b-g) = 50 µm, 10×)

4.4.3 3D cell-laden microconstructs: Preparation, cell organization and chondrogenesis

After the CS-g-PNIPAAm hydrogel has been demonstrated to be able to support cell proliferation and differentiation, we then applied cell-laden thermoresponsive hydrogel into the microengineered constructures for engineering/mimicing formation of different zones of cartilages by precise control of fabrication parameters of microconstructures. Scheme 1b illustrates the fabrication process of microengineered cell-laden thermoresponsive CS-g-PNIPAAm hydrogel patterns using microscale anisotropic PEG-DMA grooves as a micromold. Figure 4a presents a photograph of a micropatterned PEG-DMA on a TMSPMA glass slide. The overall dimension of the device was 1.5 cm (H) × 1.4 cm (W). Figures 4b-d show different microfabricated PEG-DMA patterns with the same channel dpeth (150 μm) but 3 different channel widths (50, 100 and 150 μm) at the same spacing between microchannels (200 μm). From these micrographs, channel sizes weree in precise agreement with their nominal dimension and all grooves on each patterned surafce were identical. To ensure that CS-g-PNIPAAm hydrogel was well located within the PEG-DMA microchannels, different fluorescence beads were used to distinguish the PEG-DMA and CS-g-PNIPAAm hydrogel. PEG-DMA was mixed with red fluorescent beads before lithography, while CS-g-PNIPAAm solution was mixed with green fluorescent beads, deposited into the channels and gelled at 37˚C. The construct was visualized under a fluorescence microscope equipped with a temperature control chamber. Figure 4e demonstrates that CS-g-PNIPAAm was adequately patterned within the PEG microgrooves.

After the cells has been successfully encapsulated in the hydrogel and solidified within the microgrooves, the cells were continuously incubated for 5 days. Cell-laden microconstructs were stained with calcein AM and EthD-1 to verify cellular viability and proliferation. At day 1 (Figure 5a), viable cells were individually distributed in a round morphology within micropatterned hydrogel. Cells exhibited an interconnected network with neighboring cells at a longer culture time (Figure 5b). A higher green intensity at day 5 in comparison to day 1 denoted an increase in cell number, demonstrating cells have

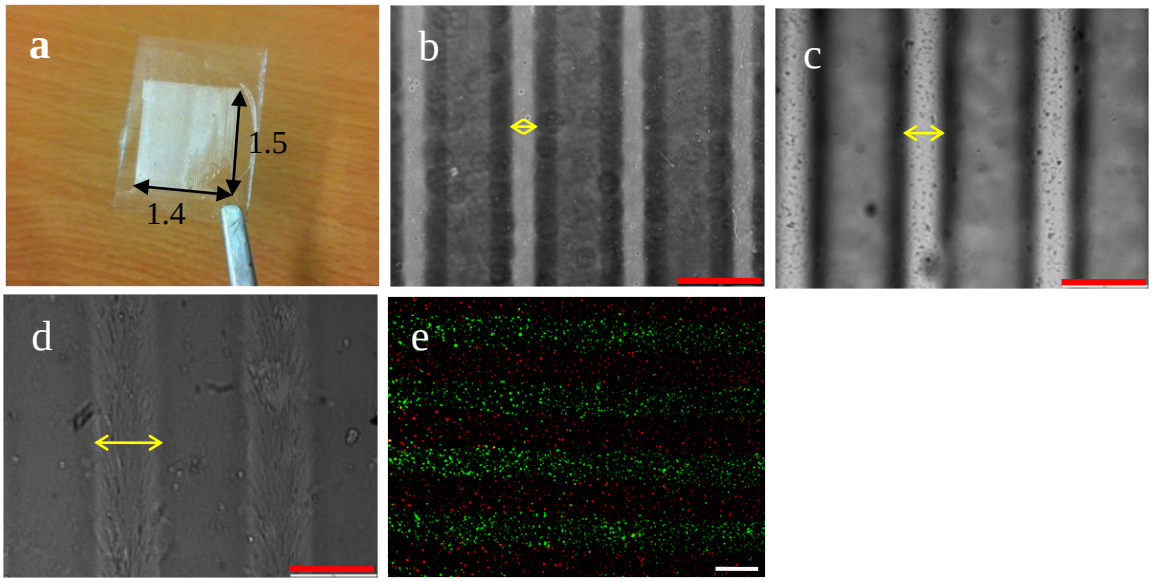

Figure 4. Images of micromolds and fabrication of micropatterned hydrogels. (a) Overview of a PEG-DMA micromold, with the dimensions of 1.4 cm × 1.5 cm. (b-d) Representative phase contrast images of PEG-DMA micromolds fabricated in different channel sizes: (b) 50 µm, (c) 100 µm, (d) 150 µm. Yellow arrows show the channel width. (scale bars: 200 µm, 10× magnification). (e) Fluorescent microscopic image of micropatterned hydrogel without cells. Green and red fluorescent beads were embedded in CS-g-PNIPAAm and PEG-DMA gels, respectively before gelation (scale bar = 100 µm).

proliferated inside the hydrogel in the microgrooves. The majority of cells remained viable and biologically active while a few dead cells (stained in red) can be found at day 1 and day 5.

The microconstructs were also stained with phalloidin and DAPI to visualize filamentous F-actin of the cytoskeleton and cell nuclei, respectively. Figure S1 displays a low

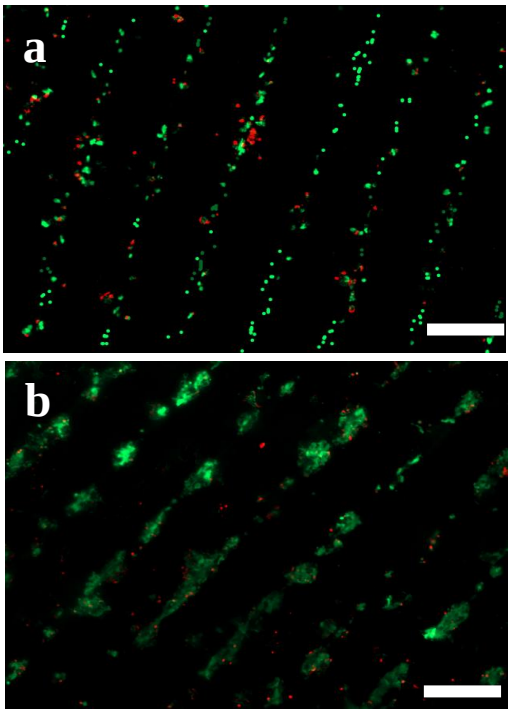

Figure 5. Live/dead cell staining of cell-laden micropatterned hydrogel (50 µm) after (a) 1 day and (b) 5 days' incubation. Green colour indicates live cells and red spots represent dead cells. (scale bars= 200 µm, 4×)

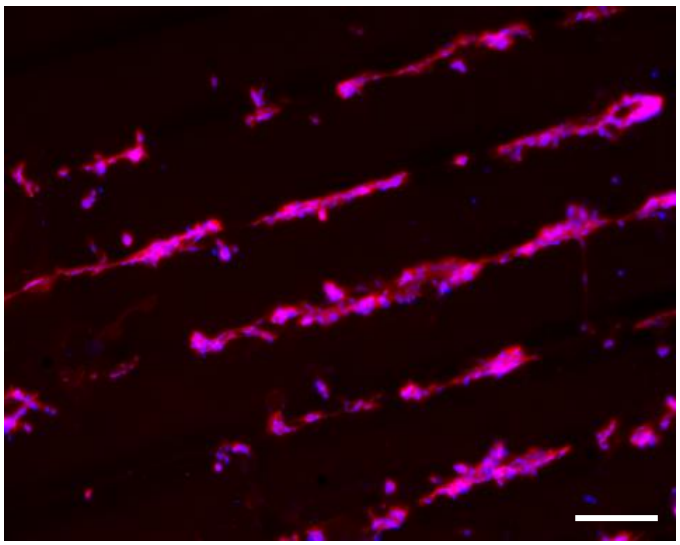

Figure S1. Representative low magnification (4X) F-actin/DAPI stained microconstruct (50 µm microchannel width) at day 5 of incubation. (scale bar = 200 µm)

magnification fluorescence image of cell-laden 3D CS-g-PNIPAAm micropatterned hydrogel with multiple alternating parallel microconstructs at a width of 50 μm after 5 day incubation. It can be seen that cells were well organized within the microconstructs. At some regions close to the top surafce, cells were spread over the lateral ridges. A few cells were also left on top of the spacing walls during preparation of microconstructs because it was impossible to prevent all the cell-polymer solution from leaking out of the channels. While some parts in the microchannels might be peeled off during the staining and washing steps, the integral structure could be maintained without washing steps as will be seen in a few paragraphs later.

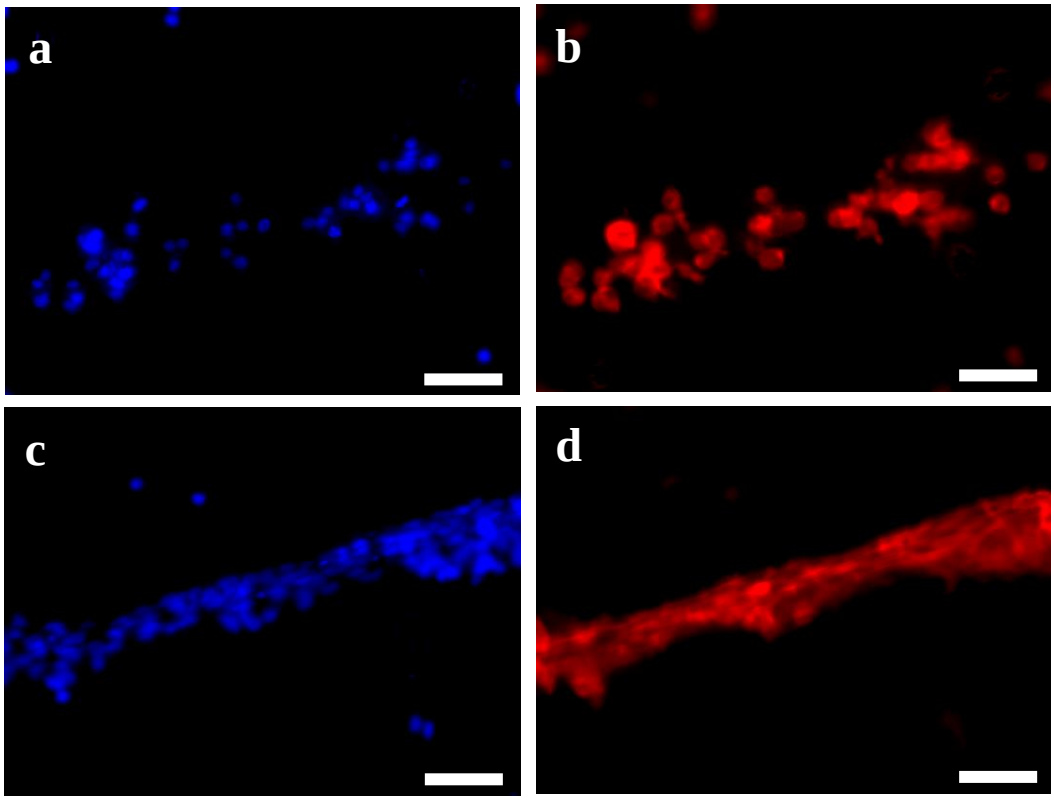

Figure 6. Fluorescence micrographs of cell alignment and elongation in microconstructs. Representative (a,c) DAPI and (b,d) F-actin-stained microconstruct (50 μm) of a cell-seeded hydrogel at days (a,b) 1 and (c,d) 5 of culture. (scale bars= 50 μm, 20X)

The cellular nucleus images at day 1 and day 5 are presented in Figures 6a & c, respectively. It can be seen that the individual cell nuclei were scattered in the hydrogel at day 1 in a round shape (Figure 6a). More cell nuclei could be found at day 5 in a stretched shape (Figure 6c). This confirmed that cells proliferate inside the hydrogel within the grooves. Cells have also been oriented along the horizonal axis of the microchannels. The cellular cytoskeleton was also stretched along the main horizontal axis of the microgrooves at day 5 (Figure 6d) in comparison to a round shape at day 1 (Figure 6b), which demonstrateed that cells have been re-oriented in the hydrogel. Long stressed fibers were found to run in parallel according to the orientation of the cells. Cells have been reported to induce the generation of stressed fibers when cells are exposed to their surrounding materials with a high mechanical property (64). Our results are in agreement with previous studies that cells could be aligned and elongated when cultured on the surface of microgrooves (65-67) or encapsulated in patterned microconstructs (54, 68).

Cell alignment was further quantified by the nuclear alignment angle which is defined as the orientation of the major axis of the nuclear shape by fitting in the best ellipse with respect to the horizontal axis of the microgrooves. Figures 7a-d represent the histogram of cell nuclear orientation in 10˚ increments within typical unpatterned and patterned microconstructs with a width of 150, 100 and 50 μm at day 5, respectively. The corresponding phalloidin and DAPI staining micrographs are also inserted as an internal panel in the histograms. The unpatterned histogram (Figure 7a) shows that cell nuclei were randomly oriented in various directions. However, cell nuclei were stretched to some extent. This again confirmed that cells have been responsive to the supporting microenvironment with a high mechanical storage moduli. Histograms of 150, 100, 50 μm wide microconstructs (Figure 7b-d) revealed that more cells intend to have small nuclear angels with respect to the channel longitude axis by reducing the channel sizes, suggesting higher alignment at a smaller channel width. Figure 7e summarizes the percentage of the aligned cells in unpatterned and patterned gels with different widths. Cells were considered to be aligned when their nuclear angles were less than 20˚ with respect to the microchannel longitude axis represented by mean cell nuclear angles (53). Figure 7e demonstrates that cells became more aligned over time in all patterned microconstructs, while there was no

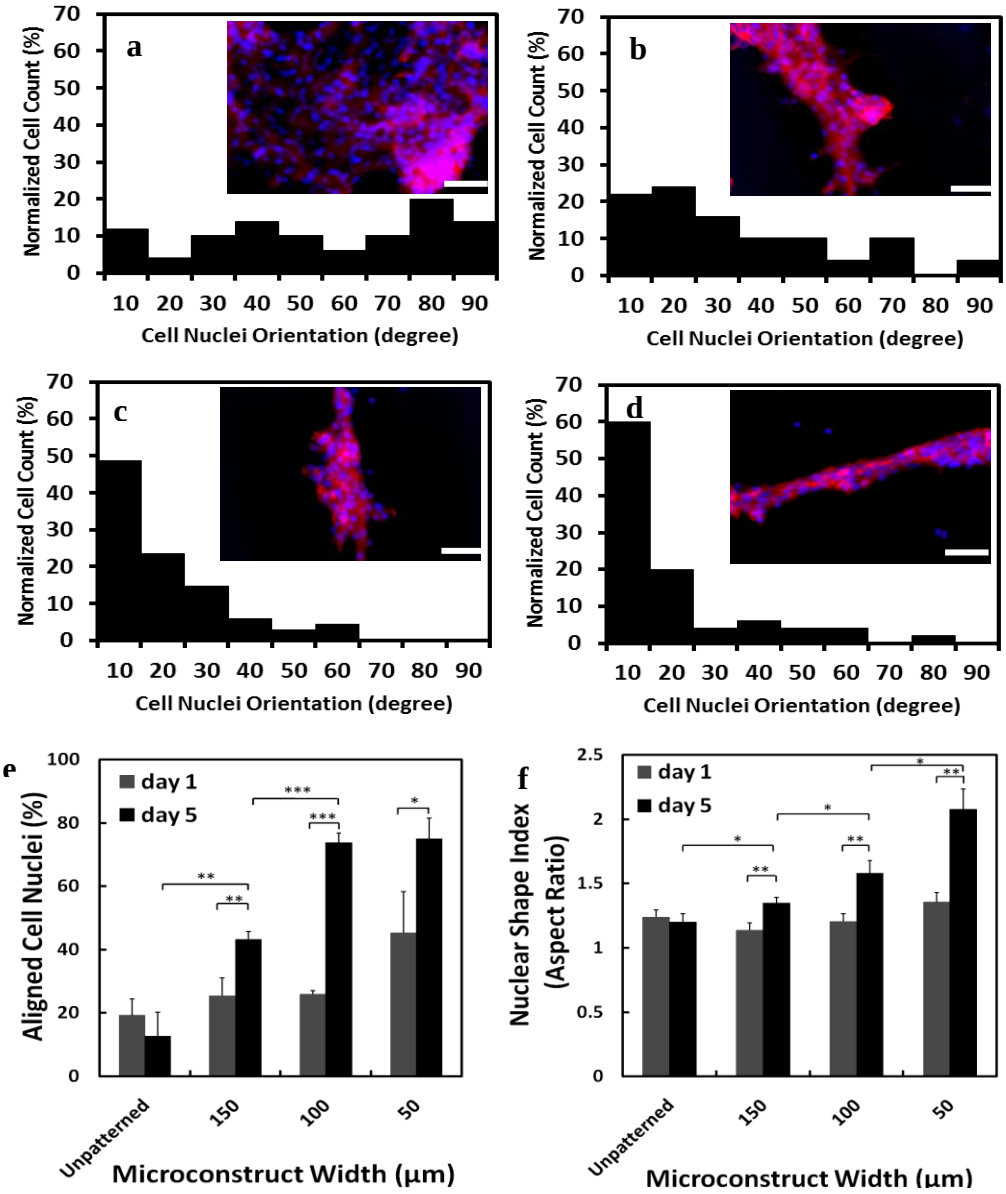

Figure 7. Quantification of cell alignment and elongation as a function of microconstruct width and incubation time. (a-d) Representative histograms of relative alignment in 10° increments on day 5 of culture in unpatterned and 150, 100 and 50 µm microchannel widths, respectively. Embedded images represent high magnification (20X) F-actin/DAPI stained microconstructs (scale bars (a-d) = 50 µm). (e) Mean percentage of aligned cell nuclei (within 20° of preferred nuclear orientation) in unpatterend and patterned gels at days 1 and 5. (f) Mean nuclear shape indices (spect ratio) of unpatterned and patterned microconstructs at days 1 and 5. (n=3, mean±SD, *P< 0.05, **P< 0.01, ***P< 0.001)

significant changes in cell alignment in unpatterned constructs. The most significant increment over time was found in 100 μm microconstructs (from 25±1% at day 1 to 74±3% at day 5). At day 1, cells in 50 μm microgrooves were more aligned (45±12%) in comparison with two other widths, while no significant difference could be seen between unpatterned, 150 and 100 μm micropatterns. At day 5, cells in 50 and 100 μm microconstructs (75±6% and 74±3%, respectively) were more aligned than those in 150 μm (43±3%). A significant increase has been found for the percentage of cell alignment in all widths at day 5 in comparison with day 1. The significant increase was also applied to patterned structure when compared to the unpatterend constructs at day 5. Interestingly, a similar percentage of aligned cells were found for 100 and 50 μm micropatterns at day 5. Jadin et. al. quantified the chondrocyte organization by their angles to the nearest neighboring cell. They found that neighboring cells were arranged horizontally in the superficial zone with an averaged angle of 20° and vertically in the deep zone with an angle of 60°. In other regions of the cartilage, the angle was 32°, indicative of an isotropic organization (69). Our experiments suggested that cells incubating within 50-100 μm microgooves were aligned in the pattern similar to the superficial zone and in gaps at 150 μm or wider were more likely to form the middle zone.

Cell elongation was quantitatively studied by estimating the cell nuclear shape index. The aspect ratio, the ratio of the major to the minor axis of the best fit ellipse from individual cell nucleus, was empolyed as the shape index. Figure 7f summarizes the results of cell shape indices in the unpatterned and patterned microconstructs with a width of 150, 100 and 50 μm at day 1 and day 5. At day 1, there was no significant difference between the shape indices of the nuclei in different groups including unpatterned and patterned hydrogels. The aspect ratio was close to 1 for all groups suggesting an almost round shape of cell nuclei. The shape index did not change at day 5 in unpatterned gels (1.202±0.07) in comparison with day 1 (1.239±0.06). In contrast, within all patterned groups, the nuclear aspect ratios at day 5 were greater than those of the same group at day 1 ($P < 0.01$). The change became more significant by decreasing the microconstruct width. At day 5, the shape indices were significantly different ($P < 0.05$) between the unpatterned and patterned groups. The highest aspect ratio of 2.075±0.161 was found for cells in the 50 μm

micropatterns. These results suggest that cells became more elongated in the more narrow microgroovers and the extent of elongation can be adjusted by controlling the widths of the microgrooves.

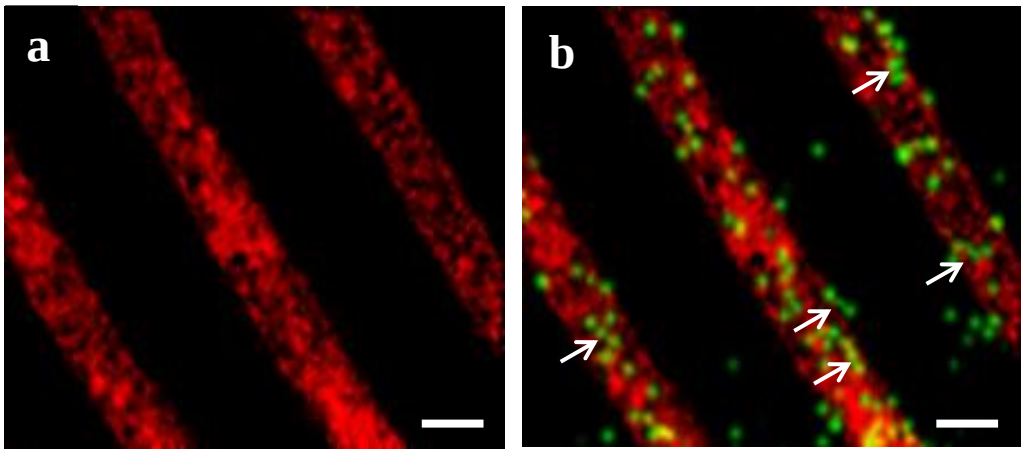

Figure 8. Multiphoton microscopy image of micropatterned cell-laden hydrogel after 21 days' incubation. (a) Autofluorescence (AF) of cell-laden CS-g-PNIPAAm gel. (b) Overlay of AF (red) and second harmonic generation signals (green), indicating collagens in extracellular matrix. White arrows indicate combined collagens from different cells. (scale bars = 100 µm, 10× magnification).

The cell-laden microconstructs were further incubated in the chondrogenic medium for 21 days and visualized under a multiphoton microscope. Some cellular components and biomaterials are detectable under the multiphoton microscope due to their autofluorescent (AF) properties; and these include some cell contents such as NADH coenzymes (70), and cell derbis (71) as well as some biomaterials used as scaffolds in tissue engineering (72, 73) including chitosan (74). Collagen in ECM can also be distinguishable from their SHG signals. Collagen is the strong source of second harmonics in animal tissues due to its unusual noncentrosymmetric structure and high degree of crystallinity (75). An integrated architecture of AF signal (red) (Figure 8a) confirmed that the structure of microconstructs was well preserved after 21 day incubation. As the multiphoton microscope can detect

autoflorescence signals, microconstructs did not need any staining and hence, washing steps and solution changes were avoided before imaging. As mentioned before, these preparation steps might bring partial damage to the microconstructs as shown in previous staining assays. SHG signals of collagen (green) are observed in Figure 8b. The detectable collagen signals denoted that MSCs have become differentiated or partially differentiated cells (74). Collagen was presented as a round shape, surrounding the individual cells. At some regions indicated by white arrows collagen was aligned along the horizonal axis. The reason for the scattered collagen distribution might be due to the low cell density. As described earlier in DNA quantification (Figure 2a), the cell number did not increase up to day 14, and the cells started to proliferate after 14 days. It is expected that after culturing in the chondrogenic medium for a longer time, collagen will be integrated and aligned.

Images of safranin O histologically and collagen II immunohistologically stained microconstructs (cultured in the chondrogenic medium for 2 weeks) are presented in Figure S2. Although it was difficult to visualize the positive stains due to the high thickness of the microconstructs under the phase contrast microscopy, positive stains could be seen at the edges and broken regions of the gel (Figure S2a). Collagen type II-positive components were not distinguishable by immunostaining within the micropatterns due to the dark background of the thick gel (Figure S2b). However, The darker stained spots could be cells being stained.

The chondrocyte spatial arrangement is vital in the functionality of the mature articular cartilage. It is an essential requirement for homeostasis (76). In addition, the spatial cellular organisation regulates cells through direct cell–cell contact and paracrine or autocrine factors. Cellular organization has also a great impact on the local solid and fluid environment in which the cells reside, when the cells are exposed to external mechanical or chemical stimuli (69). Moreover, the actin cytoskeleton and cell shape play a role in determining the zone-specific characteristics (77). To create an artificial microenvironment for allowing spatial cellular organisation and maintaining cell shape in each zone is an important step for successful cartilage tissue engineering. Among three zones, the superficial zone is the most imporant for cartilages. It has been recently shown that superficial zone chondrocytes modulate the surface mechanical properties of engineered

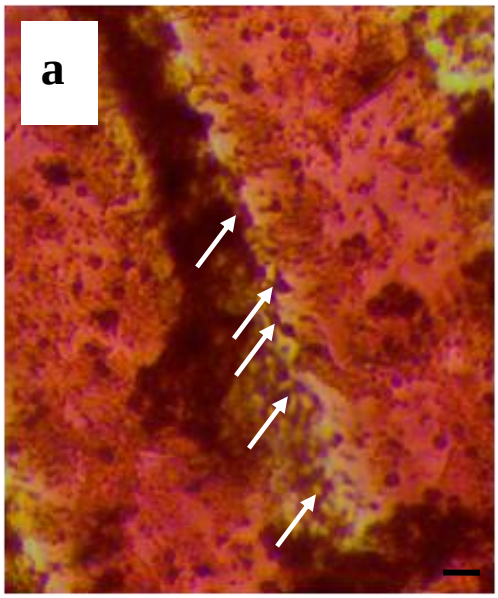

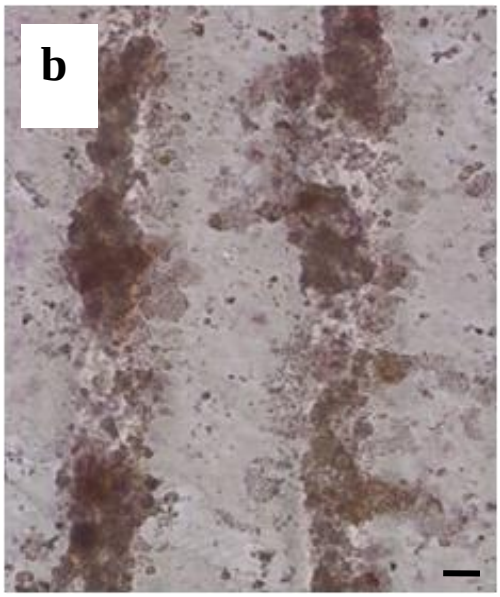

Figure S2. Histological and immunohistochemical staining of the cell-seeded patterned (100 µm channel width) hydrogels. Samples were stained (a) with Safranin O for GAGs, and (b) immunohistochemically for collagen type II after 21 days incubation. White arrows point out the positive GAG stained spots. (scale bars = 50 µm, 10×)

cartilage tissue (77). The flattened geometry of chondrocytes encourages the superficial zone phenotype (78). The changes in cellular arrangement at the superficial zone of the articular cartilage arose at the onset of osteoarthritis (79). Micropatterning was employed in this study to form the superficial zone and middle zone with the thermoresponsive hydrogels. The cellular alignment and elongation in the narrow microgrooves (50-100 µm) after culturing cells in the hydrogels for several days could mimic the superficial zonal structure, while cells in a wide microgroove (above 150 µm) or in bulk hydrogel could

form an isotropic structure in the middle zone of the cartilage. While these initial results are very promising for regenerating layered cartilage, recreating an integrated macroscale tissue by stacking the microconstructs remains to be addressed in our future research.

4.5 Conclusions

Mesenchymal stem cells incorporated in chitosan-g-PNIPAAm as a thermoresponsive hydrogel proliferated fast in the copolymer with a mechanically strong structure. By incubating MSCs in the thermoresponsive hydrogel in the chondrogenic medium for over 28 days, cartilaginous tissue formation was confirmed by biochemical, histochemical and immunohistochemical assays. The cell-laden thermoresponsive hydrogel was further micropatterned using PEG-DMA stamps by simply incubation at 37 °C without UV radiation and photoinitiators. Cells were aligned and elongated in the narrow microchannel gaps, suggesting that the microfabrication method can be exploited for 3D cell orientation and elongation to mimic the cell shape and organization in the superficial zone of native cartilages. However, cells in the wide microchannel as unpatterned microstructures served to resemble the middle zone of articular cartilage. Our results suggest that micropatterning of 3D cell-laden CS-g-PNIPAAm hydrogel is a promising method for bi-zonal cartilage tissue engineering.

4.6 References

1. Mansour JM. Biomechanics of cartilage. Kinesiology: the mechanics and pathomechanics of human movement. 2003:66-79.
2. Newman AP. Articular cartilage repair. The American journal of sports medicine. 1998;26(2):309-24.
3. Temenoff JS, Mikos AG. Review: tissue engineering for regeneration of articular cartilage. Biomaterials. 2000;21(5):431-40.
4. Hunziker EB, Quinn TM, Häuselmann HJ. Quantitative structural organization of normal adult human articular cartilage. Osteoarthritis and Cartilage. 2002;10(7):564-72.
5. Poole AR, Kojima T, Yasuda T, Mwale F, Kobayashi M, Laverty S. Composition and structure of articular cartilage: a template for tissue repair. Clinical orthopaedics and related research. 2001;391:S26-S33.
6. Wise JK, Yarin AL, Megaridis CM, Cho M. Chondrogenic differentiation of human mesenchymal stem cells on oriented nanofibrous scaffolds: engineering the superficial zone of articular cartilage. Tissue Engineering Part A. 2008;15(4):913-21.
7. Keeney M, Lai JH, Yang F. Recent progress in cartilage tissue engineering. Current opinion in biotechnology. 2011;22(5):734-40.
8. Hunziker EB. Articular cartilage repair: basic science and clinical progress. A review of the current status and prospects. Osteoarthritis and Cartilage. 2002;10(6):432-63.
9. Johnstone B, Alini M, Cucchiarini M, Dodge GR, Eglin D, Guilak F, et al. Tissue engineering for articular cartilage repair--the state of the art. Eur Cell Mater. 2013;25:248-67.
10. Lanza R, Longer R, Vacanti J, editors. Principles of Tissue Engineering. 3 ed: Elsevier Academic Press; 2007.
11. Coates EE, Fisher JP. Engineering Superficial Zone Chondrocytes from Mesenchymal Stem Cells. Tissue Engineering Part C: Methods. 2014.
12. Spiller KL, Maher SA, Lowman AM. Hydrogels for the repair of articular cartilage defects. Tissue Engineering Part B: Reviews. 2011;17(4):281-99.

13. Fedorovich NE, Alblas J, Wijin JR, Hennink WE, Verbout AJ, Dhert WJA. Hydrogels as Extracellular Matrices for Skeletal Tissue Engineering: State-of-the-Art and Novel Application in Organ Printing. TISSUE ENGINEERING. 2007;13(8):1905-25.
14. Kim I-Y, Seo S-J, Moon H-S, Yoo M-K, Park I-Y, Kim B-C, et al. Chitosan and its derivatives for tissue engineering applications. Biotechnology Advances. 2008;26(1):1-21.
15. Di Martino A, Sittinger M, Risbud MV. Chitosan: A versatile biopolymer for orthopaedic tissue engineering. Biomaterials. 2005;26(30):5983-90.
16. Francis Suh JK, Matthew HWT. Application of chitosan-based polysaccharide biomaterials in cartilage tissue engineering: a review. Biomaterials. 2000;21(24):2589-98.
17. McCullen SD, Autefage H, Callanan A, Gentleman E, Stevens MM. Anisotropic fibrous scaffolds for articular cartilage regeneration. Tissue Engineering Part A. 2012;18(19-20):2073-83.
18. Klein T, Schumacher B, Schmidt T, Li K, Voegtline M, Masuda K, et al. Tissue engineering of stratified articular cartilage from chondrocyte subpopulations. Osteoarthritis and Cartilage. 2003;11(8):595-602.
19. Sharma B, Williams CG, Kim TK, Sun D, Malik A, Khan M, et al. Designing zonal organization into tissue-engineered cartilage. Tissue engineering. 2007;13(2):405-14.
20. Kim T-K, Sharma B, Williams C, Ruffner M, Malik A, McFarland E, et al. Experimental model for cartilage tissue engineering to regenerate the zonal organization of articular cartilage. Osteoarthritis and Cartilage. 2003;11(9):653-64.
21. Bhumiratana S, Eton RE, Oungoulian SR, Wan LQ, Ateshian GA, Vunjak-Novakovic G. Large, stratified, and mechanically functional human cartilage grown in vitro by mesenchymal condensation. Proceedings of the National Academy of Sciences. 2014;111(19):6940-5.
22. Sharma B, Elisseeff JH. Engineering structurally organized cartilage and bone tissues. Annals of biomedical engineering. 2004;32(1):148-59.
23. Nguyen LH, Kudva AK, Saxena NS, Roy K. Engineering articular cartilage with spatially-varying matrix composition and mechanical properties from a single stem cell population using a multi-layered hydrogel. Biomaterials. 2011;32(29):6946-52.

24. Klein TJ, Rizzi SC, Schrobback K, Reichert JC, Jeon JE, Crawford RW, et al. Long-term effects of hydrogel properties on human chondrocyte behavior. Soft matter. 2010;6(20):5175-83.

25. Walker KJ, Madihally SV. Anisotropic temperature sensitive chitosan‐based injectable hydrogels mimicking cartilage matrix. Journal of Biomedical Materials Research Part B: Applied Biomaterials. 2014.

26. Lee CS, Gleghorn JP, Won Choi N, Cabodi M, Stroock AD, Bonassar LJ. Integration of layered chondrocyte-seeded alginate hydrogel scaffolds. Biomaterials. 2007;28(19):2987-93.

27. Ng KW, Wang CCB, Mauck RL, Kelly TAN, Chahine NO, Costa KD, et al. A layered agarose approach to fabricate depth‐dependent inhomogeneity in chondrocyte‐seeded constructs. Journal of Orthopaedic Research. 2005;23(1):134-41.

28. Bryant SJ, Anseth KS. Controlling the spatial distribution of ECM components in degradable PEG hydrogels for tissue engineering cartilage. Journal of Biomedical Materials Research Part A. 2003;64(1):70-9.

29. Woodfield T, Blitterswijk CV, Wijn JD, Sims T, Hollander A, Riesle J. Polymer scaffolds fabricated with pore-size gradients as a model for studying the zonal organization within tissue-engineered cartilage constructs. Tissue engineering. 2005;11(9-10):1297-311.

30. Erisken C, Kalyon DM, Wang H. Functionally graded electrospun polycaprolactone and β-tricalcium phosphate nanocomposites for tissue engineering applications. Biomaterials. 2008;29(30):4065-73.

31. Steele J, McCullen S, Callanan A, Autefage H, Accardi M, Dini D, et al. Combinatorial scaffold morphologies for zonal articular cartilage engineering. Acta biomaterialia. 2014;10(5):2065-75.

32. Marsano A, Wendt D, Quinn T, Sims T, Farhadi J, Jakob M, et al. Bi-zonal cartilaginous tissues engineered in a rotary cell culture system. Biorheology. 2006;43(3):553-60.

33. Spitters TW, Leijten JC, Deus FD, Costa IB, van Apeldoorn AA, van Blitterswijk CA, et al. A dual flow bioreactor with controlled mechanical stimulation for cartilage tissue engineering. Tissue Engineering Part C: Methods. 2013;19(10):774-83.

34. Kock LM, Ito K, van Donkelaar CC. Sliding indentation enhances collagen content and depth-dependent matrix distribution in tissue-engineered cartilage constructs. Tissue Engineering Part A. 2013;19(17-18):1949-59.

35. Chen T, Hilton MJ, Brown EB, Zuscik MJ, Awad HA. Engineering superficial zone features in tissue engineered cartilage. Biotechnology and bioengineering. 2013;110(5):1476-86.

36. Schrobback K, Malda J, Crawford RW, Upton Z, Leavesley DI, Klein TJ. Effects of oxygen on zonal marker expression in human articular chondrocytes. Tissue Engineering Part A. 2012;18(9-10):920-33.

37. Spitters TW, Mota CM, Uzoechi SC, Slowinska B, Martens D, Moroni L, et al. Glucose gradients influence zonal matrix deposition in 3D cartilage constructs. Tissue engineering. 2014(ja).

38. Thorpe SD, Nagel T, Carroll SF, Kelly DJ. Modulating gradients in regulatory signals within mesenchymal stem cell seeded hydrogels: a novel strategy to engineer zonal articular cartilage. PloS one. 2013;8(4):e60764.

39. Hwang NS, Varghese S, Lee HJ, Theprungsirikul P, Canver A, Sharma B, et al. Response of zonal chondrocytes to extracellular matrix-hydrogels. FEBS letters. 2007;581(22):4172-8.

40. Nichol JW, Koshy ST, Bae H, Hwang CM, Yamanlar S, Khademhosseini A. Cell-laden microengineered gelatin methacrylate hydrogels. Biomaterials. 2010;31(21):5536-44.

41. Schuurman W, Gawlitta D, Klein TJ, ten Hoope W, van Rijen MH, Dhert WJ, et al. Zonal chondrocyte subpopulations reacquire zone-specific characteristics during in vitro redifferentiation. The American journal of sports medicine. 2009;37(1 suppl):97S-104S.

42. Albrecht DR, Tsang VL, Sah RL, Bhatia SN. Photo-and electropatterning of hydrogel-encapsulated living cell arrays. Lab on a Chip. 2005;5(1):111-8.

43. Liu VA, Bhatia SN. Three-dimensional photopatterning of hydrogels containing living cells. Biomedical microdevices. 2002;4(4):257-66.

44. Yamato M, Konno C, Utsumi M, Kikuchi A, Okano T. Thermally responsive polymer-grafted surfaces facilitate patterned cell seeding and co-culture. Biomaterials. 2002;23(2):561-7.

45. Tsuda Y, Kikuchi A, Yamato M, Nakao A, Sakurai Y, Umezu M, et al. The use of patterned dual thermoresponsive surfaces for the collective recovery as co-cultured cell sheets. Biomaterials. 2005;26(14):1885-93.

46. Jun I, Kim SJ, Lee JH, Lee YJ, Shin YM, Choi E, et al. Transfer Printing of Cell Layers with an Anisotropic Extracellular Matrix Assembly using Cell‐Interactive and Thermoresponsive Hydrogels. Advanced Functional Materials. 2012;22(19):4060-9.

47. Tekin H, Anaya M, Brigham MD, Nauman C, Langer R, Khademhosseini A. Stimuli-responsive microwells for formation and retrieval of cell aggregates. Lab on a Chip. [10.1039/C004732E]. 2010;10(18):2411-8.

48. Tekin H, Tsinman T, Sanchez JG, Jones BJ, Camci-Unal G, Nichol JW, et al. Responsive Micromolds for Sequential Patterning of Hydrogel Microstructures. Journal of the American Chemical Society. 2011 2011/08/24;133(33):12944-7.

49. Mellati A, Dai S, Bi J, Jin B, Zhang H. A Biodegradable Thermoresponsive Hydrogel with Tuneable Properties for Mimicking Three-Dimensional Microenvironments of Stem Cells. RSC Advances. 2014.

50. Hwang NS, Varghese S, Elisseeff J. Cartilage tissue engineering. Stem Cell Assays: Springer; 2007. p. 351-73.

51. Hoemann CD. Molecular and biochemical assays of cartilage components. Cartilage and osteoarthritis: Springer; 2004. p. 127-56.

52. Chung R, Cool JC, Scherer MA, Foster BK, Xian CJ. Roles of neutrophil-mediated inflammatory response in the bony repair of injured growth plate cartilage in young rats. Journal of Leukocyte Biology. 2006 December 1, 2006;80(6):1272-80.

53. Annabi N, Tsang K, Mithieux SM, Nikkhah M, Ameri A, Khademhosseini A, et al. Highly elastic micropatterned hydrogel for engineering functional cardiac tissue. Advanced functional materials. 2013;23(39):4950-9.

54. Aubin H, Nichol JW, Hutson CB, Bae H, Sieminski AL, Cropek DM, et al. Directed 3D cell alignment and elongation in microengineered hydrogels. Biomaterials. 2010;31(27):6941-51.

55. Lutolf MP, Hubbell JA. Synthetic biomaterials as instructive extracellular microenvironments for morphogenesis in tissue engineering. Nat Biotech. 2005;23(1):47-55.

56. Guilak F, Cohen DM, Estes BT, Gimble JM, Liedtke W, Chen CS. Control of Stem Cell Fate by Physical Interactions with the Extracellular Matrix. Cell Stem Cell. 2009;5(1):17-26.

57. Kim M, Lee JY, Jones CN, Revzin A, Tae G. Heparin-based hydrogel as a matrix for encapsulation and cultivation of primary hepatocytes. Biomaterials. 2010;31(13):3596-603.

58. Bae H, Ahari AF, Shin H, Nichol JW, Hutson CB, Masaeli M, et al. Cell-laden microengineered pullulan methacrylate hydrogels promote cell proliferation and 3D cluster formation. Soft matter. 2011;7(5):1903-11.

59. Dillon GP, Xiaojun Y, Sridharan A, Ranieri JP, Bellamkonda RV. The influence of physical structure and charge on neurite extension in a 3D hydrogel scaffold. Journal of Biomaterials Science, Polymer Edition. 1998 ;9(10):1049-69.

60. Lin H, Cheng AW-M, Alexander PG, Beck AM, Tuan RS. Cartilage Tissue Engineering Application of Injectable Gelatin Hydrogel with In Situ Visible-Light-Activated Gelation Capability in both Air and Aqueous Solution. Tissue Engineering Part A. 2014.

61. Dai W, Kawazoe N, Lin X, Dong J, Chen G. The influence of structural design of PLGA/collagen hybrid scaffolds in cartilage tissue engineering. Biomaterials. 2010;31(8):2141-52.

62. Jin R, Moreira Teixeira L, Dijkstra P, van Blitterswijk C, Karperien M, Feijen J. Enzymatically-crosslinked injectable hydrogels based on biomimetic dextran–hyaluronic acid conjugates for cartilage tissue engineering. Biomaterials. 2010;31(11):3103-13.
63. DeKosky BJ, Dormer NH, Ingavle GC, Roatch CH, Lomakin J, Detamore MS, et al. Hierarchically designed agarose and poly (ethylene glycol) interpenetrating network hydrogels for cartilage tissue engineering. Tissue Engineering Part C: Methods. 2010;16(6):1533-42.
64. Walboomers X, Ginsel L, Jansen J. Early spreading events of fibroblasts on microgrooved substrates. Journal of biomedical materials research. 2000;51(3):529-34.
65. Hosseini V, Ahadian S, Ostrovidov S, Camci-Unal G, Chen S, Kaji H, et al. Engineered contractile skeletal muscle tissue on a microgrooved methacrylated gelatin substrate. Tissue Engineering Part A. 2012;18(23-24):2453-65.
66. Thompson DM, Buettner HM. Schwann cell response to micropatterned laminin surfaces. Tissue engineering. 2001;7(3):247-65.
67. Charest JL, García AJ, King WP. Myoblast alignment and differentiation on cell culture substrates with microscale topography and model chemistries. Biomaterials. 2007;28(13):2202-10.
68. Nikkhah M, Eshak N, Zorlutuna P, Annabi N, Castello M, Kim K, et al. Directed endothelial cell morphogenesis in micropatterned gelatin methacrylate hydrogels. Biomaterials. 2012;33(35):9009-18.
69. Jadin KD, Bae WC, Schumacher BL, Sah RL. Three-dimensional (3-D) imaging of chondrocytes in articular cartilage: Growth-associated changes in cell organization. Biomaterials. 2007;28(2):230-9.
70. Schenke-Layland K, Riemann I, Damour O, Stock UA, König K. Two-photon microscopes and in vivo multiphoton tomographs—Powerful diagnostic tools for tissue engineering and drug delivery. Advanced drug delivery reviews. 2006;58(7):878-96.
71. Schenke-Layland K, Vasilevski O, Opitz F, König K, Riemann I, Halbhuber K, et al. Impact of decellularization of xenogeneic tissue on extracellular matrix integrity for tissue engineering of heart valves. Journal of structural biology. 2003;143(3):201-8.

72. Lee H-S, Teng S-W, Chen H-C, Lo W, Sun Y, Lin T-Y, et al. Imaging human bone marrow stem cell morphogenesis in polyglycolic acid scaffold by multiphoton microscopy. Tissue engineering. 2006;12(10):2835-41.

73. Heydarkhan-Hagvall S, Schenke-Layland K, Dhanasopon AP, Rofail F, Smith H, Wu BM, et al. Three-dimensional electrospun ECM-based hybrid scaffolds for cardiovascular tissue engineering. Biomaterials. 2008;29(19):2907-14.

74. Chen W-L, Huang C-H, Chiou L-L, Chen T-H, Huang Y-Y, Jiang C-C, et al. Multiphoton imaging and quantitative analysis of collagen production by chondrogenic human mesenchymal stem cells cultured in chitosan scaffold. Tissue Engineering Part C: Methods. 2010;16(5):913-20.

75. Cox G, Kable E. Second-harmonic imaging of collagen. Cell Imaging Techniques: Springer; 2006. p. 15-35.

76. Jadin KD, Wong BL, Bae WC, Li KW, Williamson AK, Schumacher BL, et al. Depth-varying density and organization of chondrocytes in immature and mature bovine articular cartilage assessed by 3D imaging and analysis. Journal of Histochemistry & Cytochemistry. 2005;53(9):1109-19.

77. Peng G, McNary SM, Athanasiou KA, Reddi AH. Surface Zone Articular Chondrocytes Modulate the Bulk and Surface Mechanical Properties of the Tissue-Engineered Cartilage. Tissue Engineering Part A. 2014.

78. McNary SM, Athanasiou KA, Reddi AH. Transforming Growth Factor β-Induced Superficial Zone Protein Accumulation in the Surface Zone of Articular Cartilage Is Dependent on the Cytoskeleton. Tissue Engineering Part A. 2014;20(5-6):921-9.

79. Becerra J, Andrades JA, Guerado E, Zamora-Navas P, López-Puertas JM, Reddi AH. Articular cartilage: structure and regeneration. Tissue Engineering Part B: Reviews. 2010;16(6):617-27.

CHAPTER FIVE

5. Influence of Polymer Molecular Weight on the Cytotoxicity of Poly (N-isopropylacrylamide)

Influence of polymer molecular weight on the cytotoxicity of poly (N-isopropylacrylamide)

Amir Mellati, Meisam Valizadeh Kiamahalleh, Sheng Dai, Jingxiu Bi, Bo Jin, Hu Zhang*

School of Chemical Engineering, the University of Adelaide, Adelaide SA5005, Australia

*Corresponding author
E-mail: hu.zhang@adelaide.edu.au
Tel: + 61 8 8313 3810

Colloid and Interface Science Communications. (Submitted, Reference number: COLCOM-D-14-00131)

5.1 Abstract

Poly (N-isopropylacrylamide) (PNIPAAm) has been extensively used as a thermoresponsive material in various biomedical applications. In this study, we synthesized a series of PNIPAAms with well-defined molecular weights and examined polymer molecular weight-dependent cytotoxicity. Results indicated that low molecular weight PNIPAAm (degree of polymerization (DP) = 35) is inherently toxic to cells, and necrosis is the dominant cell death mechanism. Moderate-sized PNIPAAms with their DP between 100 and 200 are non-cytotoxic. For the PNIPAAm with a higher molecular weight (DP = 400), cell viability is dependent on the assay method. When cells are seeded on top of the polymer-coated surface, PNIPAAm shows non/low cytotoxicity, while when monolayer cells are exposed to the polymer solution, cell viability drops drastically, which may be due to lack of nutrient and oxygen delivery rather than intrinsic toxicity of the polymer as the polymer forms a dense polymeric layer at temperature above its LCST.

5.2 Introduction

Polymers have been widely used for biological applications. Toxicity of polymers must be evaluated before their application to human bodies. Some polymers (1, 2) and monomers (3, 4) are known to be toxic or medium-toxic, while others are low-toxic or non-toxic. Side effects of polymers including their toxicity are often molecular weight-dependent (5, 6). Understanding of the potential harmful properties of polymers and the molecular weight dependence of these effects is essential to design novel and safe polymeric biomaterials (5). Great interest in biomedical applications of thermoresponsive polymers has demanded a thorough study of their toxicity. Poly (ethylene oxide)-poly (propylene oxide)-poly (ethylene oxide) triblock copolymer (Pluronic or Poloxamer), and poly (ethylene glycol)-poly (lactic-co-glycolic acid) (PEG-PLGA) block copolymers are typical thermoresponsive polymers which have been reported to be toxic at certain concentrations and incubation times (6-8). Furthermore, the cytotoxicity of Pluronic copolymer is dependent on the molecular weight of its building blocks (7). Poly (N-isopropylacrylamide) (PNIPAAm) is another thermoresponsive polymer. Possessing a lower critical solution temperature (LCST) close to the human body temperature, PNIPAAm has become a promising biomaterial in various medical applications such as tissue engineering, regenerative medicine, drug delivery, gene delivery, cell sheet engineering and enzyme-free cell harvesting (9-11). NIPAAm is a cytotoxic monomer (12). However, to the best of our knowledge, the influence of polymer molecular weight on the cytotoxicity of PNIPAAm has not been studied. Identification of the non-cytotoxic or low cytotoxic molecular weight range will help researchers in designing less toxic biomaterials while exploiting the maximum benefits of various molecular weights in tailoring physical and mechanical properties of final products.

5.3 Materials and methods

5.3.1 Materials

N-isopropylacrylamide (NIPAAm, 97%), copper chloride (CuCl), Tris[2-(dimethylamino)ethyl]amine (Me6Tren, 97%) and ethyl 2-chloropropionate (ECP) were purchased from Sigma-Aldrich and NIPAAm was purified by recrystallization in n-hexane. Dulbecco's Modified Eagle's Medium (DMEM), trypsin-EDTA, penicillin-streptomycin and fetal bovine serum (FBS) were purchased from Gibco-BRL (Grand Island, USA). 3-(4,5-Dimethylthiazol-2-yl)-2,5-diphenyltetrazolium bromide (MTT) and the Live/dead cell apoptosis kit with annexin V- Alexa Fluor 488/ propidium iodide (PI) were ordered from Molecular Probes (Oregon, USA). All other chemicals were of analytical grades and used directly without further purification. Human Embryonic Kidney 293T (HEK 293T) cells were kindly supplied by Dr. Michael Brown at Hanson Institute, Adelaide Royal Hospital. Mesenchymal Stem Cell line (10T1/2) was obtained from RIKEN cell bank (Japan).

5.3.2 ATRP of PNIPAAm

In a typical polymerisation of PNIPAAm with a target degree of polymerization of 200 (DPn=200), NIPAAM (2.0 g, 17.6 mmol), CuCl (8.7 mg, 0.088 mmol) and 2-propanol (2 mL) were introduced into a dried Schlenk flask and fitted with a septum. Three freeze–pump–thaw cycles were performed. Me6Tren (24 µl, 0.088 mmol) was added via a nitrogen-purged syringe and the solution was stirred for 40 min at room temperature to allow formation of the CuCl/Me6TREN complex. 11 µl (0.088 mmol) of ECP was added using an air-free syringe to start the polymerization at 25°C. The reaction was exposed to air after 8 h. The solution was diluted by adding tetrahydrofuran and passed through an alumina column to remove the catalyst. The polymer was precipitated in diethyl ether, filtered and dried.

5.3.3 Dynamic light scattering (DLS)

DLS measurements were conducted using 1.0 mg mL^{-1} of the polymers in MilliQ water. The hydrodynamic diameters (d_h) were measured by DLS at different measurement temperatures using a Malvern Zetasizer (Nano-ZS). The DLS data were collected on an

autocorrelator with a detection angle of scattered light at 90°. The CONTIN software package was used to analyze the intensity autocorrelation functions.

5.3.4 Cell culture

Cells were cultured in DMEM supplemented with 10% FBS, 100 U mL^{-1} of penicillin, 100 mg mL^{-1} of streptomycin and 2 mM L^{-1} L- glutamine. The cells were incubated at 37°C in a humidified atmosphere in the presence of 5% CO_2. Cells were trypsinized, reseeded in 96-well plates at a density of 4.0×10^4 cells/mL and allowed to adhere overnight. Cell culture medium was replaced every two days until cells were harvested at the pre-set day. Harvested cells were used for the further analysis.

5.3.5 MTT assay

All cells were seeded at a density of 4.0×104 cells/mL and allowed to adhere overnight. The growth medium was replaced with fresh medium (200 μL) containing NIPAAm monomer or PNIPAAm polymer (P-35, P-100, P-200 or P-400) at concentrations of 0.5, 1.0, 2.0, 5.0 and 10.0 mg mL-1. Cells were then incubated for 48 h before measuring the cytotoxicity using MTT assay. HEK 293T cells were also treated with P-35, 200 or 400 at 5.0 mg mL^{-1} over a time range of 6 - 96 h to investigate the effect of incubation time on cell viability.

10 μL of MTT (5 mg mL^{-1} in PBS) were added to each well, including both samples and controls, and then incubated for 4 h at 37˚C. All liquid was removed from the wells and 150 μL dimethyl sulfoxide (DMSO) was added to each well to ensure complete solubilization of formazan crystals. After 1 h further incubation, the absorbance was read using an ELx808 microplate reader (BioTek, USA) at 595 nm.

To further investigate cell death in the presence of P-400 samples, P-200 and P-400 solutions (5.0 mg mL^{-1}) were added to the wells and allowed to precipitate by incubation at 37 °C for 1 h. HEK 293T cells were then seeded on top of the polymers. After 48 h further incubation at 37°C, cell viabilities were measured using the MTT assay.

5.3.6 Phase contrast and atomic force microscopy of polymer precipitates

In addition, 5.0 mg mL^{-1} of P-200 and P-400 in PBS solutions were added to the wells, made by Press-to-Seal™ silicone isolators on glass slides, and allowed to precipitate by incubation at 37 °C overnight. Precipitated polymer layers (without cell) were visualized under an inverted phase contrast microscope (Olympus IX50). Subsequently, the liquid phase was discarded and precipitates were dried in an oven. The thicknesses of the polymer layers were measured under the phase contrast microscope. The surface topographies were also analysed using an atomic force microscope (AFM) (NT-MDT Ntegra Solaris) in a tapping mode. 3D AFM images were prepared using the NOVA software.

5.3.7 Flow cytometry

HEK 293T cells (1.0 x 10^6 cells per well) were plated in 6-well plates and incubated at 37 °C for 24 h. For the detection of a chain length-related induction of apoptosis and necrosis, the cells were exposed to NIPAAm monomer, P-35 and P-200 (5.0 mg mL^{-1}) for 48 h at 37 °C. The liquid was removed, and cells were rinsed with PBS. The cells were then detached by trypsin, followed by incubation in 100 µL binding buffer containing annexin V-Alexa Fluor 488 and PI by following the manufacturer instructions. The Annexin V binds to phosphatidyl serine (secreted to the outer surface of cell membrane) as a marker of apoptosis. PI stains dead cells through reaction with nucleic acid. Therefore, it can be used to distinguish necrotic cells from apoptotic and live cells. The samples were analyzed using a FACSCalibur flow cytometer (BD, USA), equipped with an argon-ion laser for 488 nm excitation. Alexa Fluor and PI fluorescence were measured through 530/30 band-pass and 575/24 long pass filters, respectively. Data was analyzed with CellQuest software. Lower left and lower right quadrants represent live and apoptotic events. Upper right and upper left quadrants indicate necrotic events in one typical experiment.

5.4 Results and Discussion

In this study, we prepared a range of PNIPAAms with different chain lengths using the atom transfer radical polymerization (ATRP) (13-15), by which the final polymer molecular weight can be precisely adjusted (18, 19).

The hydrodynamic diameters (d_h) of polymer solutions at different measurement temperatures were evaluated by dynamic light scattering (DLS) and the onset transition temperatures were considered as the LCSTs of the polymers (20). The reaction conditions and characteristics of polymers are summarized in Table S1.

Table S1. Summary of reaction conditions and characteristics of the products

Sample	[M]:[I]:[CuCl]:[L][a]	M_n[b]	LCST (°C)[c]
P-35	35:1:1:1	3955	53
P-100	100:1:1:1	11300	38
P-200	200:1:1:1	22600	32
P-400	400:1:1:1	45200	28

[a] M: monomer, I: initiator, L: ligand

[b] Number average molecular weight

[c] Measured by dynamic light scattering.

The d_h for all samples experienced a sharp transition as the temperature increases, which is shown in Figure 1. PNIPAAm bears both hydrophilic (amide) and hydrophobic (isopropyl) groups, and water molecules can form cage-like structures to surround the hydrophobic moieties of PNIPAAm at low temperatures. Polymers molecularly dissolved in water with a d_h of around 10 nm. An increase in temperature causes the destruction of the "water cages" and the exposure of hydrophobic groups leads to the formation of PNIPAAm aggregates. Aggregation starts to form evidenced with a sharp increase in d_h when the temperature exceeded a specific phase transition temperature, which is known as the LCST (20). The LCST for low molecular weight PNIPAAm (P-35, MW = 3955) was

53 °C, while it droped to 28 °C as the polymer molecular weight increased to 45000 (P-400). This trend is consistent with previous reports (14, 15, 21, 22), but the transition temperatures differ from each other because different measuring instruments and experiment conditions were used. Xia et al. investigated the LCST of PNIPAAm at various molecular weights using differential scanning calorimetry (DSC) and found that it was raised from 30 ºC to 45 ºC when polymer molecular weight was decreased from 32500 to 3300 (14). In another study, the LCST changed from 36.1 ºC (MW= 16300) to 48.4 ºC (MW=3000) for the PNIPAAm with amine end groups (15).

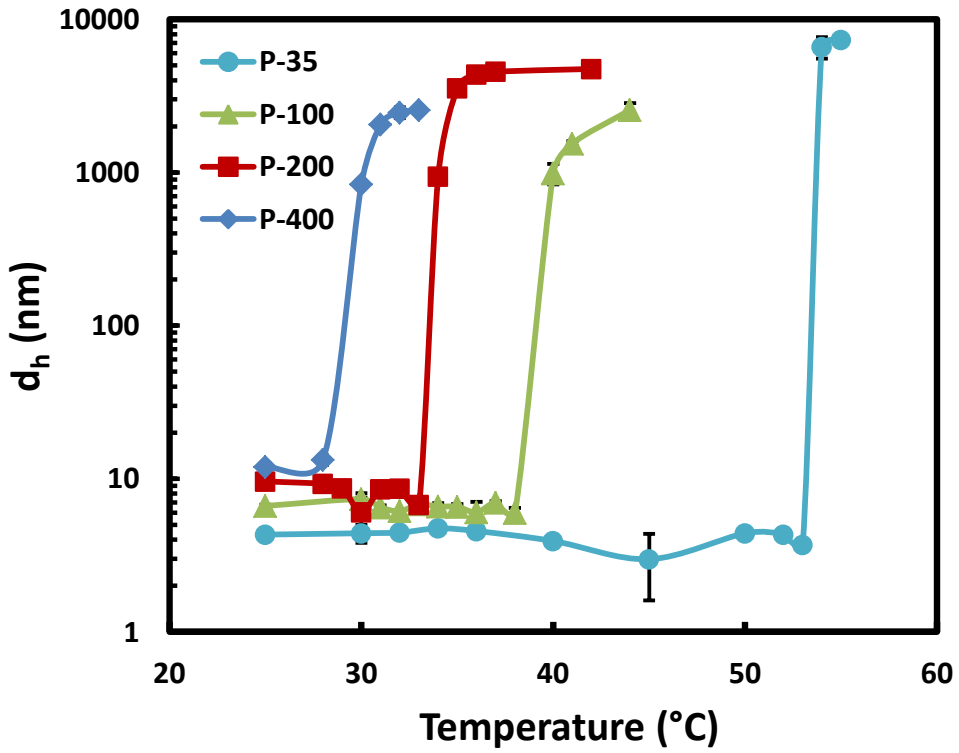

Figure 1. Temperature dependence of hydrodynamic diameter for 1.0 mg mL^{-1} PNIPAAm in water (Mean ± SD, n=3)

The cytotoxicity of polymers and monomers were examined against mesenchymal stem cells (MSCs), HEK 293T and HeLa cells. HEK 293 and HeLa cells are routinely used for evaluation of material biocompatibility (16, 17). Since in this PhD project, MSCs are used , MSCs will also be used for cytotoxicity.

The cell viabilities from the 3-(4,5-dimethylthiazol-2-yl)-2,5-diphenyltetrazolium bromide (MTT) assays are shown in Figure 2a by incubating HEK 293T cells with NIPAAm monomer and PNIPAAm with different molecular weights over a concentration range up to 10.0 mg mL^{-1} for 48 h. Viability values of NIPAAm monomer and polymer with low molecular weight (P-35) decreased by increasing concentration. P-35 is low toxic at concentrations below 5.0 mg mL^{-1} and the cytotoxicity increased as polymer concentration is raised above 5.0 mg mL^{-1}. In contrast, for the moderate-length PNIPAAms (P-100 and P-200), cell survivals were more than 80% within the whole concentration range. The decrement of cell survival was more substantial for P-400 than P-35. Cell viabilities decreased dramatically for P-400, when the concentrations exceeded 0.5 mg mL^{-1}. The experiments were also carried out with MSC and Hela cells (Figure S1). Although the MTT values varied with cell types, the general cytotoxic trends were similar for all these cell lines.

To monitor the cell viabilities at different incubation time (6, 24, 48, 72 and 96 h); we used HEK 293T cells with different molecular weight polymers at a fixed concentration of 5.0 mg mL^{-1}. As seen from Figure 2b, the viability of HEK cells had no statistically significant change over time, when treated with P-200. However, the incubation time had a significant effect on cell viabilities for P-35 and P-400. The MTT values for both samples increased during the first 24 h, which may be due to the fact that the proliferation rate suppresses the cell death rate. The following significant drop between 24 and 96 h implies a drastic cell death. The cell death was more severe for P-400 than P-35.

To further investigate cell death in the presence of P-400 samples, P-200 and P-400 solutions (5.0 mg mL^{-1}) were added to the wells and allowed to precipitate by incubation at 37 °C for 1 h. HEK 293T cells were then seeded on top of the polymers. After 48 h further incubation at 37°C, cell viabilities were measured using the MTT assay. Figure S2 shows that when the cells were seeded on top of polymer precipitates, the MTT value of P-400

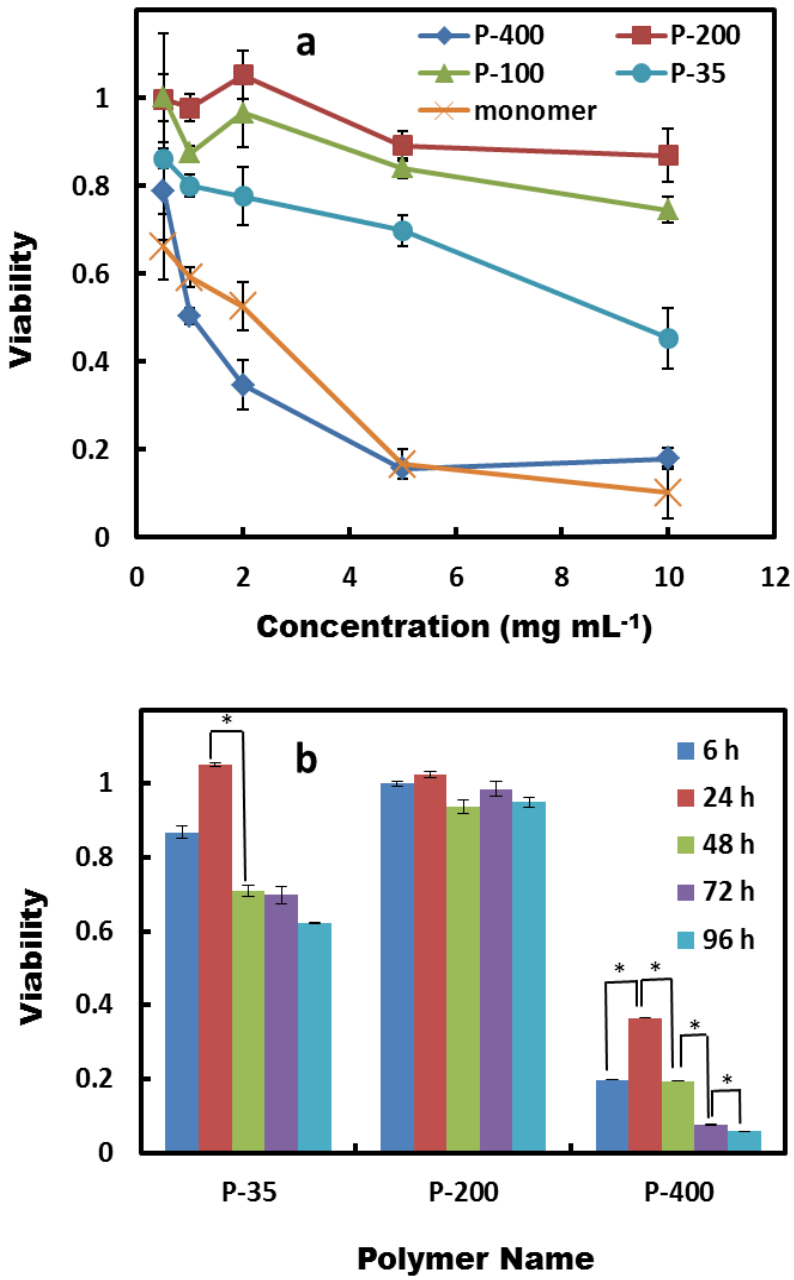

Figure 2. Viability of HEK 293T cells measured by MTT assay: (a) after 48h of incubation as a function of polymer/monomer concentration. (b) For 5.0 mg mL^{-1} polymers over time. (Mean ± SD, n=3), * p < 0.05

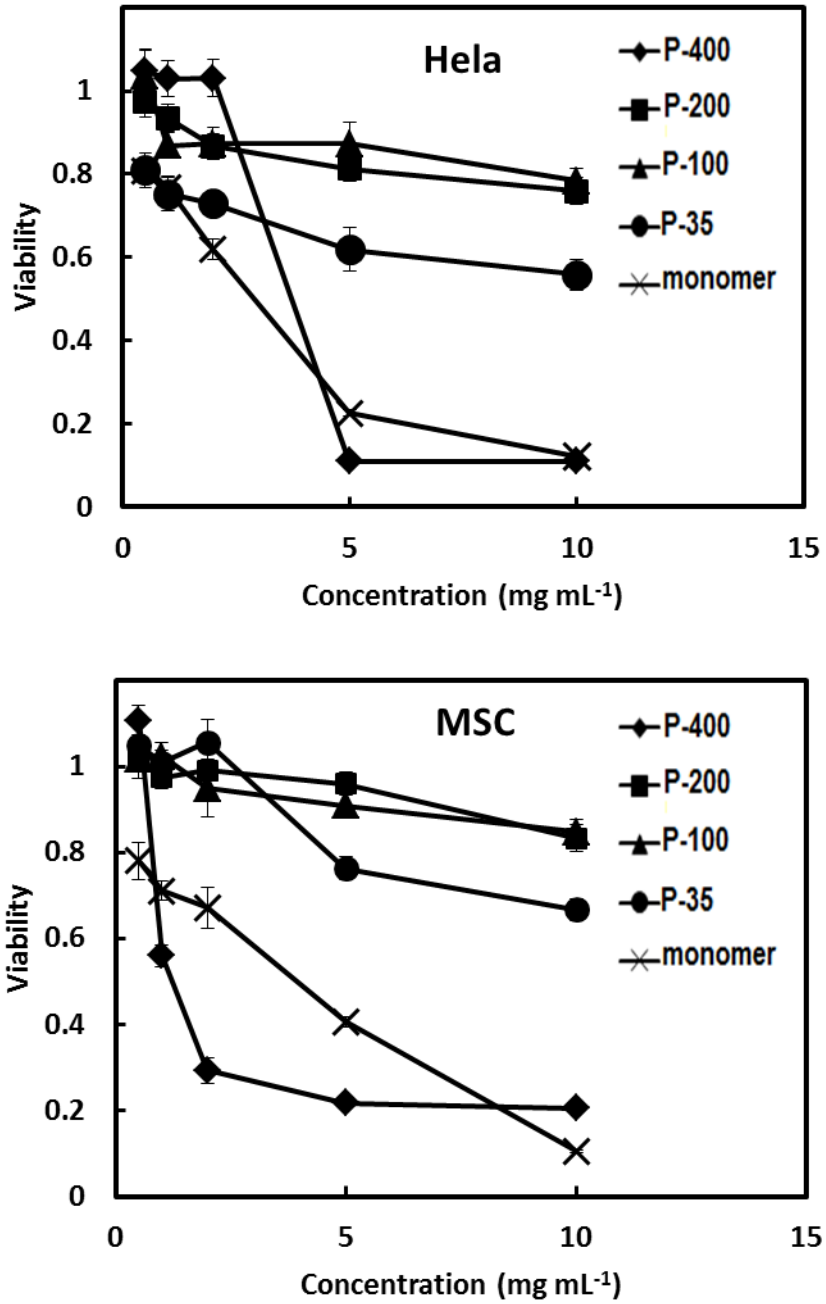

Figure S1. Viability of MSC and Hela cells after 48 h of incubation as a function of polymer concentration, measured by the MTT assay (Mean ± SE, n=3)

was similar to that of P-200 and the negative control. In addition, 5.0 mg mL^{-1} of P-200 and P-400 solutions were added to the wells, made by Press-to-Seal™ silicone isolators on glass slides, and allowed to precipitate by incubation at 37 °C overnight. Precipitated polymer layers (without cell) were visualized under an inverted phase contrast microscope. Figures 3a & b indicate that P-200 precipitates are formed as microspheres, while P-400 precipitates appeared to be an integrated, uniform and dense film. When the liquid phases were removed and the remaining precipitates were dried, a thin and transparent layer was observed for P-200, while P-400 precipitates were formed as a white thick film (Figures S3a & b). The thicknesses of the polymer layers were also measured under the phase contrast microscope. The thickness of P-200 precipitate was 49 µm (Figure 3c), whereas it was 102 µm for P-400 (Figure 3d). The surface topography was also analysed using an atomic force microscope (AFM). AFM topologies revealed that the surface of P-200 layer was bumpy (Figure S3c), suggesting a porous surface. In contrast, P-400 imparted a flat and smooth surface (Figure S3d), implying an impermeable film.

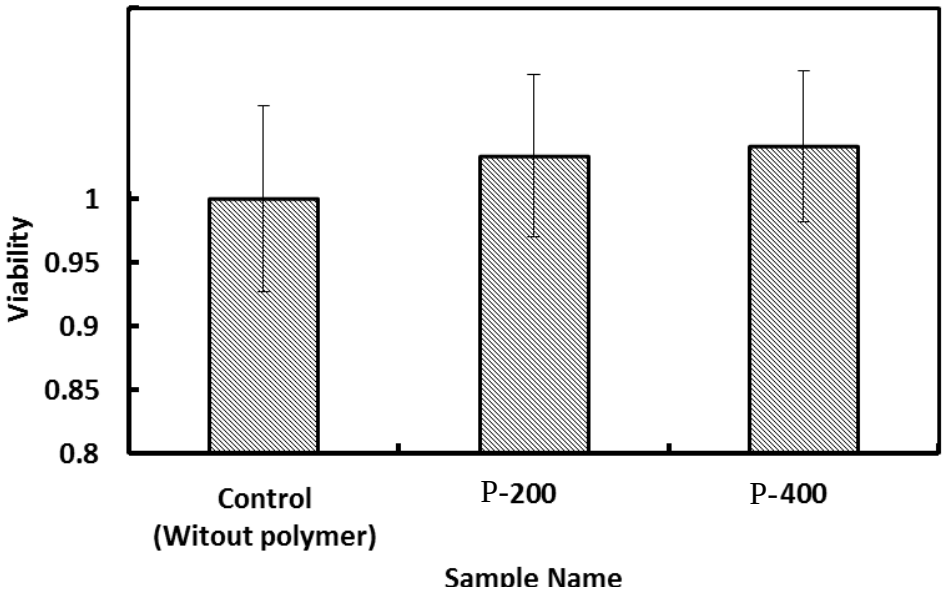

Figure S2. Viability of HEK 293T cells seeded on top of 5.0 mg mL^{-1} polymers after precipitation for 48 h, measured by MTT assay (Mean ± SE, n=3).

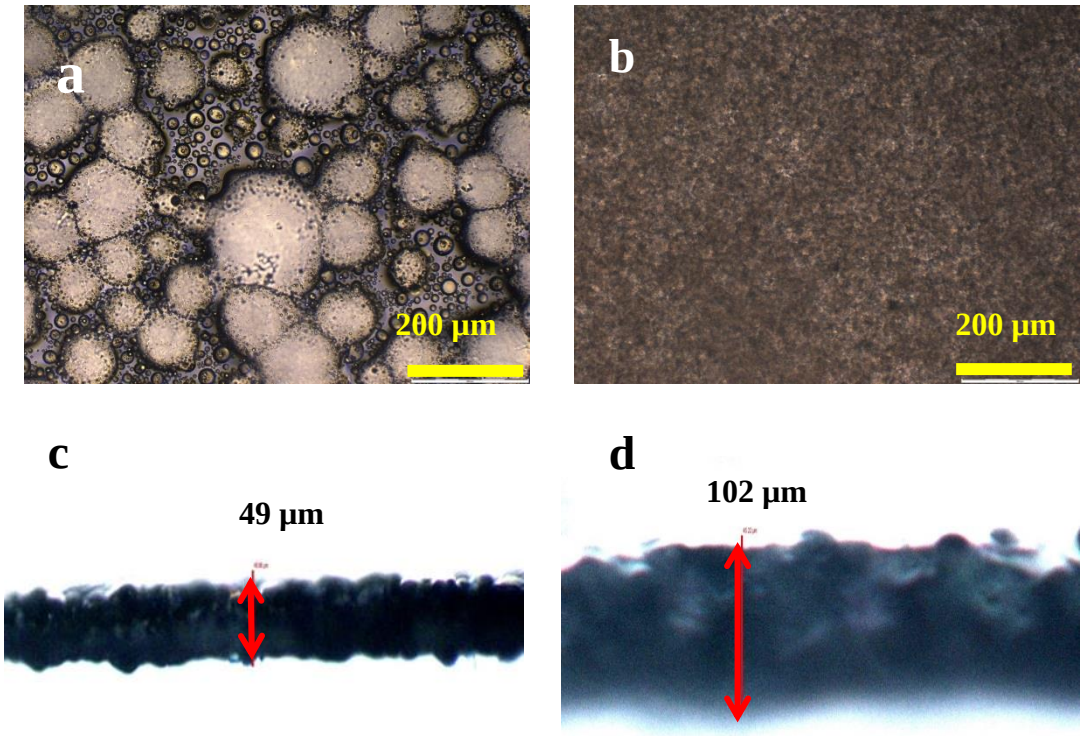

Figure 3. Micrographs of 5.0 mg mL^{-1} of P-200 (a,c) and P-400 (b,d) in PBS incubated at 37 °C for 24 h. (a,b) Top view of precipitated polymers. (c,d) Section view of dried polymers indicating the thickness of precipitated layer.

In order to distinguish the toxicity due to apoptosis or necrosis, after HEK 293T cells were exposed to P-35, P-200 and NIPAAm monomer, they were stained with annexin V-Alexa Fluor 488 and propidium iodide (PI), and analysed using a flow cytometer (23, 24). Untreated cells were employed as negative control. Results are summarized in Table 1 and the dot plots of flow cytometric analysis are presented in Figure S4. The majority of cells

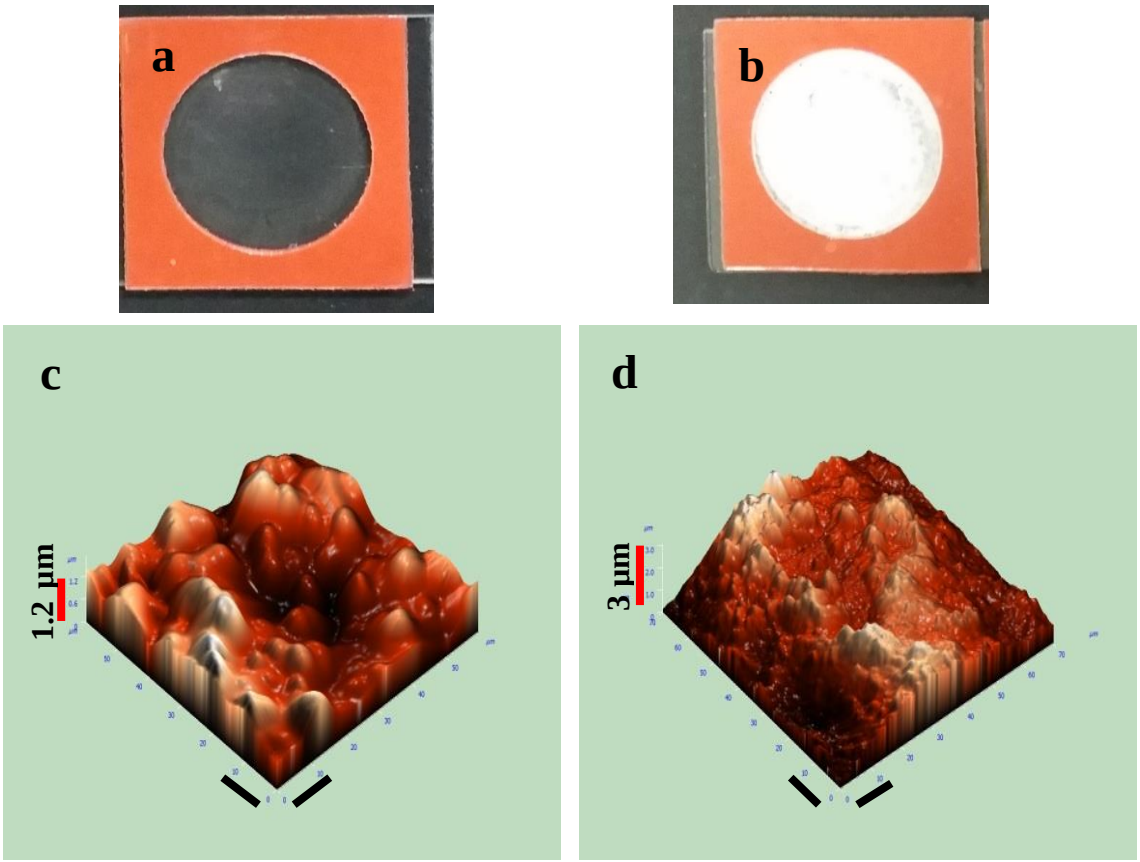

Figure S3. (a, b) Photographs of 5.0 mg mL^{-1} of P-200 (a) and P-400 (b) in PBS incubated at 37°C for 24 h, and then liquid phase was removed and dried. (c, d) 3D atomic force microscopy (AFM) topologies from the surface of a and b, respectively (scale bars are 10 µm).

in negative control (up to 83.09%) were healthy and only a few cells (6.66%) displayed apoptotic characteristics with positive annexin stains on cell surface, while other 10.25% were recognized as necrotics with positive PI stains. Cells revealed more necrotic damage when exposed to P-200 (20.91±0.67%), while apoptotic cells remained at the same level as the control. After exposure to P-35, the necrotic cell percentage nearly doubled (40.29±1.65%) compared with P-200. However, no significant change was observed in apoptosis induction. A similar trend was found for the cells treated with NIPAAm monomer: 65.08±0.87% for necrosis and 7.42±2.06% for apoptosis. Results of the flow cytometric analysis agreed with the MTT measurements. These results further indicated that the major cell death mechanism was necrosis when cells exposed to NIPAAm or PNIPAAm. These chemicals directly destroy cells rather than changing cell programming for self-suicide.

Table 1. Induction of apoptosis and necrosis in HEK 293T cells.

Sample	Negative Control	P-200	P-35	NIPAAm
Apoptotic (%)[a]	6.66±0.84	6.74±0.56	5.24±1.36	7.42±2.06
Necrotic (%)[a]	10.25±0.79	20.91±0.67	40.29±1.65	65.08±0.87

[a] Values (means ± SE) from 3 independent experiments are presented.

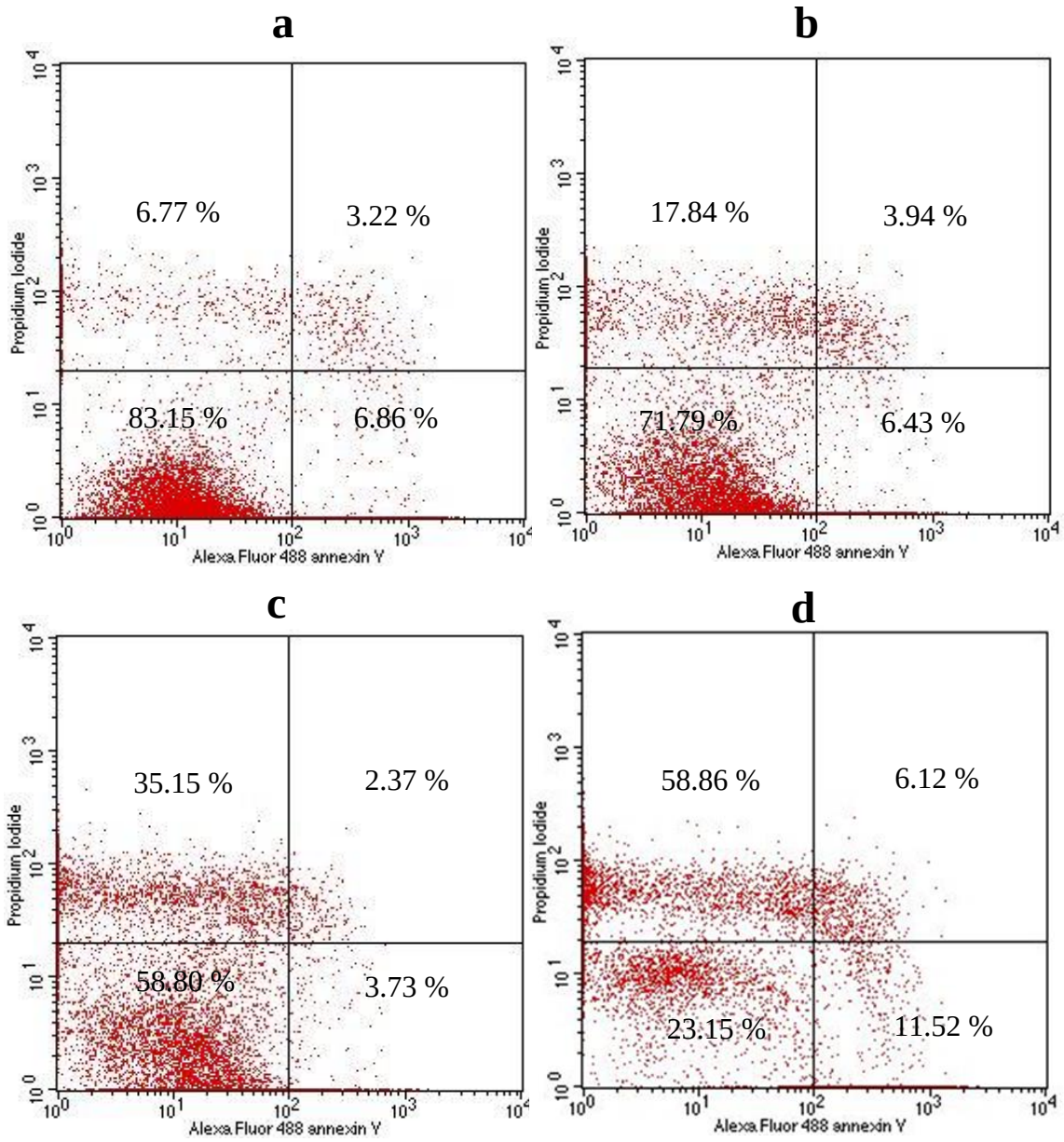

Figure S4. The influence of PNIPAAm chain length on the stimulation of apoptosis and necrosis in HEK 293T cells, measured using a flow cytometer. Cells were incubated with annexin V- Alexa Fluor 488 (apoptotic cells) and PI (necrotic cells) for 48 h. (a) Negative control without any polymer or monomer, (b) P-200, (c) P-35, (d) NIPAAm monomer. Lower left and lower right quadrants represent live and apoptotic events. Upper right and upper left quadrants indicate necrotic events in one typical experiment.

Figure 4 shows the phase contrast micrographs of MSCs after exposure to either P-200 or P-35. The majority of cells showd normal spread morphology when exposed to P-200 (Figure 4a), which were similar to the morphology of cells in negative control (Figure S5). However, the cells exhibited a spherical morphology when they were exposed to the media containing P-35 (Figure 4b). Most of cells were detached or loosened indicating cell death (12, 25). These results were consistent with the MTT assay and the flow cytometric measurements and further confirmed that cytotoxicity of PNIPAAm is dependent on polymer molecular weight.

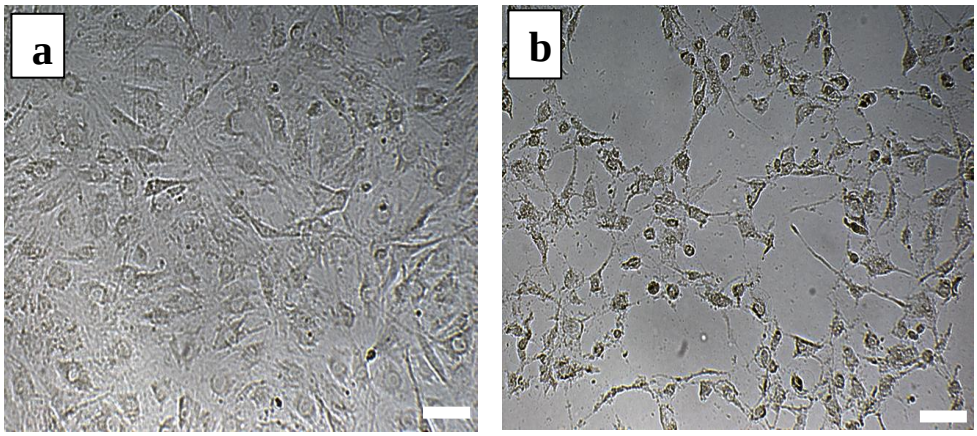

Figure 4. Morphologies of MSCs incubated for 48 h at 37 °C with 5.0 mg mL^{-1} of (a) P-200 or (b) P-35. Scale bars are 50µm. (150×)

A suggested mechanism of monomer cytotoxicity is the alteration of the lipid layers of cell membranes, which affects the permeability of the membrane (26). Likewise, the low molecular weight PNIPAAm (P-35) was fully soluble and small enough to conveniently penetrate the cell membrane and hinder cell normal activities (Scheme S1a). For medium-sized PNIPAAms (P-100 and P-200), the culture temperature was higher than their LCSTs. The formed large aggregates impeded polymer transportation through cell membrane and thus reduced the cytotoxicity (Scheme S1b). High molecular weight PNIPAAm (P-400)

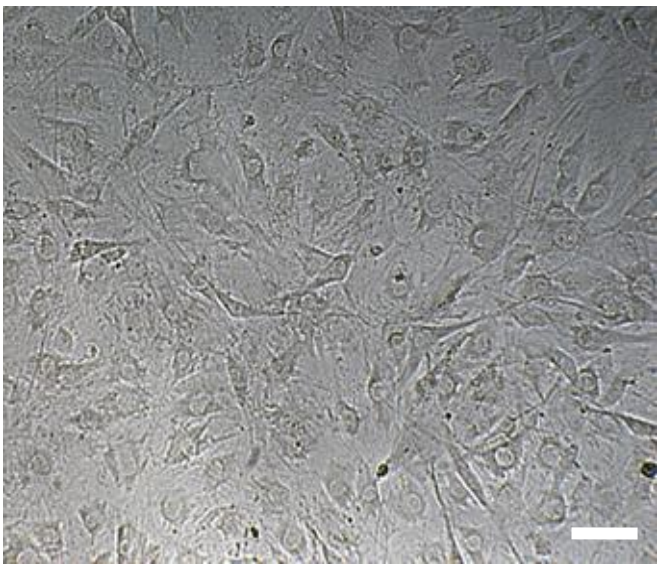

Figure S5. Morphology of MSCs incubated for 48 h at 37 °C without polymer as control. Scale bar is 50μm. (150×)

was not toxic when cells were seeded on top of the polymer coated surface. This is in agreement with previous comparable reports that PNIPAAm coated surfaces were used for cell sheeting (27). However, dramatic cell death for P-400 was found, when monolayer cells on the surface were exposed to the polymer solution. The cell death may be due to lack of nutrients and oxygen delivery from solution to the cells because entanglements of P-400 chains at culture temperature above LCST resulted in a dense and impermeable layer with blocked pores (Scheme S1c).

In this study, the influence of molecular weight on the cytotoxicity of PNIPAAm was investigated. Our results indicate that low molecular weight PNIPAAm is inherently cytotoxic and the main cell death pathway is necrosis. Moderate-sized PNIPAAms with their degrees of polymerization between 100 and 200 are non-cytotoxic or low cytotoxic. Due to chain entanglement of high molecular weight P-400, the cytotoxicity is dependent on the assay method. Our findings can provide great insights for future thermoresponsive polymer designs.

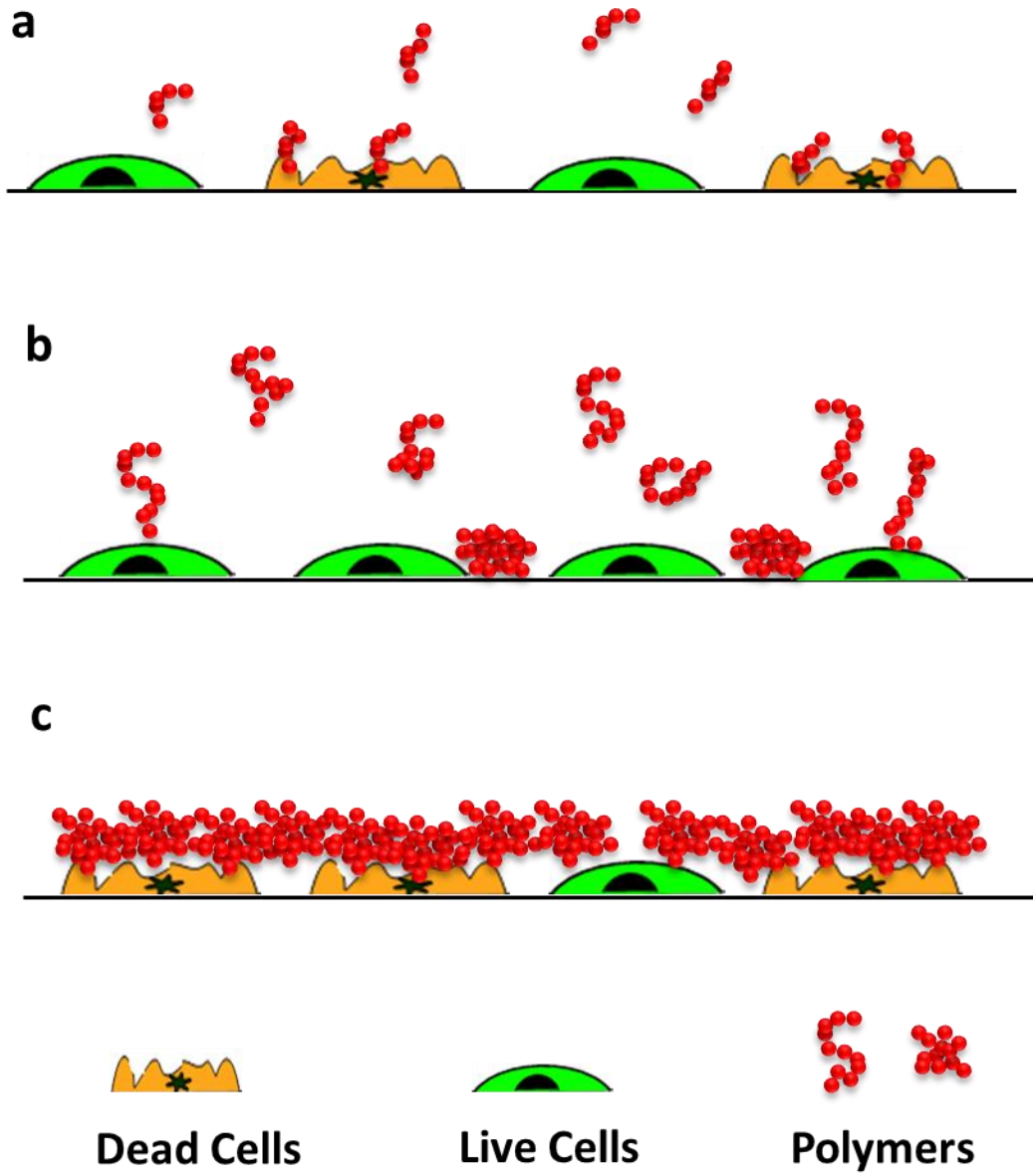

Scheme S1. The effect of PNIPAAm chain length on cell viability. (a) Short PNIPAAm chain (P-35) is toxic to cells. (b) Medium-sized PNIPAAm chains (P-100 and P-200) are non-toxic to cells. (c) Long PNIPAAm chain (P-400) precipitates at 37 ˚C and cover cell surface.

5.5 Acknowledgement

AM would like to acknowledge the Adelaide Scholarship International of the University of Adelaide. HZ thanks the MAWA Trust and the 111 Project (B12034).

5.6 References

1. Langer R, Brem H, Tapper D. Biocompatibility of polymeric delivery systems for macromolecules. Journal of Biomedical Materials Research. 1981;15(2):267-77.
2. Singh R, Singh S, Lillard JW. Past, present, and future technologies for oral delivery of therapeutic proteins. Journal of Pharmaceutical Sciences. 2008;97(7):2497-523.
3. Yoshii E. Cytotoxic effects of acrylates and methacrylates: Relationships of monomer structures and cytotoxicity. Journal of Biomedical Materials Research. 1997;37(4):517-24.
4. Salehpour S, Zuliani CJ, Dubé MA. Synthesis of novel stimuli-responsive polyglycerol-based hydrogels. European Journal of Lipid Science and Technology. 2012;114(1):92-9.
5. Duncan R. The dawning era of polymer therapeutics. Nature Reviews Drug Discovery. 2003;2(5):347-60.
6. Chang C-W, Choi D, Kim WJ, Yockman JW, Christensen LV, Kim Y-H, et al. Non-ionic amphiphilic biodegradable PEG–PLGA–PEG copolymer enhances gene delivery efficiency in rat skeletal muscle. Journal of Controlled Release. 2007;118(2):245-53.
7. Exner AA, Krupka TM, Scherrer K, Teets JM. Enhancement of carboplatin toxicity by Pluronic block copolymers. Journal of Controlled Release. 2005;106(1):188-97.
8. Yoo HS, Park TG. Biodegradable polymeric micelles composed of doxorubicin conjugated PLGA–PEG block copolymer. Journal of controlled release. 2001;70(1):63-70.
9. Klouda L, Mikos AG. Thermoresponsive hydrogels in biomedical applications. European Journal of Pharmaceutics and Biopharmaceutics. 2008;68(1):34-45.
10. Mellati A, Dai S, Bi J, Jin B, Zhang H. A biodegradable thermoresponsive hydrogel with tuneable properties for mimicking three-dimensional microenvironments of stem cells. RSC Adv. 2014;4(109):63951-61.
11. Shen Z, Mellati A, Bi J, Zhang H, Dai S. A thermally responsive cationic nanogel-based platform for three-dimensional cell culture and recovery. RSC Advances. 2014;4(55):29146-56.

12. Wadajkar AS, Koppolu B, Rahimi M, Nguyen KT. Cytotoxic evaluation of N-isopropylacrylamide monomers and temperature-sensitive poly (N-isopropylacrylamide) nanoparticles. Journal of Nanoparticle Research. 2009;11(6):1375-82.

13. Masci G, Giacomelli L, Crescenzi V. Atom transfer radical polymerization of N‐Isopropylacrylamide. Macromolecular Rapid Communications. 2004;25(4):559-64.

14. Xia Y, Yin X, Burke NA, Stöver HD. Thermal response of narrow-disperse poly (N-isopropylacrylamide) prepared by atom transfer radical polymerization. Macromolecules. 2005;38(14):5937-43.

15. Xia Y, Burke NA, Stöver HD. End group effect on the thermal response of narrow-disperse poly (N-isopropylacrylamide) prepared by atom transfer radical polymerization. Macromolecules. 2006;39(6):2275-83.

16. Chan P, Kurisawa M, Chung JE, Yang YY. Synthesis and characterization of chitosan-*g*-poly(ethylene glycol)-folate as a non-viral carrier for tumor-targeted gene delivery. Biomaterials. 2007;28(3):540-9.

17. Souza RD, Zahedi P, Allen CJ, Piquette-Miller M. Biocompatibility of injectable chitosan‐phospholipid implant systems. Biomaterials. 2009;30(23-24):2818-24.

18. Matyjaszewski K, Xia J. Atom transfer radical polymerization. Chemical Reviews. 2001;101(9):2921-90.

19. Patten TE, Matyjaszewski K. Atom transfer radical polymerization and the synthesis of polymeric materials. Advanced Materials. 1998;10(12):901-15.

20. Bao H, Li L, Leong WC, Gan LH. Thermo-responsive association of chitosan-graft-poly (N-isopropylacrylamide) in aqueous solutions. The Journal of Physical Chemistry B. 2010;114(32):10666-73.

21. Furyk S, Zhang Y, Ortiz‐Acosta D, Cremer PS, Bergbreiter DE. Effects of end group polarity and molecular weight on the lower critical solution temperature of poly (N‐isopropylacrylamide). Journal of Polymer Science Part A: Polymer Chemistry. 2006;44(4):1492-501.

22. Uchida K, Tamura A, Yajima H. Effect of the polymer chain length of poly (N-isopropylacrylamide) on the temperature-responsive phase transition behavior of its conjugates with [60] fullerene. Biointerphases. 2010;5(1):17-21.

23. Vermes I, Haanen C, Steffens-Nakken H, Reutellingsperger C. A novel assay for apoptosis flow cytometric detection of phosphatidylserine expression on early apoptotic cells using fluorescein labelled annexin V. Journal of Immunological Methods. 1995;184(1):39-51.

24. Spagnuolo G, Galler K, Schmalz G, Cosentino C, Rengo S, Schweikl H. Inhibition of phosphatidylinositol 3-kinase amplifies TEGDMA-induced apoptosis in primary human pulp cells. Journal of Dental Research. 2004;83(9):703-7.

25. May JE, Morse HR, Xu J, Donaldson C. Development of a novel, physiologically relevant cytotoxicity model: Application to the study of chemotherapeutic damage to mesenchymal stromal cells. Toxicology and Applied Pharmacology. 2012;263(3):374-89.

26. Moharamzadeh K, Van Noort R, Brook IM, Scutt AM. Cytotoxicity of resin monomers on human gingival fibroblasts and HaCaT keratinocytes. Dental Materials. 2007;23(1):40-4.

27. Takahashi H, Nakayama M, Yamato M, Okano T. Controlled Chain Length and Graft Density of Thermoresponsive Polymer Brushes for Optimizing Cell Sheet Harvest. Biomacromolecules. 2010 2010/08/09;11(8):1991-9.

CHAPTER SIX

6. Poly (N-isopropylacrylamide)/Chitosan Hybrid as a Three-dimensional Microenvironment for Stem Cells in Cartilage Tissue Engineering

Poly (N-isopropylacrylamide)/chitosan hybrid as a three-dimensional microenvironment for stem cells in cartilage tissue engineering

Amir Mellati[a], Meisam Valizadeh Kiamahalleh[a], S. Hadi Madani[b], Sheng Dai[a], Jingxiu Bi[a], Bo Jin[a], Hu Zhang[a]*

[a]School of Chemical Engineering, the University of Adelaide, Adelaide SA5005, Australia
[b]Ian Wark Research Institute, University of South Australia, SA5095, Australia

*Corresponding author
E-mail: hu.zhang@adelaide.edu.au
Tel: + 61 8 8313 3810

6.1 Abstract

Providing a well-defined three-dimensional (3D) microenvironment for chondrogenic differentiation of mesenchymal stem cells (MSCs) remains a great challenge for cartilage tissue engineering. In this work, well-defined poly (N-isopropylacrylamide) (PNIPAAm) polymers with degrees of polymerization 100 and 400 (NI100 and NI400) were prepared and the polymer solutions were introduced into chitosan porous scaffolds (CS) to form hybrids (CSNI100 and CSNI400, respectively). MSCs were incorporated within the hybrid and cell proliferation and chondrogenic differentiation were monitored. A delay time of 6 min for CSNI100 and 9 min for CSNI400 hybrids is required before incubation, in order to obtain an even distribution of cell and PNIPAAm solution inside the scaffold as well as to keep the least loss of PNIPAAm solution. The lower critical solution temperature (LCST) for both PNIPAAms alters due to hybridization with chitosan. The LCST of NI100 and NI400 drops from 37.46 °C (without chitosan) to 33.89 °C (with chitosan) and from 32.79 °C to 31.29 °C, respectively. CSNI400 have a pore volume 1.5 folds greater than CSNI100. The hybrid scaffolds show a higher swelling ratio than chitosan-alone scaffolds, and the swelling ratio of CSNI400 is also higher than that of CSNI100. SEM images indicate that the PNIPAAm gel partially occupies chitosan pores while the interconnected porous structure of chitosan is preserved. After seven-day incubation of the cell-laden constructs in a growth medium, viable cells in CSNI100 and CSNI400 are 54% and 108% higher than those in CS, respectively. Glycosaminoglycan and total collagen contents are increased 2.6 and 2.5 folds after 28-day culture in the chondrogenic medium. These results suggest that the hybrid scaffolds composed of chitosan solid scaffold and the well-defined PNIPAAm, in particular CSNI400, is suitable for 3D stem cell culture and cartilage tissue engineering.

6.2 Introduction

Cartilage failures due to diseases such as arthritis or daily accidents are one of the most reasons for disabilities around the world (1). Articular cartilage has a very limited capacity for self-healing (2). Tissue engineering is one of the most promising therapeutic strategies by regenerating a functional articular cartilage through seeding the appropriate cells in a three-dimensional matrix under the optimum microenvironment. However, obstacles for clinical treatment of cartilage failure remain to be overcome, including design and preparation of appropriate matrices as three-dimensional (3D) microenvironment for cells. Chitosan and poly (N-isopropylacrylamide) (PNIPAAm) have been used (either separately or together) in various forms to mimic the cellular microenvironment in cartilage tissue engineering (3-6).

Chitosan-based matrices are an attractive group of biomaterials as scaffolds in cartilage tissue engineering. Chitosan can promote cartilage regeneration due to its similarity with glycosaminoglycans (GAGs) and hyaluronic acid which are major components of the extracellular matrix (ECM) of the native articular cartilages. These biomolecules play a great role in inducing chondrogenesis and modulating the cell morphology, differentiation and function (4, 7, 8). PNIPAAm-based thermoresponsive hydrogels have been widely used in biomedical applications (9). PNIPAAm undergoes a thermal phase transition in an aqueous solution at a temperature termed as lower critical solution temperature (LCST). The LCST of PNIPAAm is close to the human physiological temperature at which cells reside in comfort. This fact has made PNIPAAm as one of the most studied thermoresponsive polymers.

As a thermoresponsive moiety, poly (N-isopropylacrylamide) (PNIPAAm) can be introduced to the chitosan through a variety of approaches. PNIPAAm-based thermoresponsive chitosan has been prepared in various methods, including interpenetrating polymer networks (IPN) (10, 11), semi-IPN (11, 12), surface grafted membranes (13), chemically cross-linked hydrogels in forms of discs (14-16), films (16, 17) , nanoparticles (18-22) and solutions (5, 6, 23-26).To the best of our knowledge, the

hybrid matrix composed of chitosan and PNIPAAm (without any chemical bond between chitosan and PNIPAAm or cross-linking between chitosan and/or PNIPAAm molecules), and its performance as cell microenvironment have not been reported yet.

Physical, mechanical and chemical properties of PNIPAAm polymers are molecular weight-dependent (27-29). Our previous study has demonstrated that its cytotoxicity also depends on the PNIPAAm molecular chain length (Chapter 5). However, the effect of polymer molecular weight on cellular activity in a 3D microenvironment remains to be investigated. In this study, well-defined PNIPAAms were prepared through atom transfer radical polymerization (ATRP) and the polymer solution was introduced into chitosan porous scaffolds to form hybrids upon incubating at 37 °C. These hybrids may benefit from both improved cellular compatibility of controlled PNIPAAm as well as good properties of chitosan in chondrogenesis of MSCs. PNIPAAm and PNIPAAm/chitosan hybrids were characterized and mesenchymal stem cell (MSC) proliferation within hybrid matrices was evaluated. The hybrid structure was further used as a novel scaffold for chondrogenic differentiation of MSCs.

6.3 Materials and methods

6.3.1 Materials

All chemicals were of analytical grades and used directly without further purification, unless otherwise mentioned.

6.3.2 Preparation of scaffolds

2.0 wt% chitosan (MW of 200-300 kDa, Acros Organic, NJ) solutions in 0.2 M acetic acid were prepared. 380 µL of chitosan solution was added to each well of 24-well plates and were frozen at -80 °C overnight. The frozen samples were lyophilized in an ALPHA 1-2LD plus freeze-dryer (CHRIST, Germany) for 48 h. Porous chitosan scaffolds (CS) were washed with 0.05 M NaOH for 10 min and rinsed twice in water and twice in PBS (Gibco-BRL, Grand Island).

Well-defined PNIPAAms were prepared through ATRP. To prepare PNIPAAm with a degree of polymerization (DP) of 100, the monomer n-isopropylacrylamide (NIPAAm, 97%, Sigma-Aldrich) was purified by recrystallization in n-hexane. 1.0 g (8.8 mmol) NIPAAm, 8.7 mg (0.088 mmol) copper chloride (CuCl, Sigma-Aldrich) were dissolved in 2.0 mL 2-propanol, transferred to a dried Schlenk flask and fitted with a septum. Three freeze–pump–thaw cycles were conducted before addition of 24.0 µl (0.088 mmol) of Tris[2-(dimethylamino)ethyl]amine (Me_6Tren, 97%, Sigma-Aldrich) using a nitrogen-purged syringe. The solution was stirred for 40 min at room temperature to allow formation of the CuCl/Me_6TREN complex. 11.0 µl (0.088 mmol) of ethyl 2-chloropropionate (ECP, Sigma-Aldrich) was added to start polymerization using an air-free syringe. After 8 h reaction at 25 °C, the solution was exposed to air, diluted by adding tetrahydrofuran and passed through an alumina column to separate the catalyst. The polymer was precipitated in diethyl ether, filtered and dried in an oven.

PNIPAAm with DPs of 100 and 400 (NI100 and NI400) solutions of 80 mg/mL (in PBS) were prepared. 50 µL of the PNIPAAm solution was pipetted to the top of chitosan scaffolds in 24-well plates. The plates were transferred to an oven at 40 °C to form CS/NI100 (CSNI100) and CS/NI400 (CSNI400) hybrids.

6.3.3 Dynamic light scattering

Dynamic light scattering (DLS) measurements were carried out using 1.0 mg/mL of the PNIPAAms in MilliQ water. The hydrodynamic diameters (d_h) were recorded at different measurement temperatures using a Malvern Zetasizer (Nano-ZS). The DLS data were collected on an autocorrelator with a detection angle of scattered light at 90°. The CONTIN software package was used to analyze the intensity autocorrelation functions.

6.3.4 Thermal analysis

50 µL of NI100 or NI400 aqueous solution (80 mg/mL) was pipetted on top of chitosan scaffolds and were left at room temperature at intervals of 3, 6, 9, 12, 15 and 18 min before

transferred to a 40 °C oven to solidify the PNIPAAm. Thermal gravimetric analysis (TGA) was carried out using LABSYS TG-DTA/DSC (SETARAM Instrumentation, France). Dried samples were preheated at 100 °C for 5 min to remove moisture and thermal decomposition profiles were recorded at a heating rate of 10 °C/min between 100 °C and 700 °C under nitrogen gas.

Differential scanning calorimetry (DSC) was performed using a LABSYS TG-DTA/DSC (SETARAM Instrumentation, France). NI100 and NI400 aqueous solutions as well as CSNI100 and CSNI400 hydrogels were prepared using PBS as a solvent. Samples were heated up from 25 to 60 °C at a rate of 0.5 °C/min under nitogen gas.

6.3.5 Gas absorption

Nitrogen gas adsorption experiments were carried out at 77 K using a Belsorp-Max gas adsorption apparatus (Bel, Japan). Samples were degassed prior to the adsorption experiments at ambient temperature and a background pressure of 10-5 kPa for 6 h. Ultra high purity (>99.999%) helium and nitrogen (Coregas, Australia) were used for dead-space measurements and nitrogen adsorption experiments, respectively. Pore size distributions (PSD) were calculated based on the BJH method (30), and BET surface areas were calculated using BET method (31).

6.3.6 Swelling ratio

Dried samples of the chitosan/PNIPAAm hybrid were prepared at the optimum incubation time based on TGA results. Chitosan scaffolds were prepared through the same procedure without addition of PNIPAAm. Swelling ratio was determined according to the previous reports (13, 32). Samples were weighed and then immersed into the PBS solution at various temperatures ranging from 45 °C to 4 °C for 8 h. Swollen samples were taken out from the buffer solution, wiped gently with a filter paper to remove free water from surface and weighed. The swelling ratio (SR) was defined as $SR= (W_s-W_{d)} /W_d$, where W_s and W_d were the weights of the swollen and the dry samples, respectively.

6.3.7 Preparation of cell-laden scaffolds

Mesenchymal stem cell line (10T1/2, RIKEN cell bank, Japan) was cultured in Dulbecco's Modified Eagle's Medium (DMEM, Gibco-BRL, Grand Island) supplemented with 10% fetal bovine serum (FBS, Gibco-BRL, Grand Island), 100 U/mL of penicillin (Gibco-BRL, Grand Island), 100 mg/mL of streptomycin (Gibco-BRL, Grand Island) and 2 mM/L L-glutamine (Gibco-BRL, Grand Island). The cells were incubated at 37°C in a humidified atmosphere in the presence of 5% CO_2. Cells were trypsinized from flasks and resuspended in a fresh culture medium at a density of 4.0×10^7 cells/mL.

NI100 and NI400 solutions of 160 mg/mL (in PBS) were prepared (pH of 7.4) and sterilized by autoclave. Cell suspension and polymer solution were mixed to prepare a mixture of cell and polymer at a cell concentration of 2.0×10^7 cells/mL and a final polymer concentration of 80 mg/mL. Chitosan scaffolds (neutralized and washed) were sterilized using 75% ethanol, under UV light for 3 h. The solvent was exchanged (6×) with the sterile PBS. 50 µL of the cell/polymer mixture was pipetted to the top of chitosan scaffolds in 24-well plates. The same cell concentrations were prepared by mixing cells and PBS without PNIPAAm as CS samples. Well plates were transferred to incubator at predetermined times, based on TGA results and incubated for 1 h at 37˚C to form hybrid hydrogels. 2.0 mL of fresh growth medium was topped up to each well and kept in a humidified incubator at 37˚C and 5% CO_2. Medium was replaced with fresh medium every day.

6.3.8 Scanning electron microscopy

Chitosan or chitosan/PNIPAAm hybrid samples were freeze-dried before gold coating. Cell-laden constructs (after 3 days incubation with growth medium) were first fixed in the EM fixative (4% paraformaldehyde / 1.25% glutaraldehyde (ProSciTech, Australia) in PBS + 4% sucrose (Chem Supply, Australia), pH of 7.2), washed in a washing buffer (PBS + 4% sucrose), and post-fixed in 2% OsO4 (ProSciTech, Australia) in water. Fixed

samples were dehydrated in serial ethanol followed by immersion in hexamethyldisilazane (HDMS, ProSciTech, Australia)/ethanol (1:1) and 100% HDMS. Samples were air-dried and gold coated. The morphologies of samples were observed by a Philips XL 30 FEG scanning electron microscope (SEM) (FEI, USA).

6.3.9 Mitochondrial activity measurement

Growth medium of cell-laden constructs was replaced with fresh medium at predefined times and 100 µL (5 mg/mL in PBS) of 3-(4,5-Dimethylthiazol-2-yl)-2,5-diphenyltetrazolium bromide (MTT, Molecular Probes, OR) were added to each well and incubated for 4 h at 37˚C. All liquid was removed from the wells and 2.0 mL dimethyl sulfoxide (DMSO) was added to each well to ensure complete solubilization of formazan crystals. After 1 h further incubation, constructs were transferred to centrifuge tubes and briefly vortexed to homogenize before centrifugation. The absorbance of supernatant was read using an ELx808 microplate reader (BioTek, USA) at 570 nm.

6.3.10 Confocal laser scanning microscopy

Live/Dead® viability/cytotoxicity kit (Molecular Probes, OR) was used to stain live and dead cells. 1.0 µM of acetomethoxy derivate of calcein (calcein AM) and 2.5 µM of ethidium homodimer-1 (EthD-1) working solutions were prepared freshly according to the manufacturer's protocol. At day 1 and 7, the growth medium was removed and constructs were washed with 1.0 mL of preheated PBS. The liquid was replaced with 2.0 mL of dye working solution and further incubated at 37˚C for 45 min. Samples were washed with PBS to remove unreacted dyes. For cell detachment evaluation, cells were detached by lowering the temperature to room temperature during staining and cell suspension was collected after washing the construct. The suspension was centrifuged to pellet the cells. Cell pellet was rinsed carefully with PBS and resuspended in fresh PBS. Samples were transferred carefully to a chamber made from coverslips and Press-to-Seal™ silicone isolators (Molecular Probes, OR) and observed under a Leica SP5 spectral scanning

confocal microscope (Leica Microsystems, Germany) equipped with a temperature controlled stage to keep the thermoresponsive hydrogels at 37˚C. Excitation wavelengths were set to 494 and 528 nm and emission wavelengths were at 517 and 617 nm for live (green) and dead (red) cells, respectively.

6.3.11 Chondrogenic induction

Cell-laden CSNI400 constructs were prepared as pre-described at a cell density of 1.25×10^{6} cells/well. 2.0 mL of chondrogenic medium containing high glucose-DMEM, 1% insulin, transferrin, selenous acid (ITS)+Permix (BD Bioscience, MA), 10^{-7} M dexamethasone (Sigma-Aldrich), 10.0 ng/mL transforming growth factor-beta 1(TGF-β1) (Peprotech, NJ), 50.0 µg/mL ascorbate-2-phosphate (Sigma-Aldrich), 100.0 U/mL of penicillin, 100.0 mg/mL of streptomycin and 2.0 mM/L L-glutamine was added to each well and kept in an incubator at 37 °C and 5% CO_2 for continuous 28 days. The medium was being changed every day. Eight wells at sampling days were taken out for biochemical analysis.

6.3.12 Biochemical assays

DNA, glycosaminoglycan (GAG) and total collegen content were quantified by Hoechst 33258, DMMB and hydroxyproline assays as described previously (33, 34). At each time point constructs were collected, rinsed with prewarmed PBS, freeze-dried for 48 h and incubated in papain (Sigma-Aldrich) solution at 60 °C for 16 h to digest. The supernatant of the papain-digested hydrogels was used for biochemical assays.

DNA content was measured by the Hoechst 33258 assay. 30.0 µL of the supernatant of the papain-digested constructs was added to 3.0 mL of Hoechst 33258 dye (Sigma-Aldrich) solution in TNE buffer (10 mM Tris–HCl/100 mM NaCl/1 mM EDTA) and the intensity was read using a RF-5301PC fluorospectrometer (Shimadzu, Japan) at 360 nm excitation and 460 nm emission. The corresponding DNA amount was calculated based on a ds-calf Thymus DNA type I (Sigma-Aldrich) standard curve.

For GAG analysis, the supernatant was reacted with 1,9-dimethylmethylene blue (DMMB, Sigma-Aldrich) in PBE buffer solution (100 mM sodium phosphate buffer/10 mM Na2EDTA) and absorbance was read at 525 nm by the spectrophotometer. Chondroitin sulphate (Sigma-Aldrich) was served to generate an standard curve.

Total collagen was evaluated by the hydroxyproline assay. Papain-digested supernatant was hydrolyzed in 6 N HCl for 18 h at 110 °C, then neutralized and combined with chloramine-T (Sigma-Aldrich) soultion followed by incubation at room temperature for 20 min. The solution was mixed with Ehrlich's reagent, vortexed and further incubated for 30 min at 60 °C. Finally, the absorbance was read at 550 nm using the spectrophotometer and collagen content was computed according to the trans-4-hydroxy-L-proline (Sigma-Aldrich) standard curve. All values of biochemical assays were normalized to the dry weight of the constructs.

6.3.13 Statistical analysis

All measurements were performed in triplicates for every measure points unless otherwise stated. Data obtained from our experiments are presented as mean ± SD (standard deviation). Statistical significance was determined by application of student's t-test. The differences were considered to be significant when $P < 0.05$.

6.4 Results and discussion

6.4.1 Scaffold preparation and characterization

The ATRP of NIPAAm using ECP as an initiator and CuCl/Me6TREN as the catalyst was previously demonstrated to be an effective method to achieve PNIPAAms with well-defined and narrow-dispersed molecular weights (35). Therefore, we employed this technique to prepare PNIPAAms with DPs of 100 (molecular weight (MW) =11300) and 400 (MW=45200) by adjusting the concentration ratio of the monomer to the initiator (Table 1). NI100 and NI200 have very similar properties as evidenced in Chapter 5. P-100

Table 1. Summary of reaction conditions and characteristics of the PNIPAAms

Sample	[M]:[I]:[CuCl]:[L][a]	M_n[b]	d_h (nm)[c]
NI100	100:1:1:1	11300	6.65±0.14
NI400	400:1:1:1	45200	12.47±0.65

[a] M: monomer, I: initiator, L: ligand

[b] Number average molecular weight

[c] Hydrodynamic diameter, measured by DLS, (Mean ± SD, n=3)

may form smaller particles under the precipitation conditions in comparison to P-200. But in this chapter, we would like to investigate the effect of different degree of polymerization of hydrogels on cell growth in 3D; and either P-100 or P-200 could be chosen for this purpose. The hydrodynamic diameter (d_h) of NI400 molecules (12.47 nm) was almost twice the d_h of NI100 (6.65 nm) as measured by DLS. It was expected because the DP of NI400 was higher than that of NI100.

Ice removal by lyophilization of frozen chitosan solution generates a porous structure (4). Solution concentration and freezing temperature affect the final average pore size as reported previously (36). Thus, we selected preparation conditions in order to obtain pore sizes of around 100 µm. This is large enough for MSCs with an average cell size of 10-15 µm (37).

The chitosan/PNIPAAm hybrid constructs were prepared by addition of PNIPAAm solutions on top of chitosan scaffolds. The PNIPAAm solution penetrated through the pores of chitosan and the hybrid structure formd by raising the environmental temperature to above LCST of PNIPAAm. The preparation process is illustrated in Scheme 1.

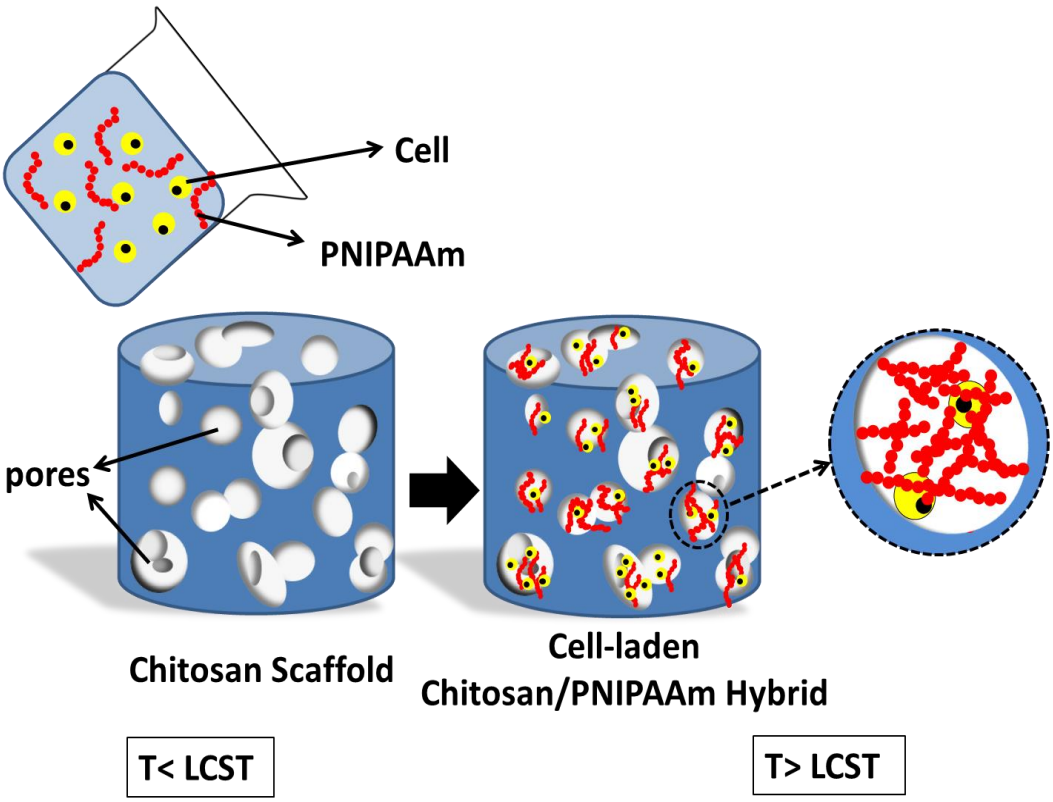

Scheme 1. Preparation of cell-laden chitosan/PNIPAAm hybrids.

After addition of the PNIPAAm solution on top of chitosan scaffold, it penetrates into the porous structure of chitosan, passes through the pores and eventually exits from the bottom of the construct. It is important to incubate the hybrid structure at a predetermined temperature above the LCST just in time when the PNIPAAm spreads over the whole depth but still retains inside the construct. To find such an optimum time, CSNI100 and CSNI400 were transferred to an oven at various intervals after addition of PNIPAAm solution and the samples were analyzed by TGA. Figures 1a and 1b show the thermal degradation curves of CSNI100 and CSNI400, respectively. As expected, both samples exhibited the degradation in two stages, which are due to thermal decompositions of chitosan and PNIPAAm, respectively (38). The degradation temperature was almost constant for both samples at different intervals. However, the percentage of weight loss

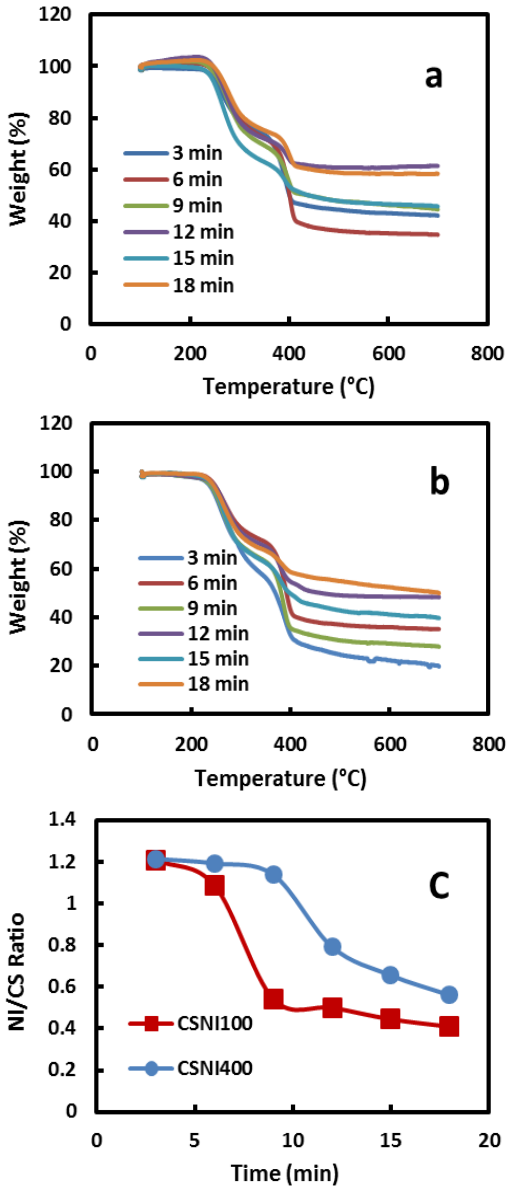

Figure 1. Thermogravimetric analysis of (a) CSNI100 and (b) CSNI400 samples prepared by transferring the PNIPAAm-loaded scaffolds to a temperature above its LCST (40 °C) at various intervals after addition of PNIPAAm solution on top of chitosan scaffolds. (c) The ratio of weight percent changes of PNIPAAm to chitosan versus time, calculated from (a) and (b).

after the onset temperature of PNIPAAm was different in each curve. This is attributed to the different amount of PNIPAAm retained in each sample and can be used to quantify the composition of the chitosan/PNIPAAM hybrid (39). The ratio of weight loss for PNIPAAm to chitosan for each sample was calculated and plotted versus time in Figure 1c. It revealed that in CSNI100 and CSNI400, the amount of PNIPAAm started to decrease with an onset at 6 and 9 min after addition of PNIPAAm solution, respectively. The time from the TGA analysis was suggested to be the optimum time to raise the environmental temperature above the LCST for PNIPAAm-loaded constructs, in order to achieve the best distribution of PNIPAAm over the chitosan scaffold along with the minimum polymer (also cell, in case of cell-laden polymer solution) loss.

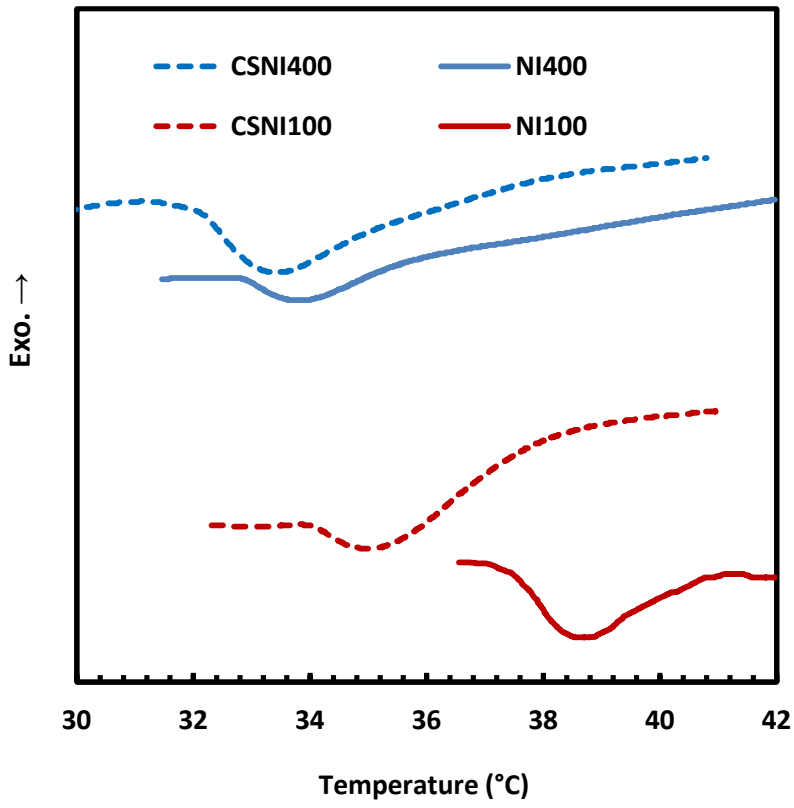

Figure 2. DSC thermograms of PNIPAAm and chitosan/PNIPAAM hybrids.

Differential scanning calorimetric analysis was conducted to investigate the LCST of PNIPAAm and the hybrids. LCST is determined as the onset temperature of the endothermic peak (40, 41). The thermograms are shown in Figure 2. LCSTs of NI100 and NI400 were 37.46 °C and 32.79 °C, respectively, while they reduced to 33.89 °C in CSNI100 and 31.29 °C in CSNI400. The increase in LCST of PNIPAAM polymers by decreasing the molecular weight is in agreement with the previous report (42). However, the absolute values might be different in various analysis methods and conditions. Hybridization of PNIPAAm with chitosan alters the LCST due to the change in hydrophilic/hydrophobic interactions by introducing chitosan moiety (43). DSC results revealed that the thermal phase transition behavior of PNIPAAm is retained after hybridization with chitosan, and the transition temperature was within the acceptable range for cell culture and tissue engineering applications.

Nitrogen gas adsorption was conducted to investigate the textural porosity of macropore walls. Nitrogen adsorption isotherms (Figure 3a) and calculated pore size distributions (PSD) (Figure 3b) on CS, CSNI100, and CSNI400 are presented in Figure 3. The isotherm plots the amount of gas adsorbed versus the relative pressure P/P_0, where P_0 is the saturation pressure of pure nitrogen. Nitrogen adsorption isotherms for all the three samples showed a type II isotherm based on the IUPAC classification (44), indicating presence of mesopores (pores larger than 2 nm) with negligible contribution of micropores (pores smaller than 2nm). The isotherms also showed H3 type hysteresis loop at high pressures, suggesting slit-shaped pores (45). Negligible adsorption on PNIPAAm dried samples (NI400 in Figure 3a) demonstrated that the mesoporosity origins from CS, and PNIPAAm had no contribution in textural porosity. Comparison between isotherms in Figure 3a revealed that amount of gas adsorption decreased for both CSNI100 and CSNI400 as a result of textural pores filling by PNIPAAm. Textural properties for all the samples are reported in the embedded table in Figure 3a. The data denoted a significant reduction in pore volume for CSNI100 and a moderate reduction in pore volume for CSNI400. However, the calculated surface areas for CSNI100 and CSNI400 were almost the same. Calculated PSDs for the three samples in Figure 3b showed presence of pores ranging in size from 3 nm to beyond 80 nm. The PSD for CSNI100 was similar in shape to

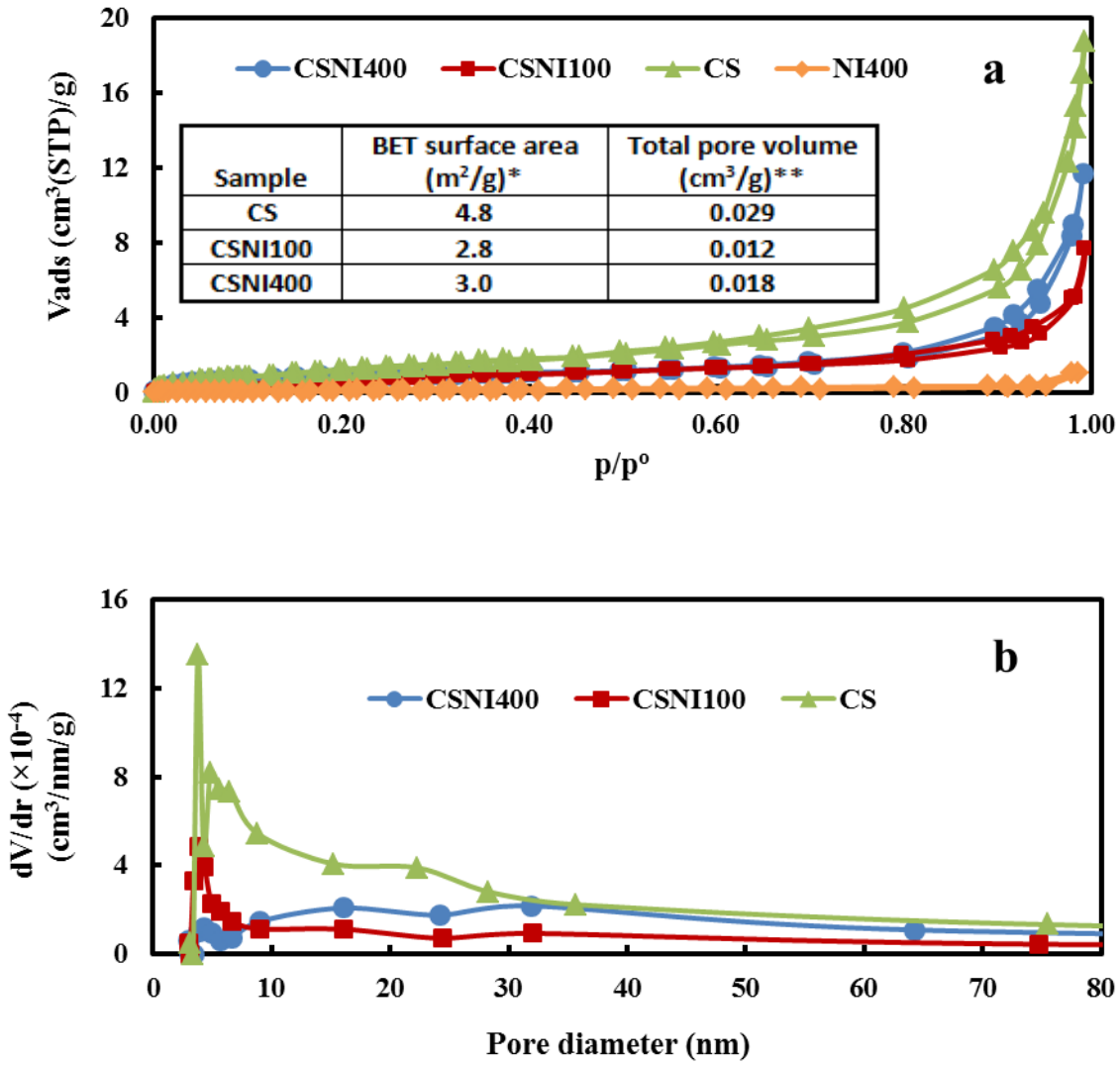

Figure 3. (a) Nitrogen adsorption isotherms and (b) calculated pore size distributions (PSD) based on the BJH method for CS, CSNI100, CSNI400, and NI400 samples. Embedded table: textural properties of CS, CSNI100, and CSNI400 derived from nitrogen adsorption isotherms. * Calculated by BET method; ** Calculated based on nitrogen amount adsorbed at near saturation pressure converted to liquid volume.

that for CS but with a smaller intensity, suggesting a uniform and non-selective pore-filling mechanism. On the other hand, the PSD for CSNI400 followed a selective pattern. Pores with sizes smaller than 30 nm in CSNI400 were more favorable sites for adsorption. The textural porosities play a significant role in micro and macroscale behaviors of scaffold (46, 47) and the properties can be tuned for cell proliferation and differentiation. Such nano-sized pores filled with thermoresponsive polymers have also been employed for encapsulation of bioactive molecules and sustained release of these biomolecules facilitates generation of engineering tissues (48).

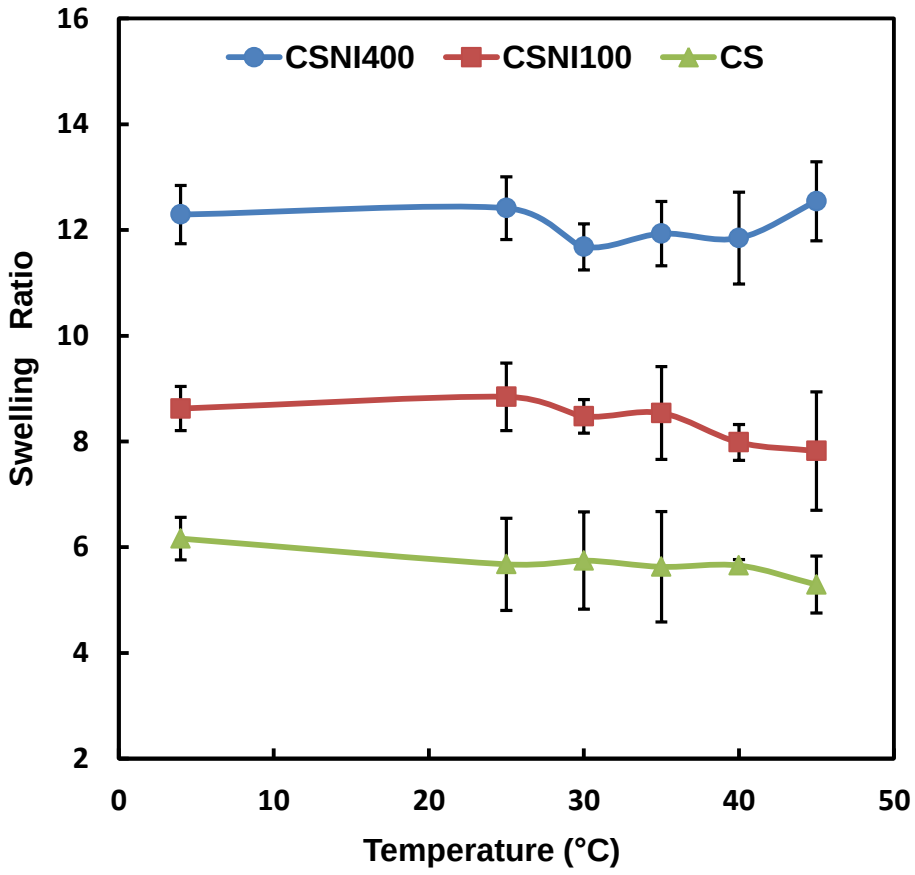

Figure 4. Swelling ratio of CS, CSNI100 and CSNI400 in PBS in the temperature range from 4-45 °C (Mean ± SD, n=3).

The swelling behavior of CS, CSNI100 and CSNI400 samples is shown in Figure 4. The hybrid constructs had a higher swelling ratio (SR) than chitosan alone, indicating a higher equilibrium water content. It is attributed to the presence of hydrophilic PNIPAAm chains in solution. Similar behavior has been reported for copolymers of chitosan and PNIPAAm (16). Furthermore, CSNI400 possessed 1.33 folds water content higher than CSNI100. It may occur due to a higher pore volume of CSNI400. The pore volume of CSNI400 was 1.50 folds larger than that of CSNI100 as calculated from gas adsorption, which allowed more water content in the swollen hybrid structure. The ratio of pore volume of CSNI400 to CSNI100 was interestingly in good agreement with the order of magnitude of the swelling ratio between two hybrid matrices. The graph also indicated that SR remained constant when temperature changed, even above LCST. SR often decreases for PNIPAAm-based thermoresponsive hydrogels beyond their LCST (38). PNIPAAm becomes hydrophobic above LCST and hence, expels water from the gel. However, little water was expelled from the chitosan/PNIPAAm hybrids because there were no chemical bonds between PNIPAAm and chitosan or cross-linking between PNIPAAm molecules. Therefore, above LCST, PNIPAAm molecules underwent a coil-to-globule transition and discharge water. Nevertheless, chitosan did not collapse and retained its swollen structure. As a result, the expelled water from PNIPAAm remained in the chitosan network.

The morphology and porous structure of the constructs were studied using SEM. The scaffold from chitosan alone in Figure 5a had a porous internal structure which was interconnected with random pore sizes and shapes. The majority of pores were between 10 and 100 µm. The pore walls were thin with a thickness of around 1 µm. Pore wall surfaces possessed a soft texture in microscale, with no visible pore or wrinkle. Pores were partially filled with PNIPAAm polymer after addition of CSNI100 (Figure 5b) and CSNI400 (Figure 5c). However, the hybrids preserved their porous structure. CSNI100 macropores seem to be slightly more occupied probably due to shorter chain lengths of NI100. Partial occupation of pores may not hindered cell activities, because of its soft and flexible structure. Cell-laden CSNI100 and CSNI400 micrographs are shown in Figures 5d-f. Cells were located within the porous structure and kept their spherical shape which is acceptable

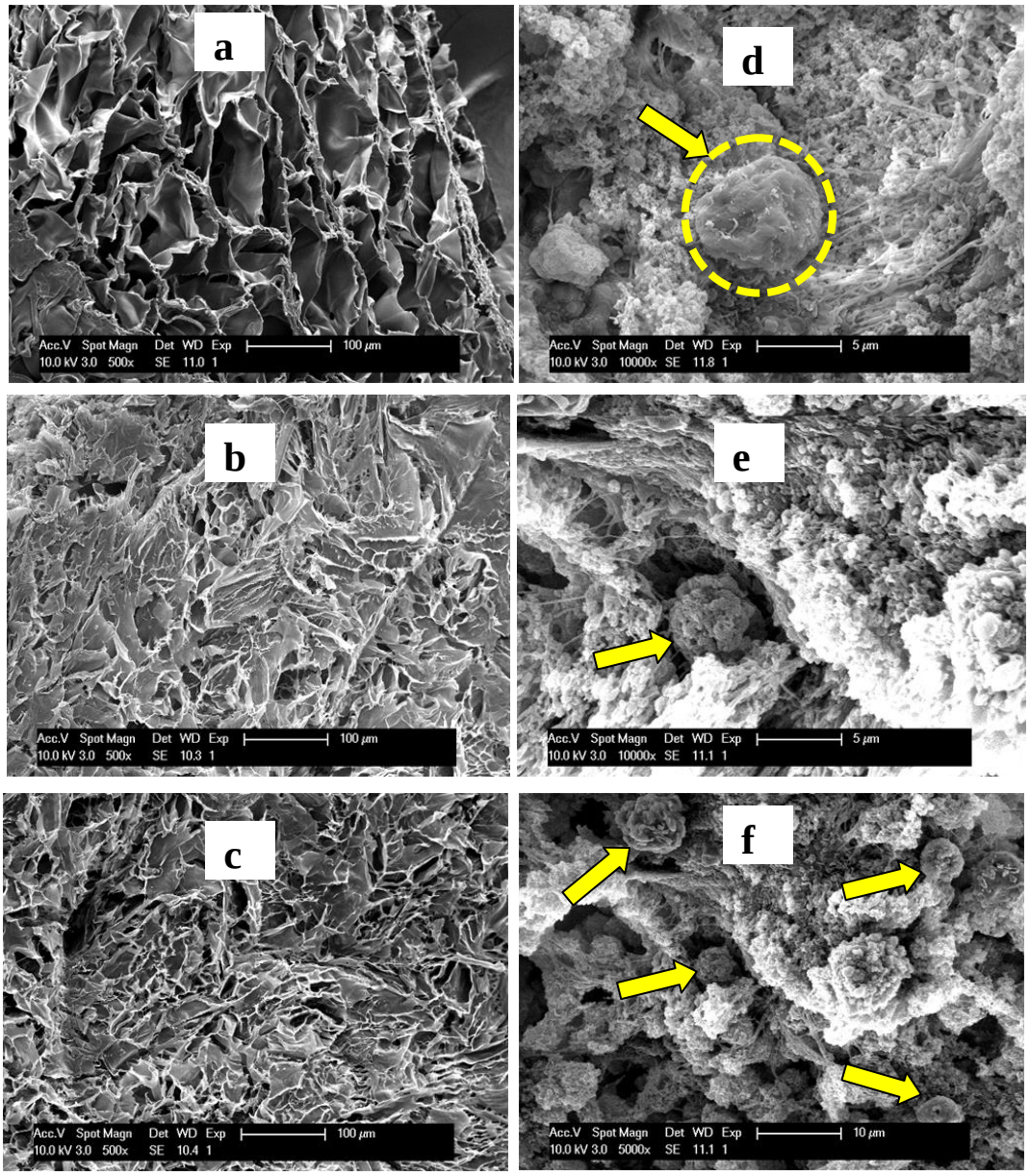

Figure 5. SEM micrograph of (a) CS , (b) CSNI100, (c) CSNI400; (500×), (d) cell-laden CSNI100, (e) cell-laden CSNI400; (10000×), and (f) cell-laden CSNI400 (5000×). Cell-laden constructs were incubated for 3 days. Yellow arrows and dashed circle point cells.

as they were cultured within a 3D microenvironment rather than a 2D monolayer. The texture of pore walls was altered with an uneven and wrinkled surface. It can be due to the ECM components excreted by cells. Sample preparation for the cell-encapsulating scaffold as well as various ions and ingredients in cell culture medium may also affect the topography of scaffolds. Macropores are a determinant parameter of cell matrices. It should provide adequate space for efficient cell seeding, cellular interactions, migration, proliferation, and ECM deposition (49). They also contribute to the scaffold mechanical property which is an important microenvironmental variable (50).

6.4.2 Cell proliferation

The MTT assay was conducted to investigate cell viability and proliferation when MSCs were cultured in chitosan scaffold and chitosan/PNIPAAm hybrids. The yellow-colored water-soluble tetrazolium salt, MTT, converts to water insoluble, purple-coloured formazan crystals as a consequence of its metabolization by mitochondrial dehydrogenase of live cells. Damaged or dead cells do not have any mitochondrial dehydrogenase activity. Therefore, the optical density of the soluble crystal represents the amount of viable cells. The cell viabilities were at the same level for CS, CSNI100 and CSNI400 at day 1 as shown in the blue bar in Figure 6a. The viabilities decreased for all three groups at day 7 in comparison with day 1. However, cell number in CSNI400 was significantly higher ($P<0.05$) than that in CSNI100, and CSNI100 was greater than CS. It might happened because some cells died when cultured in a new 3D microenvironment and then started to proliferate which was more significant in CSNI400. The photographs of cell-laden constructs incubated with MTT at day 7 are shown in Figures 6b-d. The purple-coloured viable cells were mostly located near to the top surface of CS scaffold (panel b). In contrast, viable cells were well distributed over the whole depth of CSNI100 (panel c) and CSNI400 (panel d) constructs, and the color was even more intense and uniformly dispersed in CSNI400.

The cell viability was further visualized by staining the live and dead cells encapsulated within the constructs. This assay is based on a two-color fluorescence dye. Viable cells are

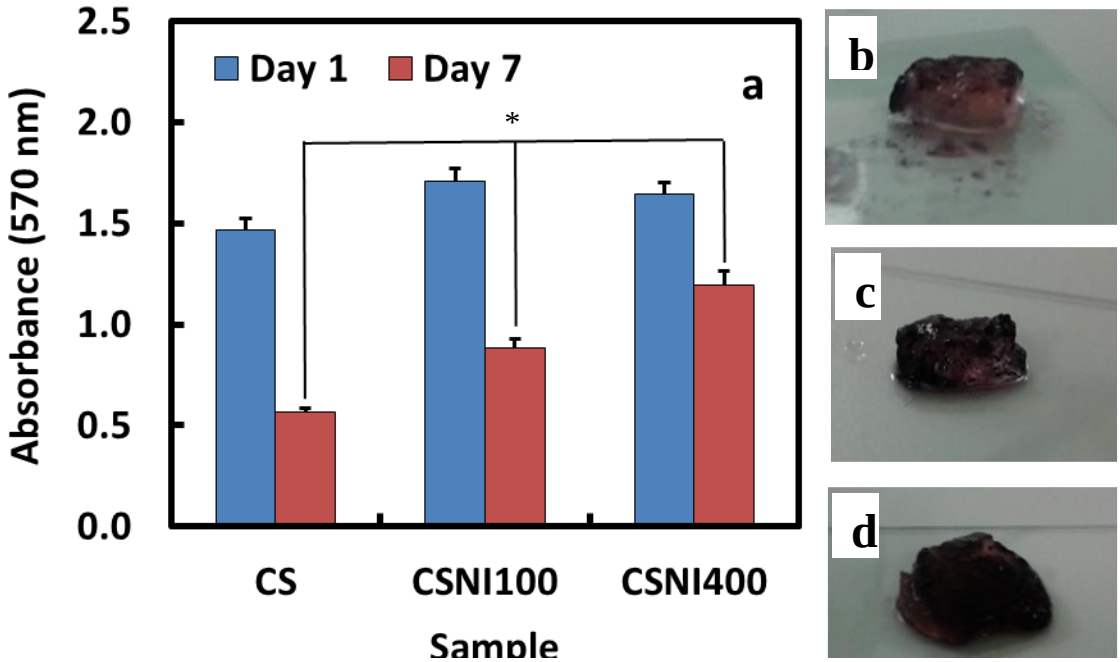

Figure 6. (a) Mitochondrial activity quantification of MSCs cultured in CS, CSNI100 and CSNI400. The MTT assay was performed at day 1 and 7 after incubation (Mean ± SD, n=3; * p < 0.05). Photograph of Cell-laden (b) CS, (c) CSNI100, and (d) CSNI400 constructs stained with MTT at day 7.

stained by cell-permeant calcein AM. Non-fluorescent calcein AM is converted to intensely fluorescent calcein as a result of enzymatic intracellular esterase activity of live cells. Cell-impermeant Ethidium homodimer-1 dye can only enter dying and dead cells with damaged membranes and binds to their DNA, and the DNA/dye complex consequently emits red fluorescence. Stained CS, CSNI100 and CSNI400 constructs were observed under a confocal laser scanning microscope. Green and red spots in Figure 4 display live and dead cells, respectively. Live cell density in CS (Figure 7a) was less than CSNI100 (Figure 7b). The viable cell number was the highest in CSNI400 (Figure 7c) in comparison to CS and CSNI100, while comparatively more dead cells were distinguishable in the CS construct. Live/dead staining results were in agreement with the MTT readings. High live to dead cell ratio of CS/NI hybrids supports the idea that the cell

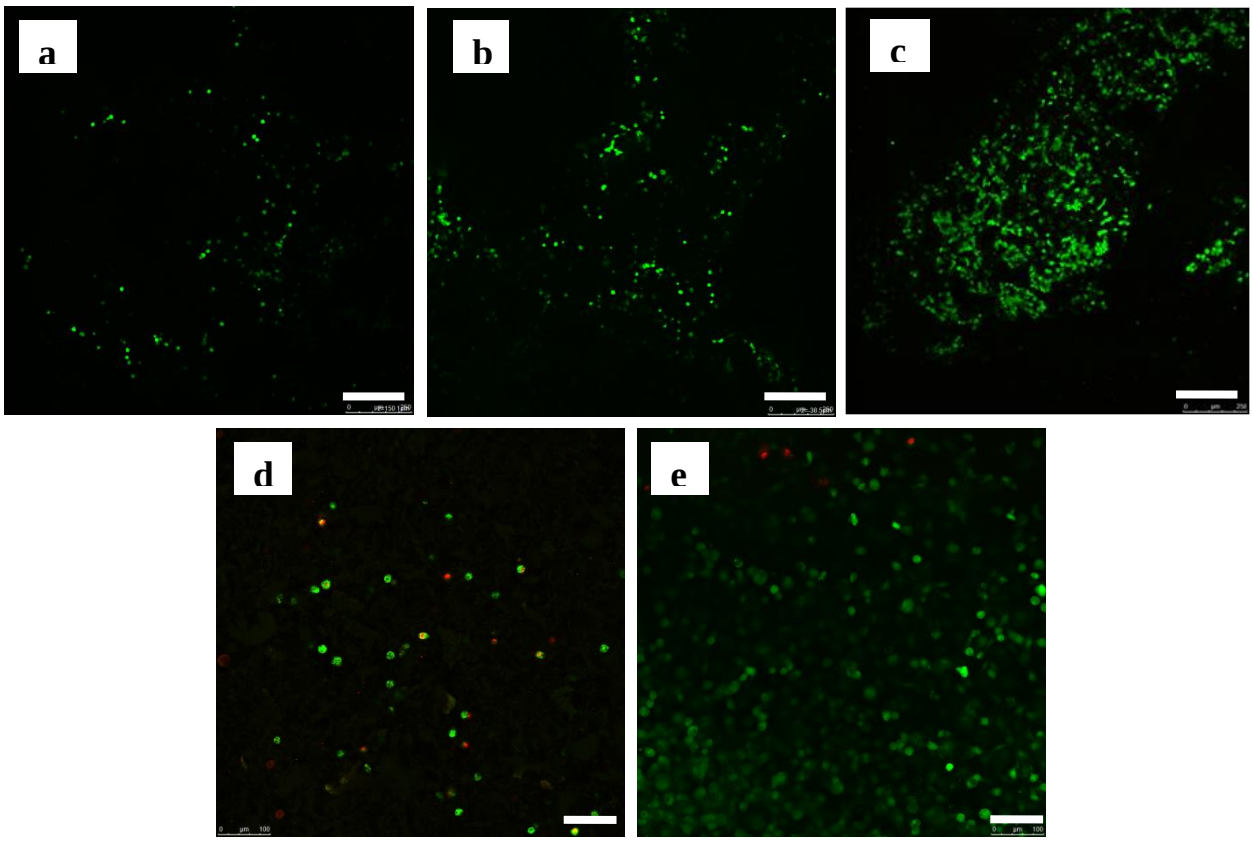

Figure 7. Confocal laser scanning images of MSCs cultured in: (a) CS, (b) CSNI100 and (c) CSNI400 at day 7 (10× oil immersion objective, scale bars 250 µm). After cells were detached from CSNI400 at day 7 by reducing the temperature to room temperature, (d) a few cells retained in the scaffold, and (e) the majority of cells were recovered and suspended in the solution (20× oil immersion objective, scale bars 100 µm).

viability decrement between day 1 and 7 in MTT assay was not a continuous phenomenon. After culturing MSCs in growth medium for 7 days, cells were detached from the scaffolds by simply lowering the temperature below the LCST of PNIPAAm. The majority of cells were recovered as a cell suspension (Figure 7e), while a few cells were entrapped within the scaffolds (Figure 7d). It suggests that this hybrid system can also be used as a platform for 3D stem cell expansion. In this approach, stem cells are cultured in a 3D

microenvironment rather than conventional monolayer cultures. This system mimics their native 3D niche which is essential to preserve cell biological capabilities and to govern cell fate (51, 52). Subsequently, cells can be detached at confluency or use time, by reducing the temperature and without using detrimental enzymes.

In general, these results suggest that stem cells were biologically more active in PNIPAAm-loaded constructs in comparison with chitosan alone, probably due to more swollen structure as shown in SR studies. The highly hydrated and swollen structure of microenvironment provides larger space which facilitates cell migration, nutrient delivery, waste removal and ECM secretion. In addition, PNIPAAm may promote cell adhesion to the chitosan macropore walls during its shrinkage above LCST. CSNI400 was also more favorable for cell proliferation in a same manner because of its bigger SR originated from greater textural pore volume.

6.4.3 Chondrogenic differentiation

Chondrogenic differentiation of MSCs in the hybrid structure was evaluated using biochemical assays. The CSNI400 has shown a better cell proliferation rate. Therefore, this structure was chosen for evaluation in the application of cartilage tissue engineering. By continuously incubating MSC in the CSNI400 hybrid structure with the differentiating medium for 28 days, ECM (GAGs and total collagen) production was monitored to confirm cartilage formation.

Cell proliferation was assessed by the Hoescht 33258 assay. The Hoescht assay results (Figure 8a) indicate that the DNA content increased from 0.73 µg DNA/mg dry scaffold at day 14 to 1.15 µg DNA/mg dry scaffold at day 28, suggesting the increase in total cell number. The DMMB and the hydroxyproline assay were employed to quantify GAG and collagen deposition, respectively. The GAG level (Figure 8b) increased 2.6 folds from day 14 to day 28, and a similar increment in total collagen accumulation was also noted in Figure 8c. GAG and collagen are the main components of cartilagous tissues. Enhanced GAG and collagen deposition revealed the chondrogenic differentiation of MSCs within the 3D microenvironment provided by the chitosan/PNIPAAm scaffold.

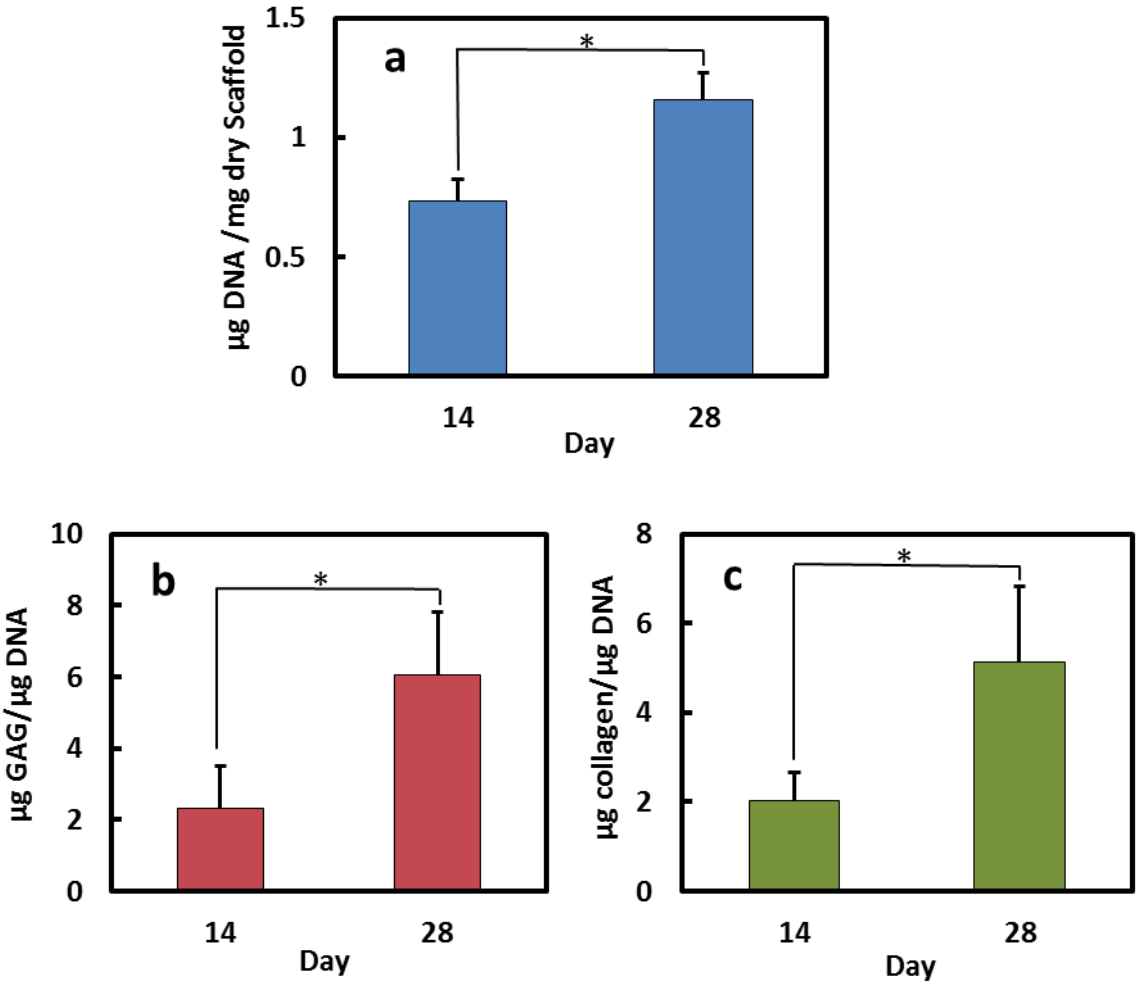

Figure 8. Biochemical analysis of cell-laden CSNI400 incubated with chondrogenic medium. (a) DNA, (b) GAG, and (c) total collagen content at various culture times. (Mean ± SD, n=3; * P<0.05)

Various chitosan-based scaffolds have been investigated for cartilage tissue engineering by other researchers. For example, gene expression analysis of chitosan/poly(butylene terephthalate adipate) blend showed less than 20% increase in aggrecan accumulation during the same culture time (53). In another study, MSCs were cultured in a hybrid scaffold composed of chitosan/β-glycerophosphate solution and demineralized bone matrix. During 11 days of culture, almost 2.0 and 2.5 folds of increase in GAG and collagen type II contents of ECM were reported, while no significant change was seen in the amount of GAG in case of chitosan alone matrix during the same time. Although the collagen type II content showed around 2.0 folds of increase (54). These results suggest that CSNI hybrid system shows better or comparable support for chondrogenesis of MSCs.

6.5 Conclusions

In this study, well-defined PNIPAAm/chitosan hybrids were prepared. Delay time before incubation to gain a well-distribution of cell and PNIPAAm as well as the less PNIPAAm loss is 6 min for CSNI100 and 9 min for CSNI400. LCST of PNIPAAm is dropped slightly by hybridization with chitosan, while still remains in desirable range. CSNI400 have 1.5 folds greater pore volume than CSNI100. Hybrid scaffolds show higher swelling ratio than chitosan-only scaffolds, and swelling ratio of CSNI400 is also higher than CSNI100. SEM images indicate that the interconnected porous structure of chitosan was preserved. The number of mesenchymal stem cells (MSCs) increased 58% and 108 % in comparison with chitosan scaffold in CSNI100 and CSNI400, respectively after seven days incubation in growth medium. Glycosaminoglycan and total collagen contents increased 2.6 and 2.5 folds after 28 days culture in chondrogenic medium. Therefore, we examined the hypothesis that a hybrid matrix composed of a soft PNIPAAm gel with controlled molecular weight (which can improve the cell compatibility of the structure) and a chitosan porous scaffold can support stem cell culture. These results suggest that hybrid scaffolds of chitosan and PNIPAAm with degree of polymerization of 400 are promising matrices for 3D stem cell culture and cartilage tissue engineering.

6.6 Acknowledgements

AM would like to acknowledge the Adelaide Scholarship International of The University of Adelaide. HZ thanks The MAWA Trust and the 111 Project (B12034).

6.7 References

1. Keeney M, Lai JH, Yang F. Recent progress in cartilage tissue engineering. Current opinion in biotechnology. 2011;22(5):734-40.
2. Hunziker E. Articular cartilage repair: basic science and clinical progress. A review of the current status and prospects. Osteoarthritis and cartilage. 2002;10(6):432-63.
3. Van Vlierberghe S, Dubruel P, Schacht E. Biopolymer-Based Hydrogels As Scaffolds for Tissue Engineering Applications: A Review. Biomacromolecules. 2011 2011/05/09;12(5):1387-408.
4. Di Martino A, Sittinger M, Risbud MV. Chitosan: A versatile biopolymer for orthopaedic tissue-engineering. Biomaterials. 2005 10//;26(30):5983-90.
5. Cho JH, Kim S-H, Park KD, Jung MC, Yang WI, Han SW, et al. Chondrogenic differentiation of human mesenchymal stem cells using a thermoresponsive poly (N-isopropylacrylamide) and water-soluble chitosan copolymer. Biomaterials. 2004;25(26):5743-51.
6. Chen JP, Cheng TH. Thermo-Responsive Chitosan-graft-poly (N-isopropylacrylamide) Injectable Hydrogel for Cultivation of Chondrocytes and Meniscus Cells. Macromolecular Bioscience. 2006;6(12):1026-39.
7. Fedorovich NE, Alblas J, de Wijn JR, Hennink WE, Verbout AJ, Dhert WJ. Hydrogels as extracellular matrices for skeletal tissue engineering: state-of-the-art and novel application in organ printing. Tissue engineering. 2007;13(8):1905-25.
8. Kim I-Y, Seo S-J, Moon H-S, Yoo M-K, Park I-Y, Kim B-C, et al. Chitosan and its derivatives for tissue engineering applications. Biotechnology advances. 2008;26(1):1-21.
9. Rzaev ZM, Dincer S, Pişkin E. Functional copolymers of< i> N</i>-isopropylacrylamide for bioengineering applications. Progress in Polymer Science. 2007;32(5):534-95.
10. Kim SY, Cho SM, Lee YM, Kim SJ. Thermo-and pH-responsive behaviors of graft copolymer and blend based on chitosan and N-isopropylacrylamide. Journal of Applied Polymer Science. 2000;78(7):1381-91.

11. Lee WF, Chen YJ. Studies on preparation and swelling properties of the N-isopropylacrylamide/chitosan semi-IPN and IPN hydrogels. Journal of Applied Polymer Science. 2001;82(10):2487-96.

12. Chen X, Song H, Fang T, Bai J, Xiong J, Ying H. Preparation, characterization, and drug-release properties of pH/temperature-responsive poly (N-isopropylacrylamide)/chitosan semi-IPN hydrogel particles. Journal of Applied Polymer Science. 2010;116(3):1342-7.

13. da Silva RM, López-Pérez PM, Elvira C, Mano JF, Román JS, Reis RL. Poly (N-isopropylacrylamide) surface-grafted chitosan membranes as a new substrate for cell sheet engineering and manipulation. Biotechnology and Bioengineering. 2008;101(6):1321-31.

14. Wang J, Chen L, Zhao Y, Guo G, Zhang R. Cell adhesion and accelerated detachment on the surface of temperature-sensitive chitosan and poly (N-isopropylacrylamide) hydrogels. Journal of Materials Science: Materials in Medicine. 2009;20(2):583-90.

15. Don TM, Chou SC, Cheng LP, Tai HY. Cellular compatibility of copolymer hydrogels based on site-selectively-modified chitosan with poly (N-isopropyl acrylamide). Journal of Applied Polymer Science. 2011;120(1):1-12.

16. Lee SB, Ha DI, Cho SK, Kim SJ, Lee YM. Temperature/pH-sensitive comb-type graft hydrogels composed of chitosan and poly (N-isopropylacrylamide). Journal of applied polymer science. 2004;92(4):2612-20.

17. Don T-M, Chen H-R. Synthesis and characterization of AB-crosslinked graft copolymers based on maleilated chitosan and N-isopropylacrylamide. Carbohydrate Polymers. 2005;61(3):334-47.

18. Chuang CY, Don TM, Chiu WY. Preparation of environmental-responsive chitosan-based nanoparticles by self-assembly method. Carbohydrate Polymers. 2011;84(2):765-9.

19. Sanoj Rejinold N, Sreerekha P, Chennazhi K, Nair S, Jayakumar R. Biocompatible, biodegradable and thermo-sensitive chitosan-g-poly (N-isopropylacrylamide) nanocarrier

for curcumin drug delivery. International Journal of Biological Macromolecules. 2011;49(2):161-72.

20. Sundaresan V, Menon JU, Rahimi M, Nguyen KT, Wadajkar AS. Dual-responsive polymer-coated iron oxide nanoparticles for drug delivery and imaging applications. International journal of pharmaceutics. 2014;466(1):1-7.

21. Gui R, Wang Y, Sun J. Embedding fluorescent mesoporous silica nanoparticles into biocompatible nanogels for tumor cell imaging and thermo/pH-sensitive in vitro drug release. Colloids and Surfaces B: Biointerfaces. 2014;116:518-25.

22. Wang Y, Wang J, Ge L, Liu Q, Jiang L, Zhu J, et al. Synthesis, properties and self-assembly of intelligent core-shell nanoparticles based on chitosan with different molecular weight and N-isopropylacrylamide. Journal of applied polymer science. 2013;127(5):3749-59.

23. Lee J, Jung M, Park H, Park K, Ryu G. Synthesis and characterization of thermoresponsive chitosan copolymer as a novel biomaterial. Journal of Biomaterials Science, Polymer Edition. 2004;15(8):1065-79.

24. Cao Y, Zhang C, Shen W, Cheng Z, Yu LL, Ping Q. Poly (N-isopropylacrylamide) – chitosan as thermoresponsive in situ gel-forming system for ocular drug delivery. Journal of Controlled Release. 2007;120(3):186-94.

25. Recillas M, Silva LL, Peniche C, Goycoolea FM, Rinaudo M, Argu□elles-Monal WM. Thermoresponsive behavior of chitosan-g-N-isopropylacrylamide copolymer solutions. Biomacromolecules. 2009;10(6):1633-41.

26. Chen C, Liu M, Gao C, Lü S, Chen J, Yu X, et al. A convenient way to synthesize comb-shaped chitosan-graft-poly (N-isopropylacrylamide) copolymer. Carbohydrate polymers. 2013;92(1):621-8.

27. Tong Z, Zeng F, Zheng X, Sato T. Inverse molecular weight dependence of cloud points for aqueous poly (N-isopropylacrylamide) solutions. Macromolecules. 1999;32(13):4488-90.

28. Mellati A, Dai S, Bi J, Jin B, Zhang H. A biodegradable thermoresponsive hydrogel with tuneable properties for mimicking three-dimensional microenvironments of stem cells. RSC Adv. 2014;4(109):63951-61.

29. Zhu PW, Napper DH. Interfacial coil-to-globule transitions: the effects of molecular weight. Colloids and Surfaces A: Physicochemical and Engineering Aspects. 1996;113(1–2):145-53.

30. Barrett EP, Joyner LG, Halenda PP. The determination of pore volume and area distributions in porous substances. I. computations from nitrogen isotherms. Journal of the American Chemical Society. 1951 1951/01/01;73(1):373-80.

31. Brunauer S, Emmett PH, Teller E. Adsorption of gases in multimolecular layers. Journal of the American Chemical Society. 1938 1938/02/01;60(2):309-19.

32. Zhang J, Chu L-Y, Li Y-K, Lee YM. Dual thermo- and pH-sensitive poly(N-isopropylacrylamide-co-acrylic acid) hydrogels with rapid response behaviors. Polymer. 2007 3/8/;48(6):1718-28.

33. Hwang NS, Varghese S, Elisseeff J. Cartilage tissue engineering. Stem Cell Assays: Springer; 2007. p. 351-73.

34. Hoemann CD. Molecular and biochemical assays of cartilage components. Cartilage and osteoarthritis: Springer; 2004. p. 127-56.

35. Masci G, Giacomelli L, Crescenzi V. Atom Transfer Radical Polymerization of N-Isopropylacrylamide. Macromolecular rapid communications. 2004;25(4):559-64.

36. Madihally SV, Matthew HW. Porous chitosan scaffolds for tissue engineering. Biomaterials. 1999;20(12):1133-42.

37. Solchaga LA, Penick K, Porter JD, Goldberg VM, Caplan AI, Welter JF. FGF-2 enhances the mitotic and chondrogenic potentials of human adult bone marrow-derived mesenchymal stem cells. Journal of cellular physiology. 2005;203(2):398-409.

38. Don T-M, Chen H-R. Synthesis and characterization of AB-crosslinked graft copolymers based on maleilated chitosan and< i> N</i>-isopropylacrylamide. Carbohydrate polymers. 2005;61(3):334-47.

39. Gilding D, Reed A. Biodegradable polymers for use in surgery—polyglycolic/poly (actic acid) homo-and copolymers: 1. Polymer. 1979;20(12):1459-64.

40. Lesage de la Haye J, Pontes da Costa A, Pembouong G, Ruhlmann L, Hasenknopf B, Lacôte E, et al. Study of the temperature-induced aggregation of polyoxometalate-poly(N,N-diethylacrylamide) hybrids in water. Polymer. 2015;57(0):173-82.

41. Park JH, Lee YH, Oh SG. Preparation of Thermoresponsive PNIPAm-Grafted Mesoporous Silica Particles. Macromolecular Chemistry and Physics. 2007;208(22):2419-27.

42. Xia Y, Yin X, Burke NAD, Stöver HDH. Thermal Response of Narrow-Disperse Poly(N-isopropylacrylamide) Prepared by Atom Transfer Radical Polymerization. Macromolecules. 2005 2005/07/01;38(14):5937-43.

43. Radhakumary C, Antonty M, Sreenivasan K. Drug loaded thermoresponsive and cytocompatible chitosan based hydrogel as a potential wound dressing. Carbohydrate polymers. 2011;83(2):705-13.

44. Sing KSW, Everett DH, Haul RAW, Moscou L, Pierotti RA, Rouquerol J, et al. Reporting physisorption data for gas/solid systems with special reference to the determination of surface area and porosity. Pure and Applied Chemistry. 1985;57(4):603.

45. Rouquerol F, Rouquerol J, Sing K. Adsorption by powders and porous solids London: Academic Press; 1999.

46. Rinki K, Dutta P. Chitosan Based Scaffolds by lyophilization and sc. CO2 assisted methods for tissue engineering applications. Journal of Macromolecular Science, Part A: Pure and Applied Chemistry. 2010;47(5):429-34.

47. Kumari R, Dutta P. Physicochemical and biological activity study of genipin-crosslinked chitosan scaffolds prepared by using supercritical carbon dioxide for tissue engineering applications. International journal of biological macromolecules. 2010;46(2):261-6.

48. Jones JR, Ehrenfried LM, Hench LL. Optimising bioactive glass scaffolds for bone tissue engineering. Biomaterials. 2006;27(7):964-73.

49. Chen VJ, Ma PX. Nano-fibrous poly(l-lactic acid) scaffolds with interconnected spherical macropores. Biomaterials. 2004;25(11):2065-73.

50. Guilak F, Cohen DM, Estes BT, Gimble JM, Liedtke W, Chen CS. Control of Stem Cell Fate by Physical Interactions with the Extracellular Matrix. Cell Stem Cell. 2009;5(1):17-26.

51. Zhang H, Dai S, Bi J, Liu K-K. Biomimetic three-dimensional microenvironment for controlling stem cell fate. Interface Focus. 2011;1(5):792-803.

52. Lund AW, Yener B, Stegemann JP, Plopper GE. The natural and engineered 3D microenvironment as a regulatory cue during stem cell fate determination. Tissue Engineering Part B: Reviews. 2009;15(3):371-80.

53. Alves da Silva ML, Martins A, Costa-Pinto A, Correlo V, Sol P, Bhattacharya M, et al. Chondrogenic differentiation of human bone marrow mesenchymal stem cells in chitosan-based scaffolds using a flow-perfusion bioreactor. Journal of tissue engineering and regenerative medicine. 2011;5(9):722-32.

54. Huang H, Zhang X, Hu X, Dai L, Zhu J, Man Z, et al. Directing chondrogenic differentiation of mesenchymal stem cells with a solid-supported chitosan thermogel for cartilage tissue engineering. Biomedical Materials. 2014;9(3):035008.

CHAPTER SEVEN

7. Conclusions and future directions

To be able to regenerate functional articular cartilage, my PhD study was focused on engineering of well-defined matrices as biomimetic 3D microenvironment for stem cells. Two forms of chitosan matrices were prepared: chitosan-g-poly(N-isopropylacrylamide) (CS-g-PNIPAAm) copolymers and chitosan/well-defined PNIPAAm (CSNI) hybrids. Mesenchymal stem cells (MSCs) were cultivated in two matrices to evaluate the proliferation performance and then they were differentiated in the chondrogenic differentiation media for the cartilage regeneration. The main conclusions are summarized below:

1- The CS-g-PNIPAAm copolymer hydrogel can provide an appropriate microenvironment for 3D cultivation of MSCs. I have optimized various polymerization conditions including acid concentration in polymerisation media, monomer concentration in the feed, and reaction temperature to obtain the best hydrogel for MSC culture with desired physical and mechanical properties. The advantage of this system is to proliferate MSC in the 3D porous networks. After MSC proliferation, MSCs can be recovered by separating cells from the polymer solution at room temperature using the sol-gel thermo-reversible property of the CS-g-PNIPAAm copolymer.

2- The CS-g-PNIPAAm hydrogel with manipulated properties can be micropatterned for regenerating the superficial zone and the middle zone of articular cartilage. The CS-g-PNIPAAm hydrogel has been demonstrated to support the embedded MSCs differentiated into chondrocytes in 3D through extracellular matrix component (glycosaminoglycan (GAG), total collagen and collagen type II) analysis. GAG and total collagen contents (per DNA) increase 1.6 and 1.4 folds from day 14 to day 28 in chondrogenic medium. Histological and immunohistochemical stainings also confirm the increasing accumulation of GAG and collagen type II. Collagen type II was typically used as an indicator for cartilage produced *in vitro*. The detailed examination of the collagen forms that mimic body structure will be carried out in future work. The cell-laden hydrogel micropatterned in 50-100 μm constructs can align cells along the microchannel horizontal axis. 75 % of cells are oriented with an aspect ratio of 2.0 in 50 μm wide microconstructs at day 5. The cell shape and

alignment in the constructs is very similar to the superficial zone of chondrocytes of the native cartilage. Meanwhile, cells in the microchannel with the gap above 150 μm are randomly distributed (12% alignment and aspect ratio of 1.2, in unpatterned constructs), which can be used to mimic the middle zone of the cartilage tissue.

3- The CSNI hybrid matrices composed of chitosan scaffolds and well-defined PNIPAAm with a degree of polymerization of 400 (CSNI400) can provide a supporting platform for 3D stem cell culture and cartilage tissue engineering. Well-defined and narrow-dispersed molecular weights of PNIPAAm have been synthesized through atom transfer radical polymerization (ATRP). The cytotoxicity of PNIPAAm is molecular weight dependent, and varies with the PNIPAAm chain length. The PNIPAAm hydrogel may be detrimental to stem cells when the cells are covered with a thick layer of gel, and this layer may become a barrier for nutrient or oxygen delivery to cells. However, cells are mixed with PNIPAAm solution and the solution is incorporated in the voids of the chitosan scaffolds. The phase separation of PNIPAAm at 37 ^{o}C leads to a hybrid matrix for MSCs. After seven days incubation of CSNI400 in growth medium, viable cell number in cell-laden hybrid is 108% higher than chitosan. GAG and total collagen contents (per DNA) increase 2.6 and 2.5 folds from day 14 to day 28 in chondrogenic medium.

In conclusion, 3D microenvironment for stem cells was created and refined through manipulation of matrices in order to enhance cell proliferation and chondrogenic differentiation. The results revealed that graft copolymer of chitosan and PNIPAAm with tailored properties and microengineered architecture is appealing for zonal cartilage tissue engineering. The hybrid matrices from chitosan scaffolds with well-defined PNIPAAm hydrogels promote chondrogenesis, much better than the graft copolymer.

Thermoresponsive hydrogels were explored with controlled physical, mechanical and chemical properties for cartilage tissue engineering. Chitosan-g-PNIPAAm with random chain length (not well-defined) and chitosan/well-defined PNIPAAm hybrid were prepared in this PhD project. Graft copolymerization of chitosan and well-defined PNIPAAm and its

interactions with MSCs for chondrogenic differentiation remained to be studied in future. A novel method to address cartilage spatial organization was also developed using microengineered CS-g-PNIPAAm. On the other hand, based on the results, CSNI hybrid is a better choice for chondrogenic differentiation of MSCs than CS-g-PNIPAAm. Therefore, microengineered CSNI hybrids as well as graft copolymer of chitosan and well-defined PNIPAAm might be potential follow-up research projects. Stacking the microengineered constructs to form a macroscale 3D cartilage tissue and evaluation of the engineered cartilage needs to be further investigated. In addition, implantation of the engineered tissues to assess their actual functionality *in vivo* is essential for clinical translation. Pharmacokinetics of PNIPAAm and its exertion from body after degradation of chitosan backbone needs an additional comprehensive study. More characterization of well-defined PNIPAAm such as viscosity differences may also help us to improve the hybrid matrices.

APPENDIX: Published papers in their Journal styles

Mellati, A., Dai, S., Bi, J., Jin, B. & Zhang, H. (2014) A biodegradable thermosensitive hydrogel with tuneable properties for mimicking three dimensional microenvironments of stem cells.
RSC Advances, vol 4, pp. 63951-63961

Shen, Z., Mellati, A., Bi, J., Zhang, H. & Dai, S. (2014) A thermally responsive cationic nanogel-based platform for three-dimensional cell culture and recovery. *RSC Advances, vol 4, pp. 29146-29156*